T-3678

TRANSPORT PROPERTIES AND COUPLED FLOW PHENOMENA

IN SALTON SEA SCIENTIFIC DRILLING PROGRAM CORES
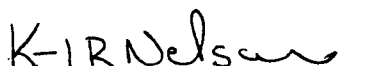
By

Elliot Yearsley

T-3678

A thesis submitted to the Faculty and Board of Trustees
of the Colorado School of Mines in partial fulfillment of
the requirements for the degree of Master of Science
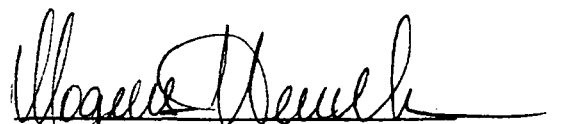(Applied Mechanics).

Golden, Colorado

Date 11/7/89

Signed _Elliot Yearsley_
Elliot Yearsley

Approved _K-1 R Nelson_
Dr. K.R. Nelson
Thesis Advisor

Golden, Colorado

Date 11/13/89

Dr. M. Henriksen
Head, Engineering Department

ii

ABSTRACT

Laboratory measurements of transport properties and coupled flow phenomena were made on six undisturbed core samples from the Salton Sea Scientific Drilling Program. The transport properties of interest were hydraulic conductivity, thermal conductivity, and electrical resistivity. Coupled flow phenomena studied were the flow of water due to chemical, electrical, and thermal gradients, and electrical potentials that result from chemical and hydraulic gradients.

The results are interpreted both in terms of fundamental processes and issues specific to the Salton Sea Geothermal System. With regard to the latter, the primary findings are: (a) pore fluid convection in the hypersaline portion of the system may be driven by a diffusion-generated coupled process described in this thesis as diffusion-osmosis, (b) pore fluid convection due to thermo-osmosis and electro-osmosis is negligible or non-existent, (c) hydraulic conductivity varies over seven orders of magnitude and is dominated by the presence or absence of fractures, (d) the

variation in thermal conductivity is small and is probably influenced more by lithology than porosity or depth, and (e) electrical resistivity is most affected by the pore fluid concentration, but surface conduction from clay minerals may be significant.

The principle findings concerning fundamental processes indicate that a chemical concentration gradient causes competing (opposite) tendencies for pore fluid flow in porous and fractured geologic media. Either chemico-osmosis (fluid flow in the direction of the more concentrated fluid), or diffusion-osmosis (fluid flow in the direction of the less concentrated fluid) can dominate depending on the abundance of clay minerals and the pore fluid concentration. Specifically, chemico-osmosis is likely to predominate for those samples that are saturated with a dilute fluid and are abundant in clays; whereas diffusion-osmosis is likely to predominate for samples saturated with a concentrated fluid and are lacking abundant clays. These competing processes are described in terms of the ion-exclusion membrane properties of clay mineral assemblages, and the effect of solute diffusion on the water phase of the pore fluid.

T-3678

TABLE OF CONTENTS

LIST OF TABLES

CHAPTER V: APPLICATION OF THE RESULTS TO THE

SALTON SEA GEOTHERMAL SYSTEM

LIST OF FIGURES

CHAPTER III: EXPERIMENTAL PROCEDURE AND SAMPLE DESCRIPTION

CHAPTER IV: DISCUSSION OF RESULTS

T-3678

ACKNOWLEDGMENTS

In reflection it is the writer's full realization that he has played but a medium-sized role in an exercise that has benefited him greatly. He recognizes, first of all, his wife Alyson and his own parents, without which completion of the thesis would have no personal meaning, and second the institution of learning so deeply rooted in our society that makes it possible for those of us so inclined to pursue learning. Individuals make up this institution, and it has been the writer's good fortune to have been associated with individuals sincerely interested in unselfish collaboration.

Karl Nelson has been the exemplary advisor and teacher. Without him the writer would have neither started nor finished this thesis, and with him the thesis has become an excellent piece of work. Hal Olsen provided clear leadership for the experimental and scientific body and essence of the thesis. Roger Morin created the opportunity for the work, and assisted Hal Olsen in formulating its goals. As committee members Eileen Poeter, Dave Munoz, and Mike Riggins have shared with the writer their experience, knowledge, and intuition.

CHAPTER I

INTRODUCTION

The Salton Sea Scientific Drilling Program (SSSDP) is a
single research borehole drilled to a depth of 10564 ft in
the Salton Sea Geothermal Field, which is located within the
Salton Trough. The physiographic province known as the
Salton Trough occupies the lowland area between the Salton
Sea and the Gulf of California (Figure 1.1). This region,
mostly flanked by mountains, includes the Imperial and
Mexicali Valleys, which are separated by the U.S. - Mexico
border.

The Salton Sea Geothermal Field is one of several
fields in the Salton Trough that are actively engaged in the
commercial generation of electrical power from geothermal
fluids.

The SSSDP borehole was drilled in 1985-86 to study the
physical and chemical processes involved in the magmatically
driven hydrothermal system. The program was funded by the
U.S. Department of Energy (DOE), managed by the U.S.
Geological Survey, and drilled under contract by Bechtel
National, Inc. A detailed history of the program is
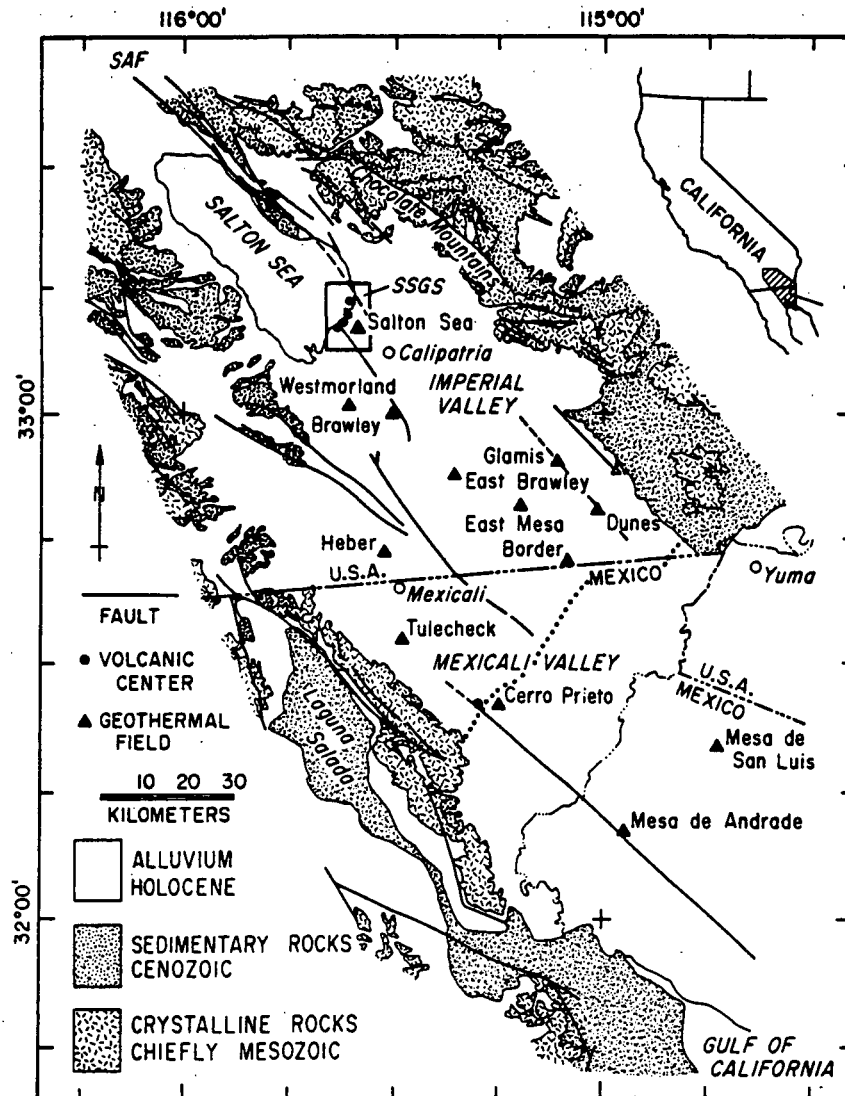
FIGURE 1.1: Geographic location of the Salton Trough. The Salton Trough is represented in outcrop by the Holocene alluvium shown in this geological map. Note the location of the Salton Sea Geothermal System (SSGS) on the southeast edge of the Salton Sea.

contained in a series of quarterly reports published by the
DOE between January, 1985, and January, 1988.

One of the main operational priorities for the program
was coring, and a total of 730 ft of core were recovered from
the borehole, ranging in depth from 1553 to 9808 ft. This
core has been described in detail (Mehegan, 1986), and much
of it has been analyzed for a variety of physio-chemical
attributes, including ore formation (McKibben et al., 1988),
hydrothermal alteration (Cho et al., 1988), and acoustic
velocity (Tarif et al., 1988).

The work in this thesis will address the transport
properties and coupled flow phenomena as measured in six
cores ranging in depth from 3113 to 8591 ft. The transport
properties of interest are hydraulic conductivity, thermal
conductivity, and electrical resistivity. Hydraulic and
thermal conductivities are the two primary parameters in the
modeling of geothermal systems, as these properties are
necessary to the calculation of heat and mass flow.
Electrical resistivity can yield information on clay content
and pore fluid concentration.

Laboratory measurements, however, provide only a limited
view of these properties, which belong to a very large,
mostly inaccessible subsurface domain. As such, the data
must be interpreted accordingly. Still, core measurements

made in the laboratory contribute to the fundamental understanding of the physical properties of rocks.

The coupled flow phenomena of interest are the fluid transport caused by chemical, electrical, or thermal gradients, and electrical potentials caused by chemical or hydraulic gradients. Studies of coupled flow are particularly germane to the Salton Sea Geothermal System because of its extreme geothermal and chemical gradients. Furthermore, unusual hydrogeologic and geochemical conditions there lend themselves to speculation concerning the interactions of these gradients. The writer's interest in coupled processes is also fundamental. There is no doubt that coupled effects contribute to a diverse variety of subsurface processes, including non-hydraulic groundwater movement (Olsen et al., 1989), naturally occurring electric potentials (Wyllie, 1949; Hanshaw, 1962), and contaminant migration (Tsang, 1987).

Therefore, the approach of this thesis will be to present laboratory data that can be interpreted in terms of fundamental processes, and can also be applied to processes specific to the Salton Sea Geothermal System. In pursuit of the latter goal, the following sections on the geology, geothermics, and geochemistry of the Salton Sea Geothermal

System will provide the context within which to interpret
the thesis data. Following those sections, Chapter II will
lay the fundamental ground work for coupled flow.

Regional Geology and Geothermics of the Salton Trough

The Salton Trough can be described as a continental
depression caused by the action of plate tectonics. This
depression has been filled primarily with sediments carried
by the Colorado River and derived from the Colorado Plateau.
The river has alternately flowed into the Gulf of California
or into the Salton Trough over the last 3 - 4 million years.
Deposition of sediments in the gulf has been in a marine
environment, whereas deposition in the Salton Trough has
been in lacustrine and deltaic environments; so that the
Salton Trough has probably remained a shallow water or sub-
aerial feature throughout its formation.

From a global tectonic perspective, the Salton Trough
is located at the southern end of the San Andreas Fault in
Southern California, where right lateral strike-slip
movement takes place between the North American and Pacific
Plates. Beginning at the Salton Sea and extending south into
the Gulf of California, the San Andreas Fault gives way to

multiple en echelon faults as the strike-slip movement of
the San Andreas grades into the Rivera Triple Junction; an
intersection of spreading, converging, and strike-slip
processes (Figure 1.2).

The multiple en echelon fault pattern consists of
right-stepping, strike-slip faults of unequal relative
movement (Elders, 1979). That these faults are offset in a
right-stepping sense results in tension between the faults
and produces "pull-apart" (terminology due to Crowell,
1974). This pull-apart mechanism is recognized as the cause
of the rifting that has formed the Salton Trough and
contributed to the formation of the Gulf of California
(Elders, 1979; Lachenbruch, 1985). The pull-apart basins are
characterized by intense seismicity and high heat flow, and
are the locus for both sediment deposition from the land
surface and magmatic emplacement from the mantle. The scale
of these pull-apart basins is relatively small compared to
the Salton Trough and the Gulf of California (Figure 1.3).
However, if the relative rates of movement between the
right-stepping faults are unequal, as Elders suggests, this
would create an unstable fault pattern that migrates in time
and space; explaining the Salton Trough and the Gulf of
California as the large regional features observed today.
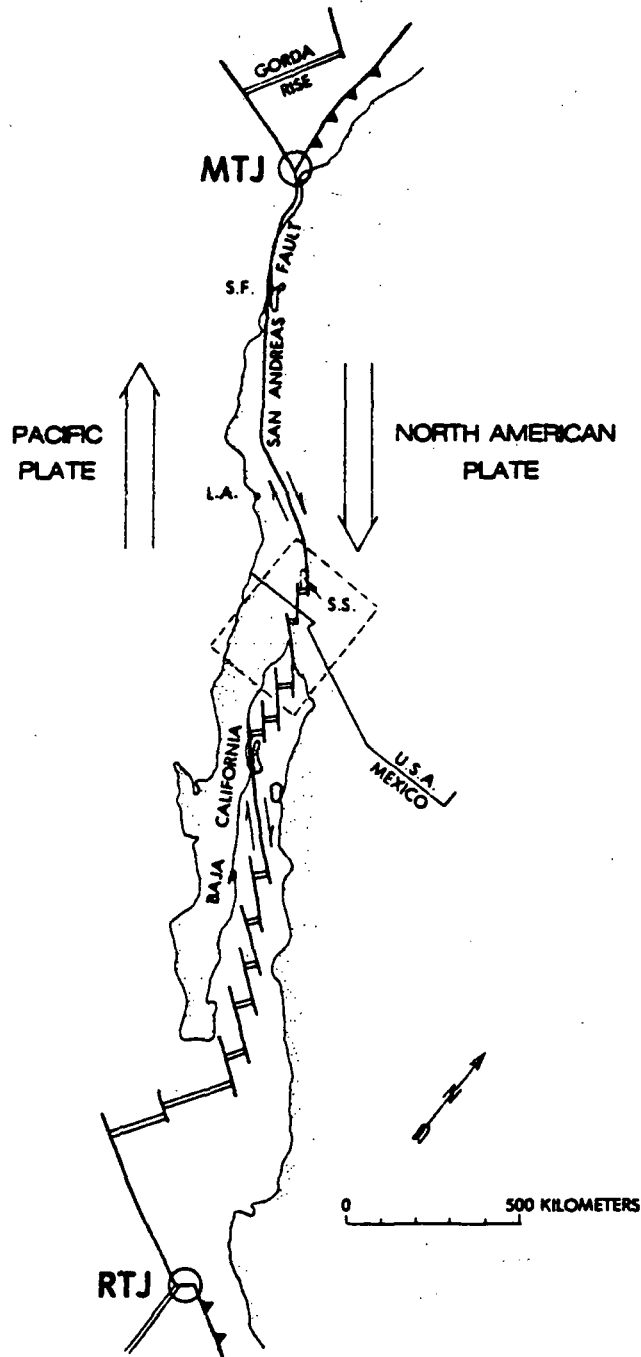
FIGURE 1.2: Boundary between Pacific and North American plates. RTJ = Rivera Triple Junction; MTJ = Mendecino Triple Junction; SS = Salton Sea.

FIGURE 1.3: The scale of the pull-apart basins with respect to the Salton Trough and the Gulf of California (Lachenbruch, 1985). Unstippled land area is Salton Trough and stippled pattern is extent of crystalline basement as inferrred by Fuis et al. (1982). The pull-apart basins are represented by the squares: S.S. = Saton Sea; C.P. = Cerro Prieto; W = Wagner basin. Heavy arrows represent plate movement.

Although the Salton Trough is the natural landward extension of the Gulf of California and both appear to be undergoing similar geologic processes today (pull-apart), they may have different origins. For example, early formation of the gulf may have been due to a volcano-tectonic rift zone similar to the rifts commonly formed behind island arc-trench systems (Karig and Jensky, 1972; from Elders, 1979). Also, palentological evidence indicates that marine deposition occurred in the gulf in Miocene time (Ingle, 1973), whereas deep drilling in the Salton Trough has penetrated 14,000 ft of no older than late Pliocene sediments (communication with Elders, 1988). Table 1.1 gives the geologic time scale for these epochs.

TABLE 1.1: Epochs of the Cenozoic

Epoch	Million years before present
Pleistocene	.01 - 2 m.y.
Pliocene	2 - 7 m.y.
Miocene	7 - 26 m.y
Oligocene	26 - 37 m.y.
Eocene	37 - 53 m.y.
Paleocene	53 - 65 m.y.

No drill bit has reached basement in the Salton Trough, and therefore the thickness of these sediments is unknown. But seismic and gravity surveys have been interpreted as indicating a sediment/basement boundary at 6 -7 km (Biehler, 1964; Elders et al., 1972). Furthermore, these surveys suggest that the basement is newly formed basalt, speculated to have derived from the mantle. Presumably then, in the Salton Trough, recent Plio-Pleistocene sediments directly overlie newly formed basalt basement. This hypothesis is supported by consideration of geothermics, as proposed by Lachenbruch (1985).

Lachenbruch's thermo-mechanical model attempts to reconcile the observed near-surface heat flows in terms of an extending crust where new crust is created simultaneously from below as a basaltic melt derived from the mantle, and above from sediment accumulation. Figure 1.4 illustrates the essential elements of his model. His conclusions indicate that he believes that the Salton Trough has been created over the last 4 million years by local extension in pull-apart zones whose locations are ephemeral with time. Figure 1.3 shows the locations of two of the currently active pull-apart zones, as identified by intense seismicity and high heat flow. These areas coincide with the
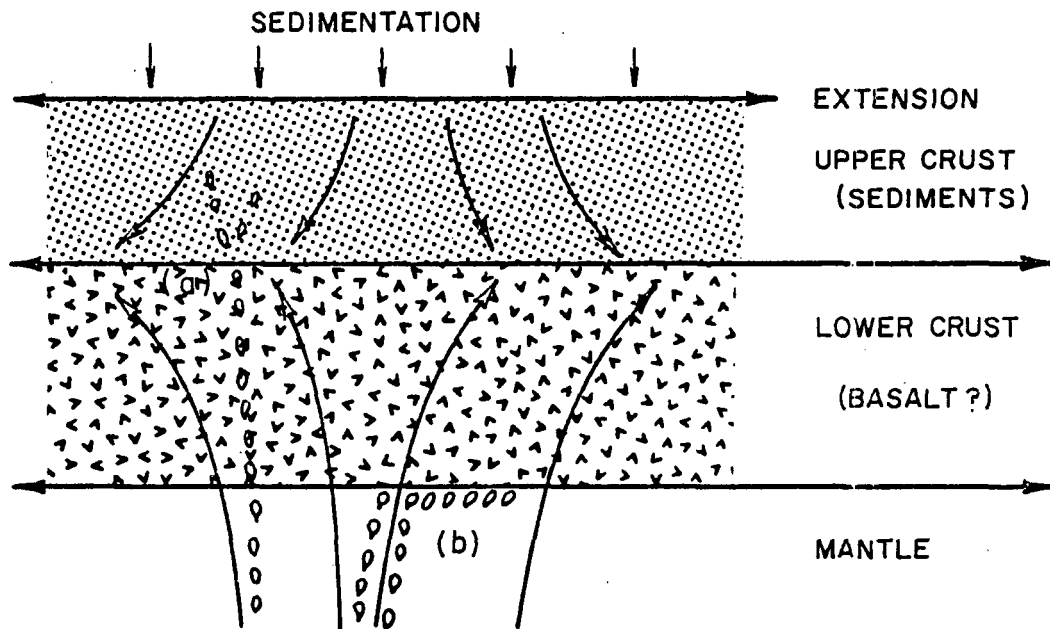
FIGURE 1.4: Essential elements of Lachenbruch's model. New crust is created in the pull-apart region by the simultaneous accumulation of sediments and mantle material. The mantle material is emplaced by two processes: (a) intrusion into previously formed crust, and (b) underplating from the mantle on the lower crust.

Salton Sea and Cerro Prieto geothermal fields.

The assumptions which form the basis of Lachenbruch's conclusions are as follows: (a) the relative rates of sedimentation and magmatic emplacement are ultimately both controlled by the extension rate (due to isostatic balance between the lower crust and the sediments), (b) the extension rate must be such that melt material from the mantle rises to the crust, but massive melting does not occur (as Biehler, 1964 and Fuis et al., 1982 have pointed out that their geophysical studies indicate that the basement underlying the Salton Trough is predominately solid), and (c) heat transfer is accomplished by advection via magmatic emplacement from the mantle to the crust. A predominately solid basement at a temperature near the mantle solidus would preclude heat transfer by conduction by virtue of similar temperatures (no temperature gradient).

Geochemistry of the Salton Sea Geothermal Field

The Salton Sea Geothermal Field is characterized by hypersaline brines (20-25% by weight total dissolved solids [TDS]), high temperatures (>300C), and high local heat flux (>200 milliwatts/m^2). Rex (1985) has described the subsurface of the Salton Sea area as a single continuous

hypersaline brine reservoir with an aerial extent of approximately 1000 km^2, based on geochemical data from numerous drill holes in the area. The following discussions will focus on the origin of the hypersaline brine, observation of a hypersaline brine/dilute pore fluid interface, and speculation for a density stable, non-advecting brine column below the interface.

Origin of the hypersaline brine:

Because of the high temperatures and high metal content of the brines, White et al. (1963; from Mckibben et al., 1988) first suggested they represented magmatic fluids. Later isotopic studies of the brine indicated that the water was meteoric in origin (Craig, 1966; from Mckibben et al., 1988). Williams and McKibben (1988) have shown that there are actually two chemically and isotopically distinct fluids in the field: the deeper, hypersaline brine, and the overlying less saline fluid.

The hypersaline nature of the deeper brines is probably due to dissolution of shallow non-marine evaporites by meteoric waters (White, 1968; Rex, 1985). McKibben et al. (1988) have also suggested that the high salinities are due in part to the hydrothermal metamorphism of lacustrine deposits. Most authors agree that the present day Salton Sea

has been the site of ancient lake and salina deposition
during the past 1-2 million years. Deposition in this
environment would produce evaporites and other sediments
with high salt contents.

Hypersaline brine/dilute pore fluid interface:

Williams (1988) has demonstrated that a relatively
sharp (a few hundred meters thick) hypersaline brine/dilute
pore fluid interface exists in the Salton Sea Field,
consisting of a 3-6% by weight TDS fluid overlying a 20-25%
by weight TDS fluid. The overlying fluid is referred to as
dilute in a relative sense. The field is known for its
hypersaline brines because production depths are generally
below the interface. Though the existence of the dilute
fluid was known previously, Williams has more fully
addressed the spatial distribution of the two fluids based
on 40 geothermal wells and 60 production intervals.

Examination of the spatial distribution of the two
fluids reveals that they cut across structural and
stratigraphic features. Similar inspection of thermal
profiles in the area shows that the shapes of the profiles
also are not controlled by structure or stratigraphy
(Williams). The latter finding departs from the previously

held view that an impermeable "caprock" restricts upward

circulation of hot brines, thereby influencing the shape of

the thermal profiles. Williams questions the caprock thesis

because: (a) the shape of the thermal profiles do not

appear to be controlled by stratigraphy, and (b) instead the

brine interface may act as a barrier to the upward

circulation of hot brines.

Based on a plot of temperature versus TDS (Figure 1.5),

Williams concludes that temperature controls the spatial

distribution of the interface. The demarcation of fluids

appears to be at approximately 260C. Thus, the interface

is most shallow at the center of the field, where the 260C

isotherm is encountered at a depth of about 2500 ft, and

deeper off the flanks, where the interface has been observed

as deep as 12,000 ft.

Geophysical log calculations done in this thesis

indicate that the interface is encountered in the SSSDP

borehole, which is near the center of the field, at 2800-

3000 ft. These calculations are performed on sandstones and

are based on Archie's (1941) relationship that assumes

the pore fluid contributes 100% of the electrical

conductance of the rock. Figure 1.6 shows the interpreted

salinity profile based on these geophysical log calculations

and two fluid analyses.
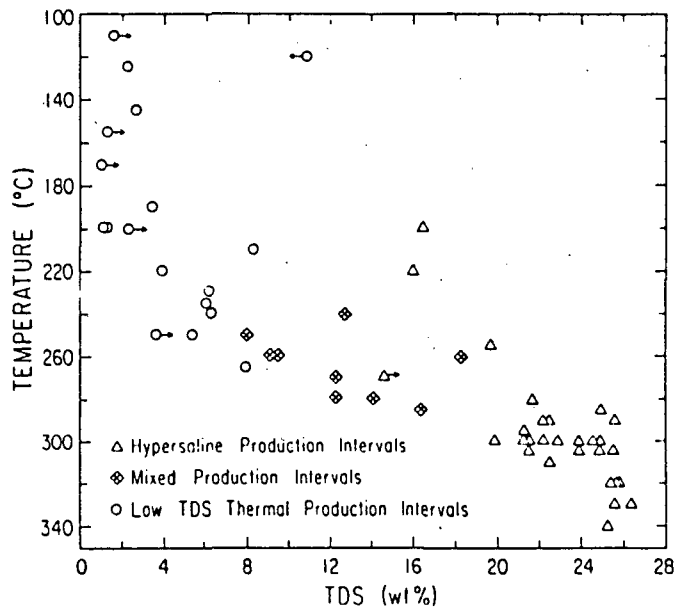
FIGURE 1.5: Salinity vs. temperature plot for the Salton Sea Field (Williams, 1988). Note the separation of fluids into three distinct groups: (1) low TDS fluids below 260C, (2) high TDS fluids above 260C, and (3) mixed fluids at approximately the 260C isotherm.

DEPTH
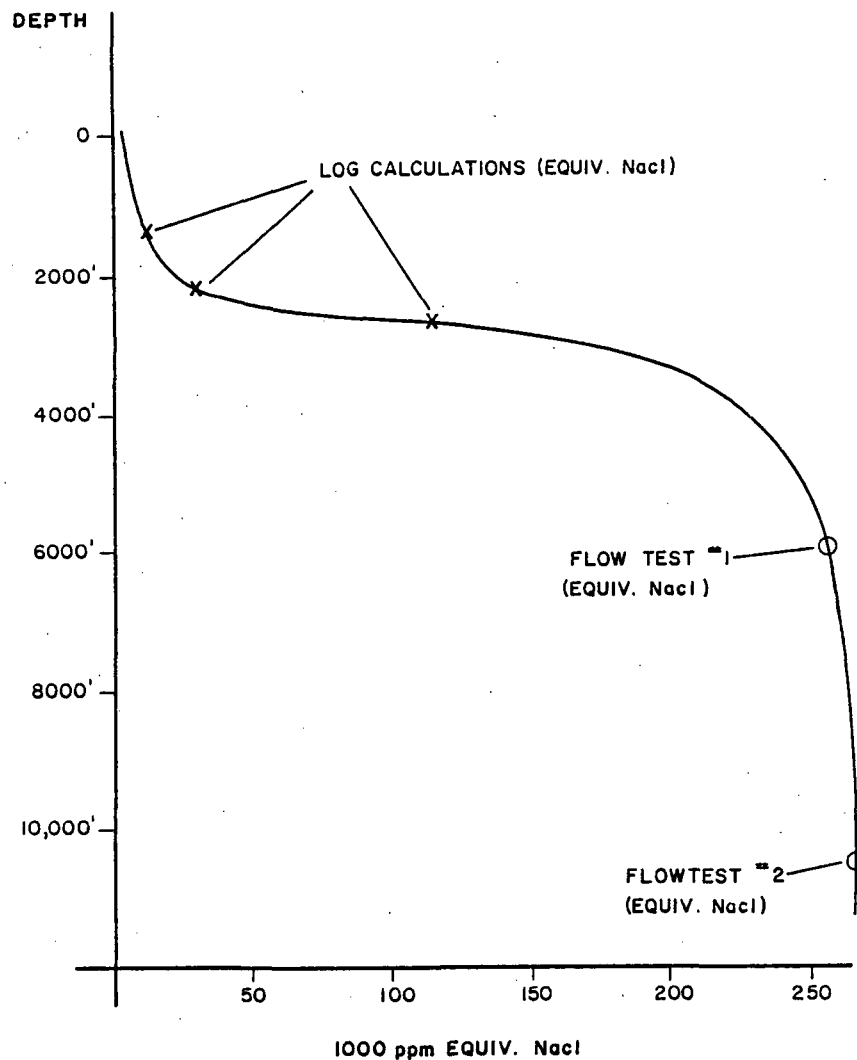
FIGURE 1.6: Estimated salinity profile at the SSSDP site.
Three sandstone intervals were amenable to log calculation
of salinity (other sandstone interval resistivities appeared
influenced by factors others than pore fluid). Two fluid
analyses were obtained from the borehole; at approximately
6000' and 10,400'. The second test (10,400') was corrected
for dilution due to contamination from drilling fluid.

A density stable non-advecting brine:

Though most or all geothermal systems are assumed to be undergoing upward advection due to thermal fluid density gradients, a stable non-advecting brine is possible. Michels (1988) explains the condition for gravitational stability in terms of offsetting thermal and chemical concentration gradients. He computes that the minimum average value for stability for a 20-25% brine is 900 ppm TDS/C (parts per million total dissolved solids per degree celsius).

Rex (1985) has reported that in the Salton Sea hypersaline system there is a consistent, reservoir wide, temperature-chlorinity balance that translates to 2200 ppm TDS/C. Since this value is larger than the minimum computed by Michels, non-advection appears sound. It must be pointed out, however, that this salinity gradient has never been verified directly by measurement in a borehole.

Still, there is other evidence which supports the stable brine column. Namely, the observed fluid density in the hypersaline portion of the reservoir appears to be a remarkably uniform 1.0 g/cm^3. For thermal plume-like advection to occur, the fluid density must decrease with depth. Neither Rex nor Michels have suggested a mechanism for the origin of a salinity gradient that stabilizes against advection; though both propose the same combination

of physical processes which would sustain and improve it.

Rex and Michels suggest that a salinity gradient in the presence of a thermal gradient may be stable due to offsetting coupled process; namely, chemico-osmosis and thermo-osmosis. They hypothesize that chemico-osmosis would drive the water phase of the brine toward the more concentrated region (down), and that thermo-osmosis would drive the water toward the cooler region (up). This process would tend to increase the stability of the brine column against advection (Michels).

The existence of a non-advecting brine has important consequences with regard to the mechanism of heat transfer within the reservoir, and this issue is re-examined in Chapter V.

CHAPTER II

CONDUCTION AND COUPLED FLOW PHENOMENA

The flow of matter and energy through geologic porous materials in the subsurface is controlled by naturally occurring gradients and the properties of the media. In the most general form the flux of matter and energy by direct conduction can be expressed as:

$$J_i = K_i X_i \qquad (2.1)$$

where J_i is the flux, X_i is the gradient, and K_i is the conduction coefficient. For water, heat, current, and solute respectively, these well known linear relationships can be written:

water flow	$J_h = K_h X_h$	Darcy's law
heat flow	$J_t = K_t X_t$	Fourier's law
electrical flow	$J_e = K_e X_e$	Ohm's law
solute flow	$J_s = K_s X_s$	Fick's law

Each of these relationships describes direct conduction, that is, flow of one type which occurs as a direct result of a gradient of the same type. However, flows which occur as a result of a gradient of a different type

may also be important in the subsurface. Flows of this type
are referred to as "coupled" flows because of the
interdependent paired nature of the process.

The proportionality constants that link flux to the
gradient responsible for transport include both direct
conduction coefficients and coupled transport coefficients.
As an analogy with direct conduction, the coupled flux of
matter or energy can be written as:

$$J_i = K_{ij}X_j \tag{2.2}$$

where K_{ij} is the coupled transport coefficient and represents
the degree to which gradient X_j causes a flux of J_i.

In this research we are primarily concerned with
thermal, hydraulic, and electrical conduction and non-
hydraulic causes of pore fluid movement. However, in the
interest of completeness Table 2.1 presents a 4x4 matrix
that relates the flow of water, heat, current, and ions to
hydraulic, thermal, electrical, and chemical gradients.

Irreversible Thermodynamics

A mathematical description for coupled flow can be
found in the field of Irreversible Thermodynamics, so called
because it is the study of irreversible processes; i.e.,
processes _not_ in equilibrium. Onsager in 1931 laid the

TABLE 2.1

Conduction and Coupled Flow Phenomena

	Gradient X			
Flow J	Hydraulic	Temperature	Electrical	Chemical
Water:	Hydraulic conduction Darcy's law	Thermo-osmosis	Electro-osmosis	Chemico- or Diffusion- osmosis
Heat:	Isothermal heat transfer	Thermal con- duction Fourier's law	Peltier effect	Dufour effect
Current:	Streaming current	Thermo- electric effect	Electric con- duction Ohm's law	Membrane and liquid junction potentials
Ions:	Streaming current	Soret effect (thermal diffu- sion of electro- lytes)	Electro-phoresis	Diffusion Fick's law

(Adapted from Gray, 1966)

modern cornerstone for irreversible thermodynamics by
proposing that, in general, thermodynamic flows can be
explicitly expressed as a linear sum of thermodynamic
forces. This expression can be written in equation form as:

$$J_1 = K_{11}X_1 + K_{12}X_2 + K_{13}X_3 + \ldots + K_{1n}X_n$$

$$J_2 = K_{21}X_1 + K_{22}X_2 + K_{23}X_3 + \ldots + K_{2n}X_n$$

$$J_3 = K_{31}X_1 + K_{32}X_2 + K_{33}X_3 + \ldots + K_{3n}X_n$$

$$\cdot$$
$$\cdot$$
$$\cdot$$

or $$\qquad J_i = K_{ij}X_j \qquad (i = 1,2,3,\ldots,n) \qquad (2.3)$$

Onsager described these as "phenomenological equations of
flow" because they can be verified only through experimental
observation.

To take a specific case, irreversible thermodynamics
establishes that the total flux of water in porous media due
to hydraulic, electric, thermal, and chemical gradients can
be written as:

$$J_h = K_h\nabla H + K_{he}\nabla E + K_{hc}\nabla C + K_{ht}\nabla T \qquad (2.4)$$

for: $\quad J_h$ = flux of water

$\qquad \nabla H$ = hydraulic gradient

$\qquad K_h$ = hydraulic conductivity

$\qquad \nabla E$ = electric potential

∇C = chemical concentration gradient

∇T = thermal gradient

The coupled transport coefficients in equation (2.4) are defined in Table 2.2, along with other coupled transport phenomena that will be of interest in this thesis.

TABLE 2.2

Coupled Transport Phenomena

Symbol	Coefficient	Process
K_{he}	electro-hydraulic	transport of water due to an electric field (electro-osmosis)
K_{eh}	hydro-electric	electric current due to hydraulic flow (streaming potential)
K_{hc}	chemico-hydraulic	transport of water due to a chemical gradient (chemico- or diffusion-osmosis)
K_{ec}	electro-chemical	electric potential caused by chemical concentration gradient (membrane potential or liquid junction potential)
K_{ht}	thermo-hydraulic	transport of water due to a thermal gradient (thermo-osmosis)

Perhaps the clearest demonstration of Onsager's
phenomenological equations of flow for a porous geologic
material is provided by Olsen (1969). Olsen presents
remarkably linear data for the flow of water resulting from
hydraulic, electric, and chemical concentration gradients
across a compacted sample of kaolinite. One of his figures
is reproduced here. Figure 2.1 plots the measured hydraulic
head differences in response to a range of electric currents
and superimposed hydraulic flow rates. Careful inspection of
this figure will show that for zero hydraulic flow the
electric currents cause proportional head differences across
the sample, which represent the tendency for electro-osmotic
coupled flow. When hydraulic flows are superimposed
additional head differences are developed which are
additive.

Another excellent example of the linearity of Onsager's
equations of flow in porous media is given by Srivastava and
Avasthi (1975). Their data clearly show the linear
relationship between thermo-osmotic flow and the
corresponding thermal gradients (Figure 2.2).

Onsager's provision for equations (2.3) were contained
within a larger work on reciprocal relations in irreversible
processes. Those relations, for our purposes, can be
described as the equality condition between coupled
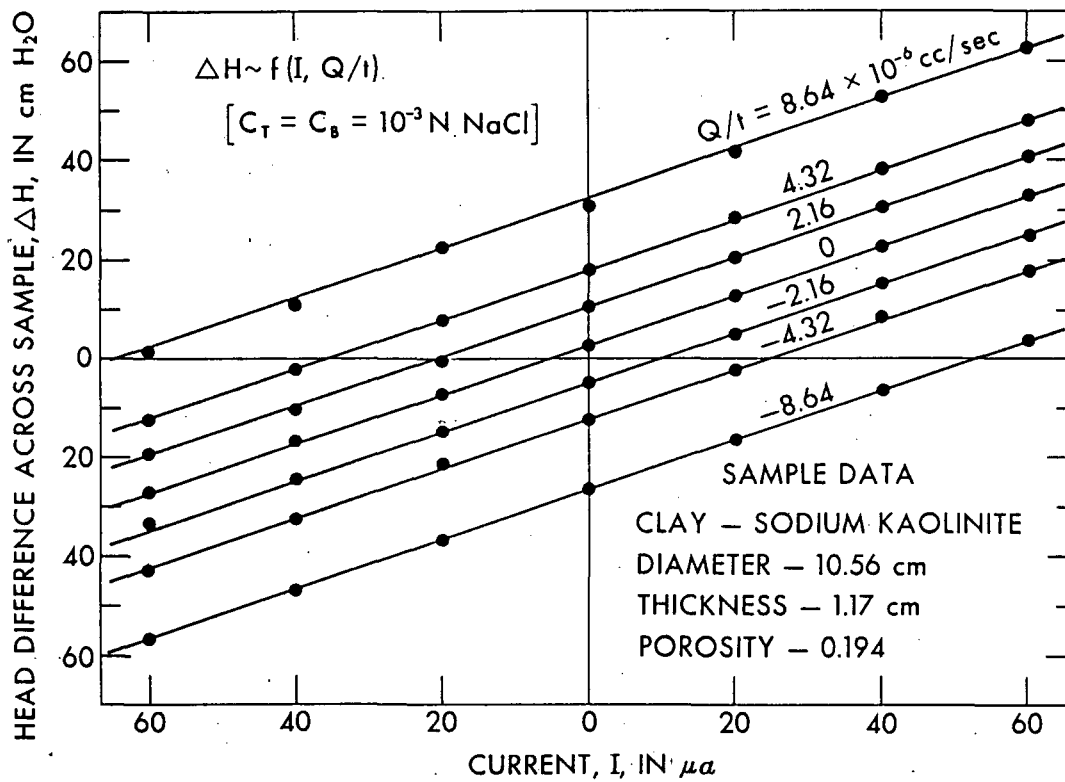
FIGURE 2.1: Measured hydraulic head differences plotted as a function of the externally imposed currents and liquid flow rates (Olsen, 1969).
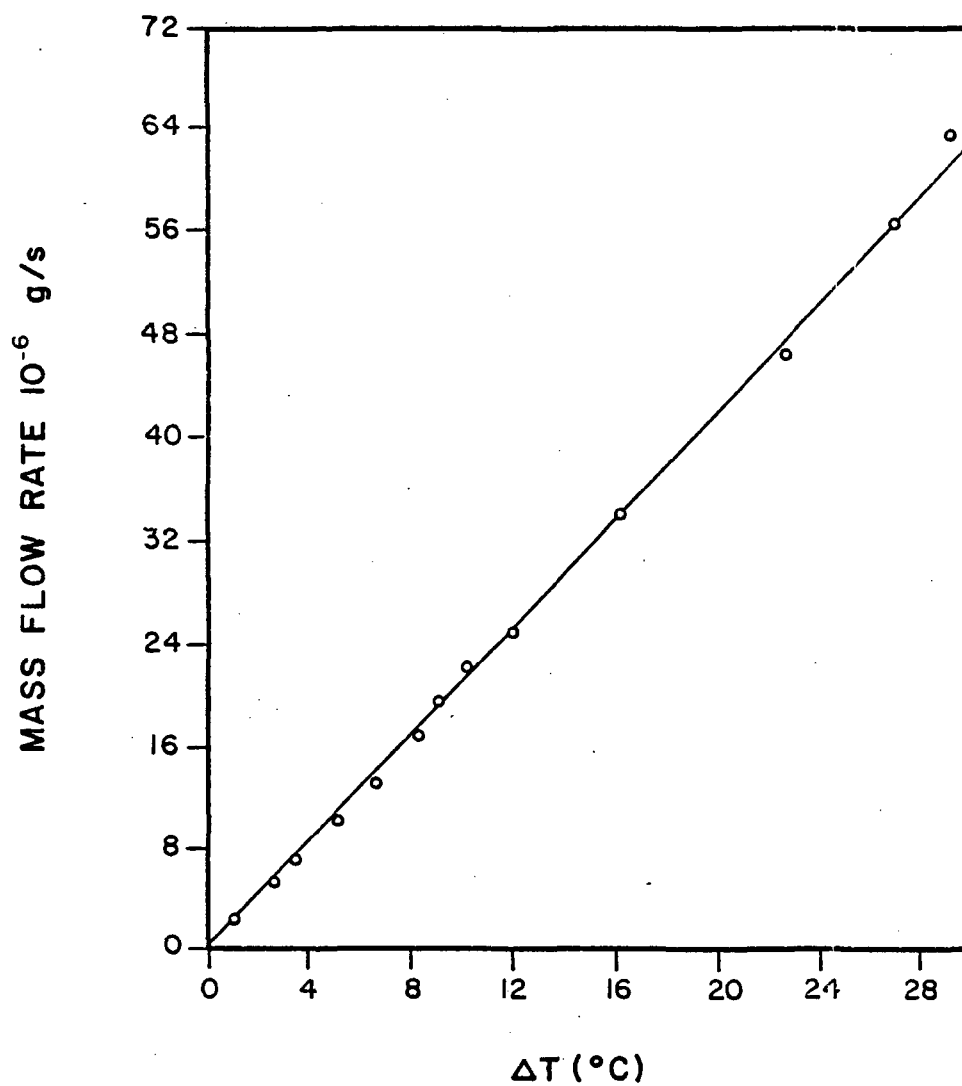
FIGURE 2.2: Linear relationship between thermo-osmotic flow and temperature difference (Srivastava and Avasthi, 1975).

transport coefficients that characterize reciprocal

processes; i.e., from equations (2.3):

$$K_{12} = K_{21}$$
$$K_{13} = K_{31}$$
$$K_{23} = K_{32}$$

in general: $K_{ij} = K_{ji}$ (2.5)

This reciprocal condition has been verified for

specific cases in geologic materials. Gray (1966) showed the

reversibility of electro-osmotic and streaming potential

data. Elrick et al. (1976) demonstrated that the flow of

ions and electric current are reciprocal processes.

Srivastava and Avasthi (1975) experimentally confirmed the

reciprocal relationship between thermo-osmotic flow due to a

thermal gradient and heat flux due to a hydraulic gradient.

Onsager's work in irreversible thermodynamics is

massive, and the field has expanded since then. An excellent

treatment of the full field of irreversible thermodynamics

can be found in a text by Katchalsky and Curran (1965).

However, our interest in this thesis lies with the simple

linear relationships expressed by equations (2.3) and (2.4),

and the reciprocal condition described by equation (2.5).

The tenets of irreversible thermodynamics represented

by equations (2.3), (2.4), and (2.5) provide a unified

approach to coupled flow phenomena that is appealing in its
simplicity and elegant in form. They are also experimentally
useful for the extrapolation of data, derivation of
consistent units, and in the deduction of reciprocal coupled
transport coefficients. Irreversible thermodynamics by
itself does not, however, suggest what causes coupled flow,
and has no predictive value for a specific soil or rock.

Here lies the crossroads of phenomenological and
mechanistic descriptions of coupled processes. The
phenomenological description expresses the relationship
between coupled forces and fluxes; the mechanistic
description explains the causes of the processes.

Mechanistic descriptions tend to be speculative,
particularly for subsurface processes in geologic materials.
With this in mind, the following sections summarize the
mechanisms for specific coupled processes of interest in
this thesis; namely, non-hydraulic causes of pore fluid
movement and naturally occurring electric potentials.
Following those sections is a brief review of subsurface
occurrences of coupled flow phenomena.

Chemico-osmosis

Chemico-osmosis is the tendency for water to flow from

less concentrated to more concentrated solutions separated by a semipermeable membrane. The semipermeable membrane restricts the flow of solute but allows the flow of water. The thermodynamic driving force for chemico-osmosis is the difference in chemical potential in the water phase between the two solutions, the more concentrated solution having the lower potential. A pressure applied to the more concentrated side that will balance the osmotic tendency so that the flow of water becomes zero is called the osmotic pressure. For a perfect semipermeable membrane that separates arbitrary solutions 'A' and 'B', the ideal osmotic pressure can be approximated by:

$$\pi = (RT/V_w)\ln(a_A/a_B) \qquad (2.6)$$

where: π = osmotic pressure

R = gas constant (in consistent units)

T = absolute temperature

V_w = mean partial molar volume of water

a_A = activity of water on less concentrated side

a_B = activity of water on more concentrated side

Derivation of equation (2.6) is given in Appendix A.

Experimenters have found that natural clays can act as semipermeable membranes (Hanshaw, 1962; Young and Low, 1965;

Marine and Fritz, 1981), and are therefore capable of
generating chemico-osmotic flow or pressure where a solute
concentration gradient exists in the subsurface.

The membrane properties of clays result from charge
deficiencies on the surfaces of clay particles which arise
primarily from the substitution of high valence cations in
the clay lattice by lower valence cations. This results in
negatively charged clay particles which tend to attract
cations to their surfaces, forming a double layer comprised
of the negatively charged clay surface and the cation
layer, or "diffuse layer". As the clay particles approach
each other (as in compacted clays) the adjoining double
layers draw closer together, lowering the concentration of
anions in the pore space between them (Figure 2.3). This
anion depletion, or cation excess, is responsible for the
semipermeable membrane properties of clays by virtue of the
electric repulsion (Kharaka and Berry, 1973). Discussion of
"membrane properties" in this thesis refers to the ion
exclusion phenomena described above.

Though clays can exhibit membrane properties, they are
not perfect semipermeable membranes, and the osmotic
pressure which develops across clay samples is generally
some fraction of that described by equation (2.6). The
degree to which osmotic pressure approaches ideal is
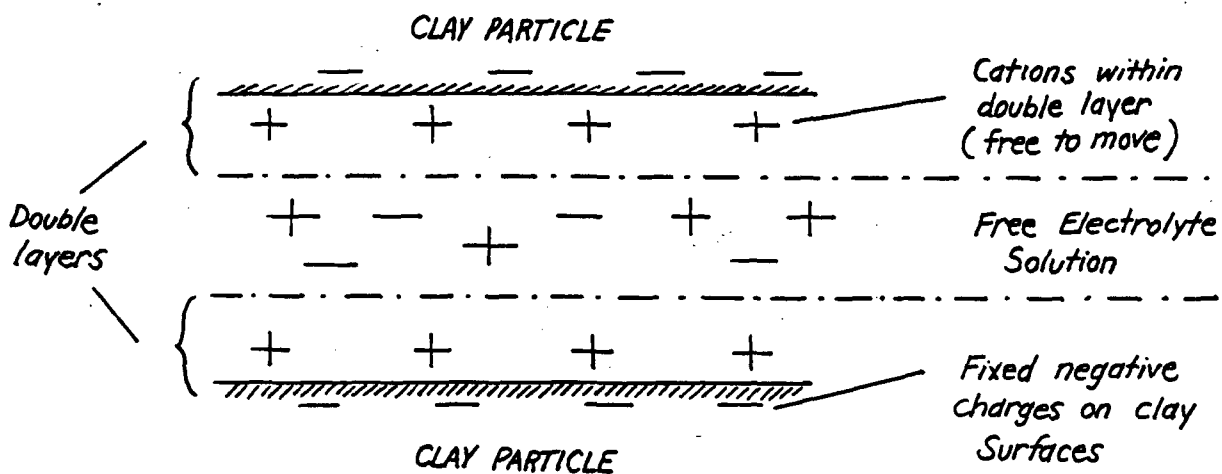
FIGURE 2.3: Schematic representation of the electric double layer in the pore space between clay particles.

represented by a term known as the "reflection coefficient" (Staverman, 1952; Groenevelt and Elrick, 1976), so named because it describes the ability of the membrane to "reflect" ions. Experimenters have found (Kharaka and Berry, 1973; Fritz and Marine, 1983; Fritz, 1986) that the reflection coefficient depends on: (1) the cation exchange capacity of the clay, (2) the degree of compaction, and (3) the concentration of the saturating solution. Table 2.3 relates these conditions to their effects on the membrane's efficiency in generating chemico-osmosis.

TABLE 2.3

Factors Affecting Membrane Efficiency

Condition	Effect
(1) Cation exchange capacity	More active substitution of cations results in a greater charge disparity and a more effective double layer (increases membrane efficiency).
(2) Compaction	Pore space distribution: proximity of the double layer increases electric repulsion (increases membrane efficiency).
(3) Saturating solution	A lower concentration in the pore space increases the ratio of cations to anions in the pore space, thereby increasing electric repulsion (increases membrane efficiency).

The entries in Table 2.3 indicate that osmotic efficiency is directly related to the ability of the clay to act as an ion-restricting membrane. It is interesting to examine this relationship in the context of the mechanism for chemico-osmosis. Membrane properties of clays, though required to generate chemico-osmosis, are not related to its driving force (chemical potential difference). Rather, those ion-restricting properties subdue a would-be competing process; namely, diffusion-osmosis.

Diffusion-osmosis

A chemical potential in the solute phase provided by a concentration gradient drives the diffusion of ions from the more concentrated to the less concentrated solution according to Fick's law already quoted. If the ions are not restricted from migrating by the membrane properties described above, their movement apparently transfers momentum to water molecules, which results in the flow of water in the direction of diffusion.

This diffusion-originated mechanism for the non-hydraulic cause of pore fluid movement in porous media is herein defined as diffusion-osmosis (the term coined by Olsen, Yearsley, and Nelson, 1989). This process was

apparently first noted in the literature by Kemper and Quirk (1972), who described it as "negative osmosis ... probably due to the limited development of the double layer and the presence of large pores [in calcium kaolinite]". The process was noted again by Elrick et al. (1976), who proposed an equation whereby a negative reflection coefficient could be calculated.

Elrick's data showed that a chemico-osmotic pressure can be flipped from the saline side to the dilute side by short circuiting reversible silver chloride electrodes in contact with opposite ends of the sample. Silver chloride electrodes will be explained in detail in Chapter III; it will suffice to say here that they allow the exchange of electrons and chloride ions.

Elrick's results nicely illustrate the difference between chemico-osmosis and diffusion-osmosis. Without the short circuit ions are electrically repelled from the clay membrane. However, water is allowed to flow from the less concentrated to more concentrated side in accordance with the difference in its chemical potential: chemico-osmosis results (Figure 2.4). With the short circuit, chloride anions are passed from the more concentrated to less concentrated side via the reversible electrodes (Figure 2.5);

| lower concentration | charged membrane: overall polarity of pore fluid is positive | ⟹ | higher concentration water molecules pass |
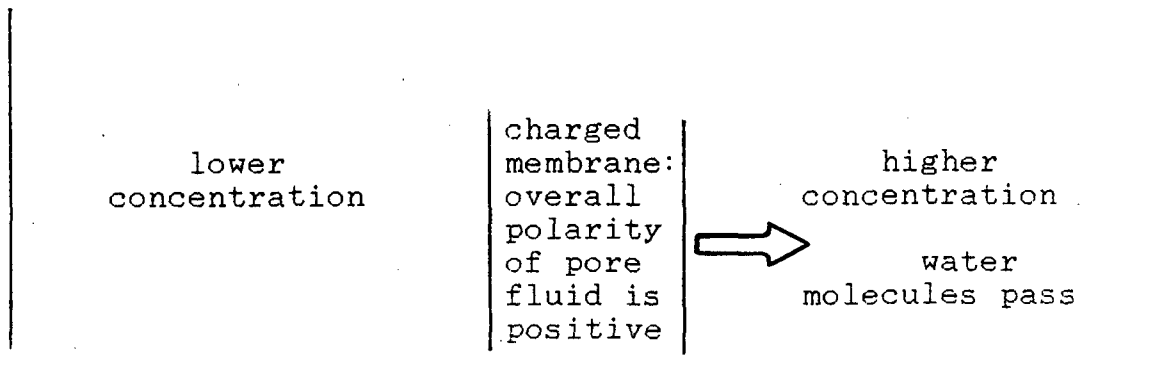
FIGURE 2.4: Schematic of chemico-osmotic process. Large arrow is direction of water flow.

reversible electrodes

lower
concentration

⟸

charged
membrane:
overall
polarity
of pore
fluid is
positive

higher
concentation

water molecules
diffuse with cations

electrons displace
chloride ions

chloride ions
displace electrons

e^-
short circuit
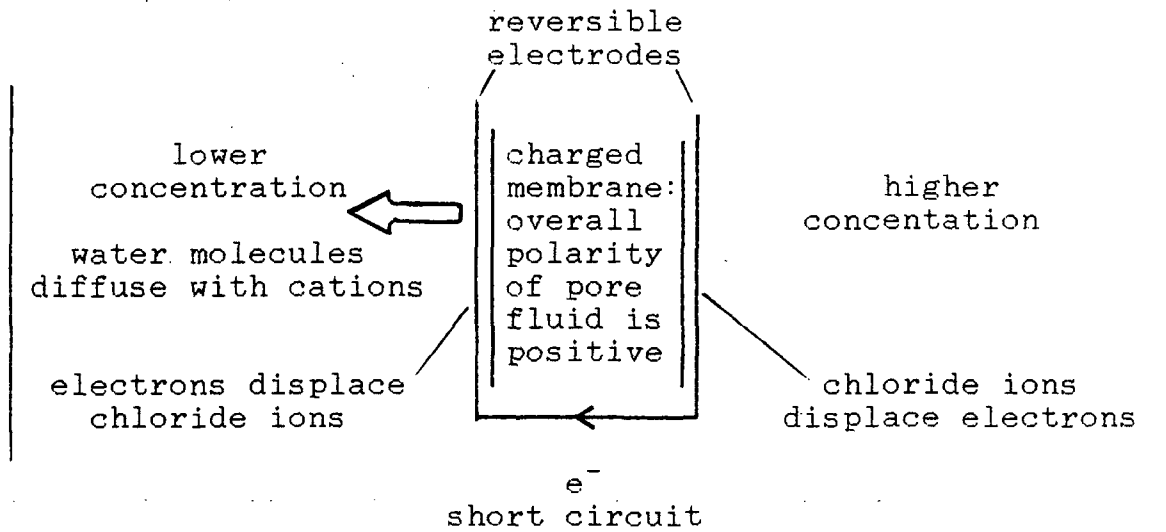
FIGURE 2.5: Elrick's short circuit resulting in diffusion-osmosis. Large arrow represents direction of water flow.

thereby freeing the cations to diffuse (due to electroneutrality requirements). The flow of cations imparts a momentum to the water molecules in the direction of diffusion that evidently overcomes the driving force provided by the difference in chemical potential in the water: diffusion-osmosis results.

Electro-osmosis

Electro-osmosis is the tendency for water to flow in geologic materials in the presence of an electric current. The mechanism that drives electro-osmotic flow is the momentum transfer from electrically driven ions to water molecules. The cations impart a net momentum to the water because of their surplus in the pore space of charged membranes, and therefore the direction of electro-osmotic flow is in the direction of cation flow. Furthermore, electro-osmosis is a process associated with those membrane properties consistent with chemico-osmosis.

Experimenters have found, however, that electro-osmotic efficiency is the greatest for materials of low exchange capacity and high porosity (Spiegler, 1958; Carr et al., 1962: from Gray, 1966). This peculiar relationship (opposite that for chemico-osmotic efficiency) can be analyzed in the context of the water to cation ratio. In high porosity, low

exchange capacity membranes there is more water associated per cation, and therefore more water flow per unit charge. This relationship cannot be extrapolated to a material with no membrane properties; i.e., electro-osmosis does not occur in a quartz sandstone.

There is a twist to the efficiency relationship described above: increased salinity severely reduces electro-osmotic flow in low exchange capacity materials due to the reduction in the cation to anion ratio in the membrane. Whereas, high exchange capacity membranes can accommodate more cations in the double layer, maintaining a higher cation to anion ratio, and therefore a greater electro-osmotic efficiency relative to increasing salinity.

These contorted relationships for electro-osmotic efficiency veil its fairly straight-forward cause. Nevertheless, the mechanics of electro-osmosis are still not well understood, and development of various electro-osmotic models can be found in Gray (1966) and Mitchell (1976).

Thermo-osmosis

Thermo-osmosis is the tendency for water to flow in the presence of a thermal gradient, without benefit of a body force. The additional qualification of the absence of a body

force is implicit in all osmotic processes, but must be stated explicitly in this case to differentiate thermo-osmosis from thermal advection driven by density gradients.

The mechanism for thermo-osmosis in saturated porous media is not known, but some have suggested that thermo-osmosis is closely related to electro-osmosis (Carr and Sollner, 1962; Kobatake and Fujita, 1964: from Gray, 1966). The thermal diffusion of electrolytes is well known (Soret effect), and the thermally-caused migration of ions through materials with membrane properties could also cause the flow of water, as in electro-osmosis. Gray argues that a consistent thermo-electric response might be expected to accompany thermo-osmosis if thermo-osmotic flow is related to electro-osmosis. He points out, however, that experimenters have found no such consistent response: both positive and negative polarities in the direction of thermo-osmotic flow, as well as no thermo-electric effect, have been measured. To the writer's knowledge, this issue is still unresolved (1989).

As an analogy with chemico-osmosis, the driving force in thermo-osmosis may be the temperature dependent chemical potential of water. Unfortunately, the variation of the chemical potential of water with temperature is not straight-forward. Several methods for calculating the

temperature dependent chemical potential of water are
available (Helgeson, 1968; Robie et al., 1978, Iwata et
al., 1988), but these methods are inconsistent with each
other. Furthermore, conflicting experimental results do not
illuminate the issue. Many researchers have measured thermo-
osmotic flow from warm to cool (Taylor and Cary, 1961;
Dirksen, 1969; Srivastava and Avasthi, 1975). However, Gray
(1966) reported thermo-osmotic flow in the opposite
direction; from cool to warm. In addition, researchers of
thermo-osmosis across non-geologic materials have reported
both directions of thermo-osmotic flow, depending on factors
such as electrolyte concentration and absolute temperature
(Tasaka, 1986).

Gray has investigated thermo-osmosis in geologic
materials with regard to electrolyte solutions (most other
researchers have used distilled water), and has suggested
that the direction of flow in his experiments may have been
controlled by the chemical potential of the solute, which is
inversely related to that of the water according to a form
of the Gibbs-Duhem equation:

$$du_w = -(n_s/n_w)du_s \qquad (2.7)$$

for: du_w = change in chemical potential of the water

        du_s = change in chemical potential of the solute

        n_w = number of moles water

        n_s = number of moles solute

Thus, for a constant molar ratio, an increase in the solute

chemical potential due to temperature will produce a

corresponding decrease in the chemical potential of the

water phase.

Naturally Occurring Electric Potentials

Naturally occurring electric potentials in the

subsurface can result from a wide variety of conditions, but

our interests are specific to saturated sedimentary rock.

For this condition, the source of natural electric

potentials can be divided into two main groups: that which

is caused by the presence of a solute concentration

gradient, and that which is caused by hydraulic flow.

With regard to the latter, hydraulic flow through

porous media possessing charged membrane properties tends to

displace diffuse layer charges (cations) in the direction of

the flow. As with its reciprocal process, electro-osmosis,

the mechanism of transport is a momentum transfer; this time

from the water molecules to the cations. The electric

potential that develops is proportional to the hydraulic

flow, in accordance with Onsager, and is known as the

streaming potential. The streaming potential has been

identified both in the soils literature (see summary by

Mitchell, 1976), and in borehole logging (Wyllie, 1951).

A solute concentration gradient in porous media may

also cause natural electric potentials, the polarity of

which depends on the presence or absence of membrane

properties. If the rock or soil has no membrane properties,

and diffusion of ions is allowed to occur freely, then a

negative polarity may develop in the direction of diffusion

due to the greater mobility of chloride ions (Kemper and van

Schaik, 1972). More properly, the polarity which develops

maintains the neutrality of diffusion by compensating for

the greater mobility of the chloride ions. This mechanism

and associated result is called the liquid junction

potential, and is recognized in physical chemistry (Barrow,

1979), the soils literature (Kemper and Quirk, 1972), and in

borehole logging (Wyllie, 1949).

If, on the other hand, the rock or soil does possess

ion-restricting membrane properties, then the solute

concentration gradient may result in a positive polarity in

the direction of diffusion due to the tendency for the
membrane to pass cations (Shainberg and Kemper, 1972). Here,
the literature differs as to terminology; the borehole
literature goes no further and calls this differential
diffusion process the membrane potential (Schlumberger,
1972). In the soils literature, Hanshaw (1962) describes the
membrane potential in the context of the Nernst potential,
which is derived in Hanshaw for differential phase boundary
potentials that arise due to the cation concentration
difference between the diffuse layers and the external
solutions. Shainberg and Kemper (1972) combine the two
processes and say the membrane potential consists of the
"diffusion potential difference caused by the differential
diffusion of ions within the membrane, and two phase
boundary potential differences".

Most authors agree, however, that the "membrane
potential" arises due to a solute concentration gradient
across a charged membrane, and that the relative sense of
the potential is positive in the direction of the diffusion
tendency.

Subsurface Occurrences of Coupled Flow Phenomena

Researchers have speculated that chemico-osmosis is

responsible for anomalous pore fluid pressures in subsurface formations. Marine (1974) and Marine and Fritz (1981) presented evidence suggesting that the Dunbarton Triassic Basin in South Carolina is approximately 10% overpressured with respect to hydrostatic as a result of the chemico-osmotic process. They indicate that hydraulic flow is not significant because the basin is isolated, and that the tendency for chemico-osmotic flow from an overlying fresher water aquifer to the more saline Triassic sediments has caused the overpressured condition. The geologic membranes required for chemico-osmosis are provided by shale lenses within the Triassic sediments. Berry (1959) and Berry and Hanshaw (1960) also identify cases of abnormal fluid pressures they think have resulted from chemico-osmosis.

The relative importance of non-hydraulic causes of pore fluid movement might be expected to be greater for deep confining beds where hydraulic conductivity is low. There, traditional analysis of groundwater flow, using Darcy's law as the predicate, may not accurately describe either the direction or the magnitude of flow. This point is exemplified by Olsen (1972), who has considered the hypothetical case of a compacted clay bed separating aquifers containing waters of different salinities. The model is based on his experimental data for kaolinite, and

suggests that flow across the clay bed could realistically be opposite to the hydraulic gradient. Though this is difficult to prove in-situ, his assumptions represent conditions that are not rare in the subsurface.

In areas where hydraulic flow does dominate, the ion-restricting properties of clay membranes could influence the geochemistry of formation waters. Bredehoeft et al. (1968) and Graf (1982) suggest reverse-osmosis, or hyperfiltration, as a mechanism for concentrating brines in the subsurface. These authors argue that hydraulic flow through geologic membranes in a direction opposite to chemico-osmosis tends to concentrate formation waters on the higher pressure side because ionic species are restricted from passing. Kharaka and Berry (1973) provide experimental work that qualifies the relative retardation of certain ionic species common to formation waters.

Natural electric potentials can occur in boreholes where the borehole is filled with a conductive fluid. "Spontaneous potentials", as they are called, can be streaming potentials, liquid junction potentials, membrane potentials, or combinations of these. The streaming potential occurs when there is hydraulic flow through the

clay mudcake[1] from the borehole into the adjacent formation
due to a greater hydraulic pressure in the borehole
(overbalanced condition). The liquid junction potential may
be present when there is diffusion of ions between the
borehole fluid and a permeable formation.

Most borehole log analysts believe that membrane
potentials dominate spontaneous potential measurements, and
usually occur at interfaces between clay rich rocks (shales)
and permeable non-clay lithology (sandstone, fractured coal
or limestone, etc.), where there is a salinity difference
between the borehole fluid and the formation fluid. Mounce
and Rust (1944) presented early experimental evidence that a
current will flow in a circuit formed by saline water, fresh
water, and a shale (Figure 2.6). They did not know at that
time the mechanism which caused the current, but
consideration of subsequent work on the membrane properties
of clays indicates they had indeed been early observers of
the charged membrane phenomena of shales.

Closer inspection of borehole potentials measured at
the interface of permeable and non-permeable formations

---

[1] "Mudcake" is a layer of clay solids formed on the borehole
wall due to the separation of solids and fluid during the
flow of the fluid phase from the borehole into the formation.

T-3678
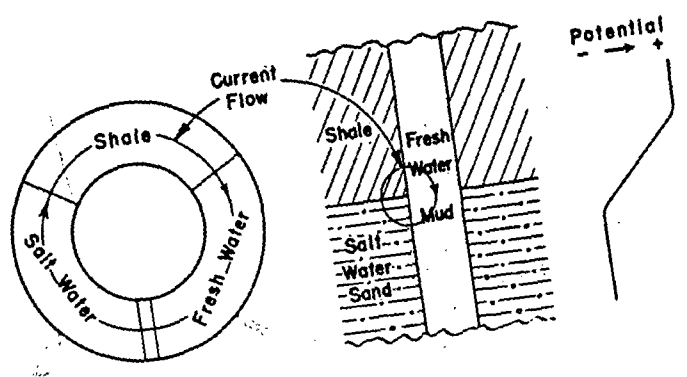
FIGURE 2.6: Current flow at a shale/salt water sandstone interface (Mounce and Rust, 1944).

reveals that they must consist of both membrane phenomena
and the liquid junction process if they are to produce a
current. An electric current that is sustained in an aqueous
solution (or saturated porous media) does so only through
charge separation. Individually, the membrane and liquid
junction potentials do not cause charge separation;
conversely, they insure by their presence that charges
(cations and anions) do not separate. Working together
however, they can produce a current whose driving force is
the differential diffusion of ions (Figure 2.7).

Continuing the general discussion of subsurface
occurrences of coupled flow phenomena, the final topic is
thermo-osmosis, which is generally thought to be of little
importance in subsurface saturated media. This is due mainly
to the premise that laboratory measurements, while
confirming the occurrence of thermo-osmosis, have been made
under conditions of unrealistically high thermal gradients.
For example, Dirksen (1969) found that a gradient of 1C/cm
across compacted kaolinite caused about half as much flow as
a hydraulic gradient of 1 cm/cm across the same sample.
Natural geothermal gradients generally range from .0002C/cm
as a global average to .0012C/cm in geothermal areas.
The latter figure is some 800 times smaller than the thermal
gradient employed by Dirksen.
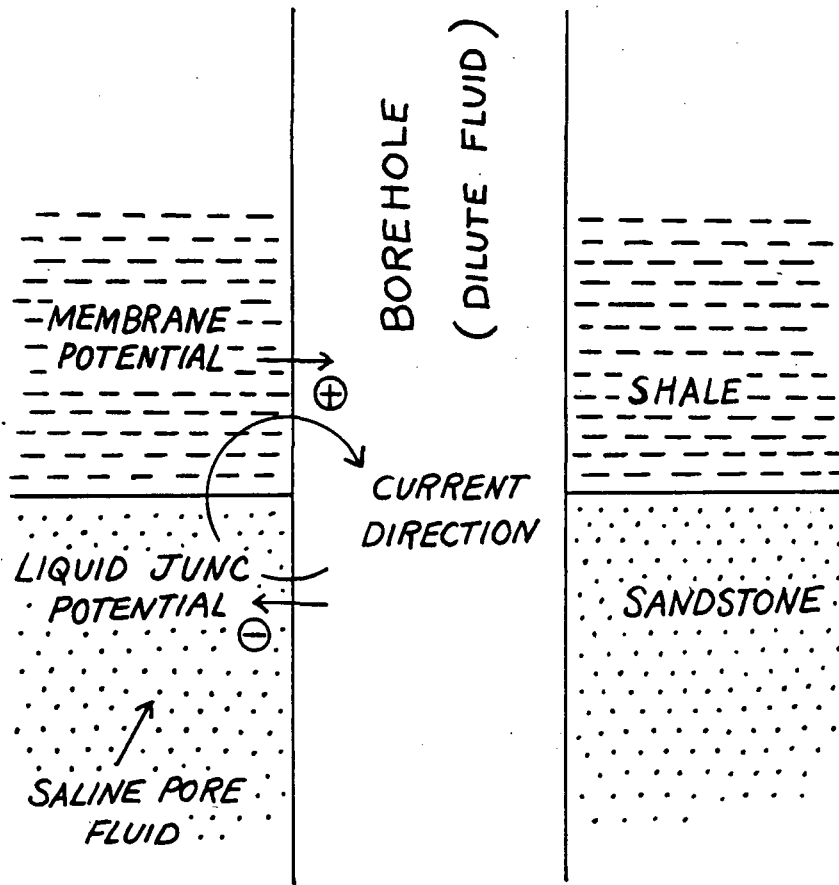
FIGURE 2.7: A close look at current flow in a borehole. An electric current is only sustained by the simultaneous differential diffusion of anions (liquid junction potential) and cations (membrane potential).

However, hydraulic gradients of 1 cm/cm are rare: .01
cm/cm is more common. Therefore, a fair comparison of
Dirksen's data for a geothermal area indicates that thermo-
osmosis may cause about one sixteenth[*] the flow that a
hydraulic gradient of .01 cm/cm causes (in compacted
kaolinite). This does not particularly shed light on the
relative importance of thermo-osmosis, and no thermo-osmotic
research has ever been conducted for in-situ geothermal
conditions (this thesis will not amend this omission, since
its experiments have not been conducted at in-situ
temperatures).

Nevertheless, thermo-osmosis could be of some
consequence in geothermal areas. As discussed in the thesis
introduction, Rex (1985) and Michels (1988) have suggested
that both chemico-osmosis and thermo-osmosis may have played
an important role in the geochemical and hydrological
evolution of the Salton Sea Geothermal System.

* If q (flow) from 1C/cm = 1/2 q from 1cm/cm, then
  q from .0012C/cm = 1/16 q from .01 cm/cm

CHAPTER III

EXPERIMENTAL PROCEDURE AND SAMPLE DESCRIPTION

The Experimental System

Experimental measurement of the transport properties of interest requires the application of known thermal, electrical, and chemical concentration gradients across a confined, saturated core sample under in-situ effective stress. Required also is the capability to measure the hydraulic pressure and electrical potential differentials between the ends of the sample during zero flow or known flow rate conditions. The imposed gradients and observed responses must be known simultaneously in order to derive the transport properties of interest and investigate coupled flow phenomena.

The essential components of the experimental system used in this thesis that achieve the above are listed as follows:

(1) Hydraulic press to provide simulated overburden stress (capable to 10,000 psi).

(2) The test cell which includes the sample, compression pistons, and instrument packages (the test cell is shown in figure 3.2 and explained in more detail in the following section).

(3) A flow pump to control the imposed flow rates ranging from 10^{-1} to 10^{-5} cm^3/sec (Harvard Model 912 dual syringe infusion-withdrawal pump).

(4) Pore pressure control provided by Bellofram cylinders (Bellofram is a trademark name of Bellofram Corp.; manufacturer of the rolling seal diaphragm type pressure regulator).

(5) Differential pressure transducers accurate to 1.0 mm H_2O (Validyne variable reluctance Model P300D). Operated with Validyne power and signal conditioner Model MC1 and Soltec Model 1243 strip chart recorder.

(6) Constant current source to impose external currents across the sample (Keithley Model 224).

(7) High impedance voltmeter accurate to 0.1 millivolt to measure electric potentials across sample (Orion Model 901).

(8) Power supply for heater (Hewlett Packard Model 6215A).

(9) Multimeter for various uses including measurement of thermistor resistance (Fluke Model 27).

(10) Pore fluid reservoirs (9 liter glass carboys) that contain different concentrations of the simulated pore fluid.

(11) Pore fluid manifold system that interconnects pore fluid reservoirs, flow pump, belloframs, and test cell.

Figure 3.1 shows most of these components as they are assembled in the laboratory. The manifold is shown in the center of the picture, the hydraulic press with test cell on the right, the dual flow pump in the left foreground, and voltmeter and current source in the center background.

The test cell:

A schematic cut-away of the test cell is shown in Figure 3.2. It consists of the instrument packages above and below the sample, and compression pistons in which the instrument packages are housed. The sample is epoxied within the sample holder (A) which is constructed of mycarta, a high strength material that is both a thermal and electrical insulator, and is impermeable. The sample holder and pistons fit inside a mycarta sleeve (B). O-rings (C) seal the sample
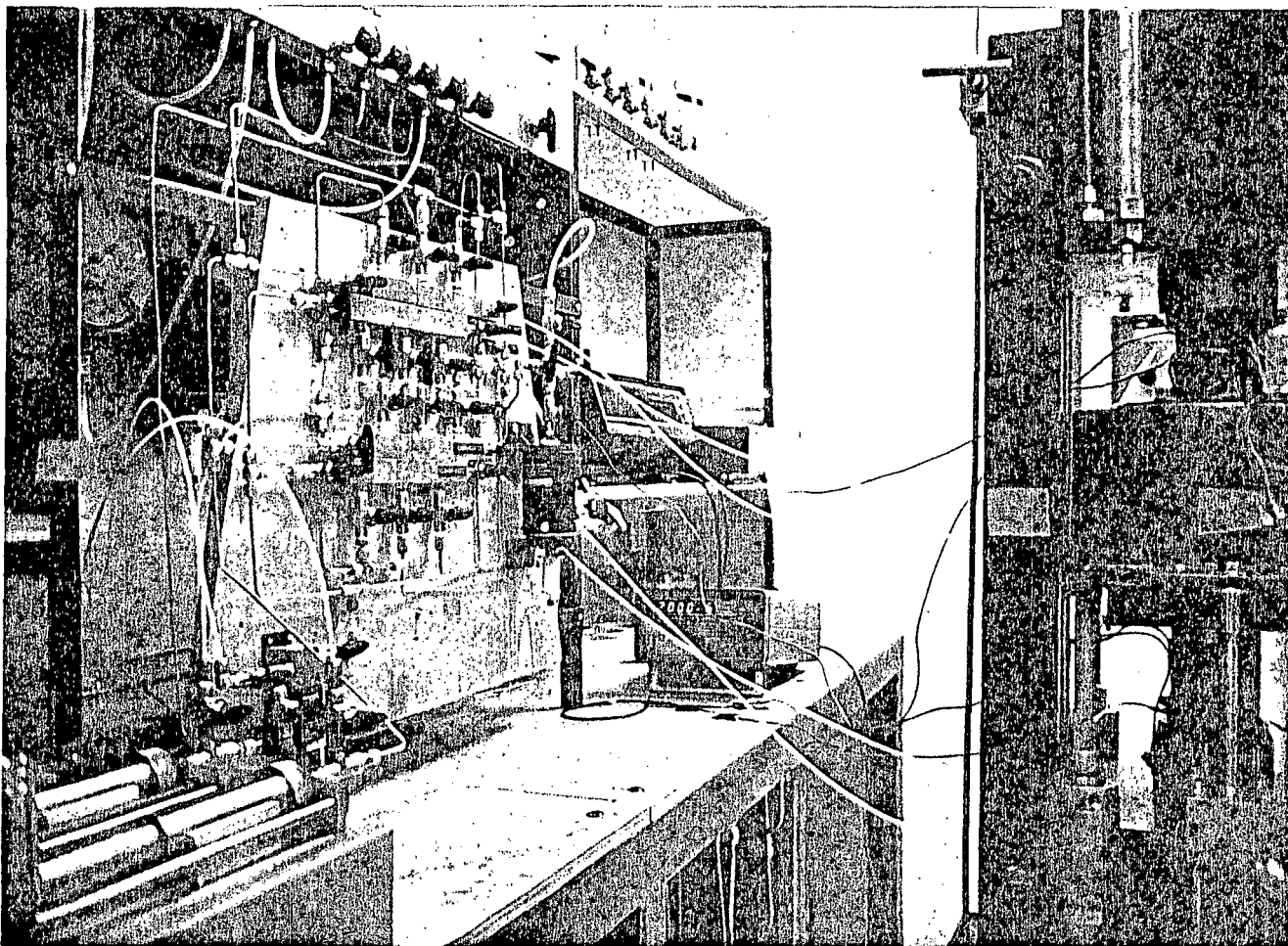
FIGURE 3.1: Photograph of assembled laboratory apparatus.
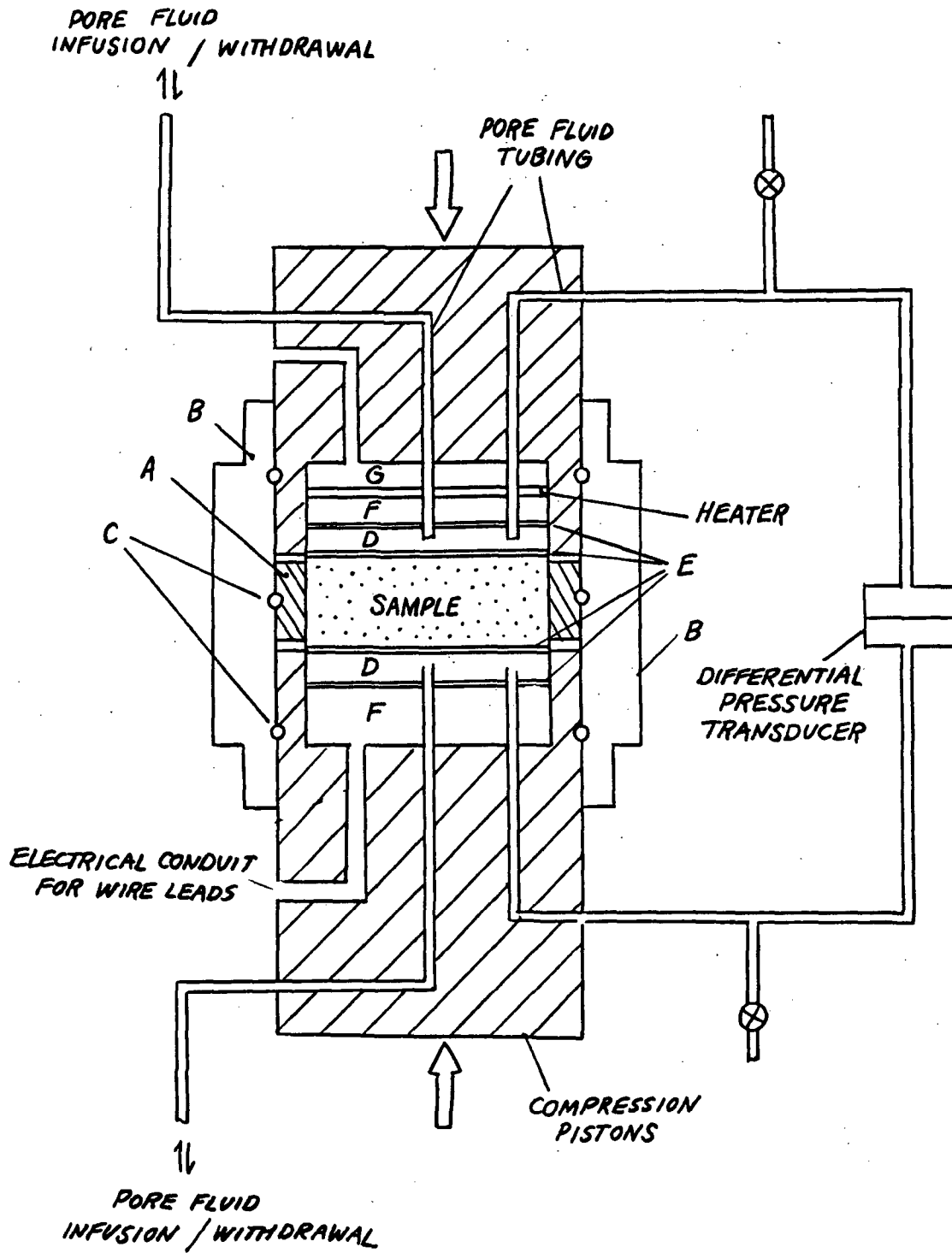
FIGURE 3.2: Schematic cut-away of test cell. See text for explanation of letters.

from the outside environment, and prevent short circuit
hydraulic flow between the sample holder and sleeve. The
pistons, with instrument packages intact, can slide in or
out of the mycarta sleeve to allow the placement of new
samples.

The instrument packages contain the following:
Porous stones (D) that are in contact with each end of the
sample for the purpose of providing uniform infusion and
withdrawal of the pore fluid. The pore fluid is brought to
the porous stones through tubing that extends from the
manifold through the pistons and instrument packages to the
porous stones. There are two tubing ports in each porous
stone to facilitate the circulation of pore fluid through
the stone, and enable static pressure measurements through
one port while the other is flowing. The flow rate to and
from the ends of the sample is controlled by the dual flow
pump.

Reversible silver-silver chloride electrodes (E) are
placed on both sides of the porous stones so that an
electrical potential can be measured across the sample as a
response to externally imposed currents, flow rates, or
differences in the pore fluid chemistry in contact with
opposite ends of the sample. Figure 3.3 depicts the four-
electrode arrangement in which the inside pair measure the
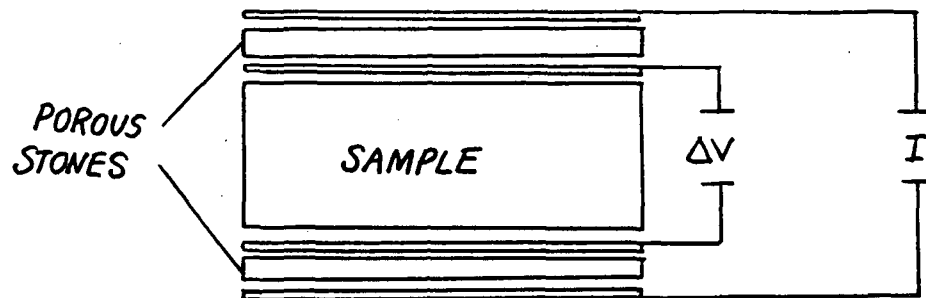
FIGURE 3.3: Four-electrode arrangement. I is electric current and ΔV is the measured voltage potential.

potential across the sample, and the outside pair serve the purpose of the current source. Details concerning electrode construction and asymmetry testing are provided in Appendix B.

A heater constructed of high resistance wire wrapped serpentine fashion inside a circular plastic frame is located in the top instrument package and provides the thermal source for the temperature gradient. The heater assembly is embedded in a thermally conductive epoxy (F), which electrically and hydraulically insulates the heater wire from fluid in the porous stone. A second layer of epoxy (G) above the heater is a thermal insulator to cut down on heat loss in the axial direction.

Thermistors are fixed within the porous stones on both ends of the sample. Wire leads from the thermistors, electrodes, and heater are insulated and diverted through conduits within the pistons to the outside where they are connected to their respective devices.

Measurements, Calibrations, Errors

The following discussions explain the test procedures for the measurement of coupled processes and direct transport data in the sequence they were executed.

The test cell, which includes the prepared sample, was placed in the hydraulic press, and the pore fluid tubing lines connected to the manifold. The voltmeter and current source wires were connected. The sample was evacuated through the base while de-aired pore fluid was allowed to enter in the top. The initial pore fluid was either distilled water or a dilute solution.

The sample was slowly loaded by the hydraulic press (axial loading) while pore pressure was applied to the fluid in the sample, such that the final resultant stress was the in-situ effective stress. The dual flow pump was used to circulate de-aired fluid through the base and top stones. After 5-7 days of circulation and exposure to 60 psi back pressure (from the belloframs), the sample was assumed to be saturated with de-aired fluid.

Hydraulic conductivity tests could then be performed at any time as per the following: A known flow rate (controlled by the dual flow pump) was caused to flow through the sample, and the hydraulic pressure difference between the top and base of the sample was detected by the differential pressure transducer and recorded on the strip chart.

Valid hydraulic flow tests were confirmed by plotting the imposed flow rate versus the resulting head difference for several different flow rates and checking for linearity,

as prescribed by Darcy's law. Figure 3.4 is an example of typical hydraulic conductivity data. As an analogy with Ohm's law and electrical resistance, the slope of the line that connects the linear trend is the hydraulic conductance of the sample. The hydraulic conductivity of the rock is derived by considering the dimensions of the sample as follows:

$$K_h = C_h \text{ X } L/A \qquad\qquad (3.1)$$

for: K_h = hydraulic conductivity

 C_h = hydraulic conductance (6.5×10^{-4}, from Figure 3.4)

 L = sample length (2.2 cm)

 A = sample cross-sectional area (32 cm^2)

Thus, for the data presented in Figure 3.4:

$$K_h = [(6.5 \text{ X } 10^{-4} \text{ cm}^2/\text{s}) \text{ X } (2.2 \text{ cm})] / (32 \text{ cm}^2) = 4.5 \text{ X } 10^{-5} \text{ cm/s}$$
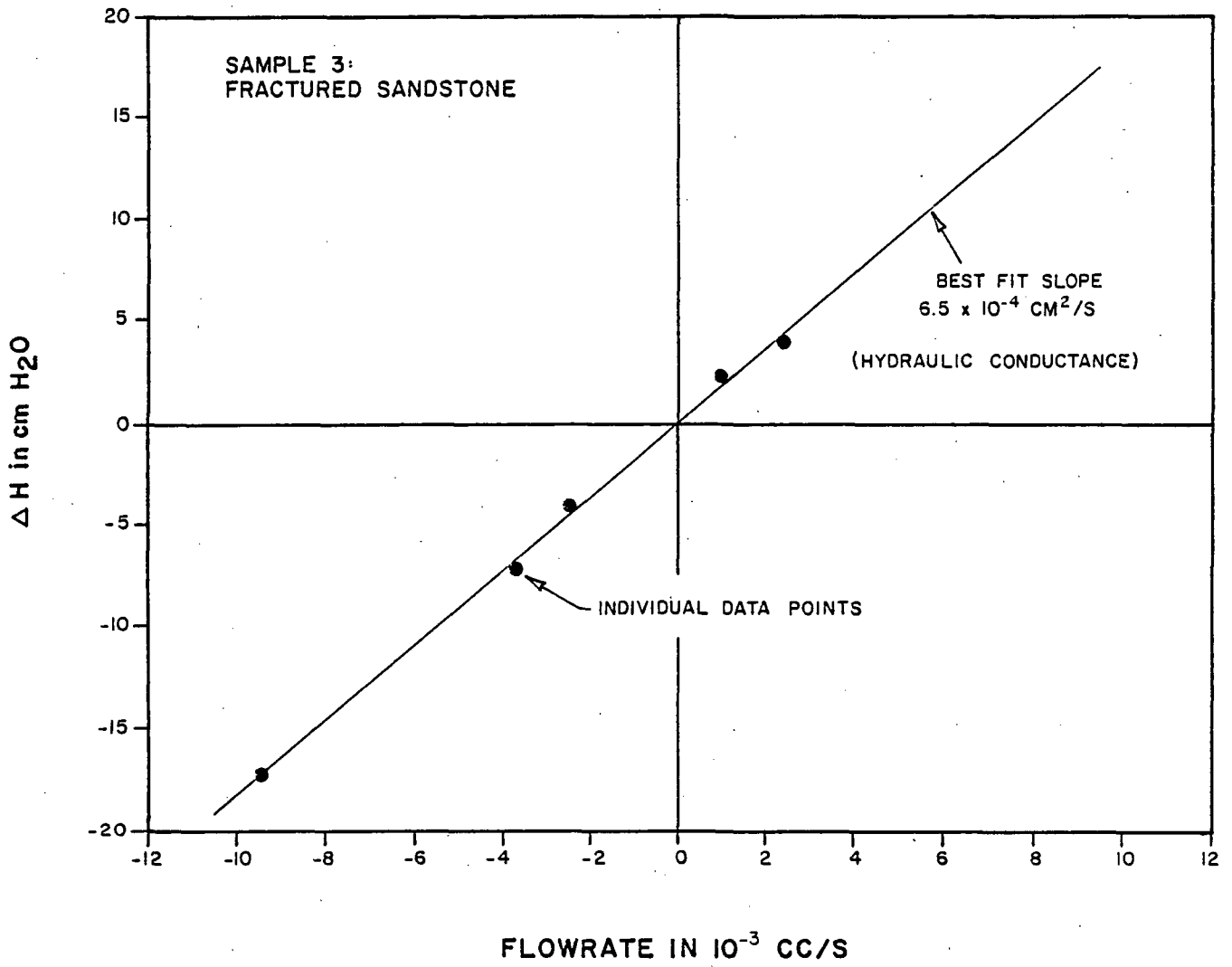
FIGURE 3.4: Typical hydraulic conductivity data.

The flow pump was also used to circulate pore fluids of differing solute concentrations into either the top or base porous stone in order to provide solute concentration gradients. Continuous hydraulic and electric responses to the imposed concentration difference between the ends of the sample were recorded on the strip chart. During this circulation phase no flow is allowed through the sample. This is achieved by closing the valve to the dynamic line on the end not being circulated (Figure 3.5). For this condition, the direction for the tendency for flow is indicated by the side with the higher pressure.

This is an extremely reliable and accurate method for detecting the tendency for fluid transport within the sample. Care must be taken, however, to establish and monitor a zero baseline for a manifold short circuit configuration (valves open both to top and base imposes equal hydraulic potential on the top and base, and therefore zero ΔH condition across the sample).

Establishing the manifold short circuit baseline is particularly critical with highly concentrated brines in the system because density gradients can and do form within the manifold. This condition is recognized by a non-zero short circuit reading, and can be accounted for by deducting the manifold short circuit value from the reading obtained when
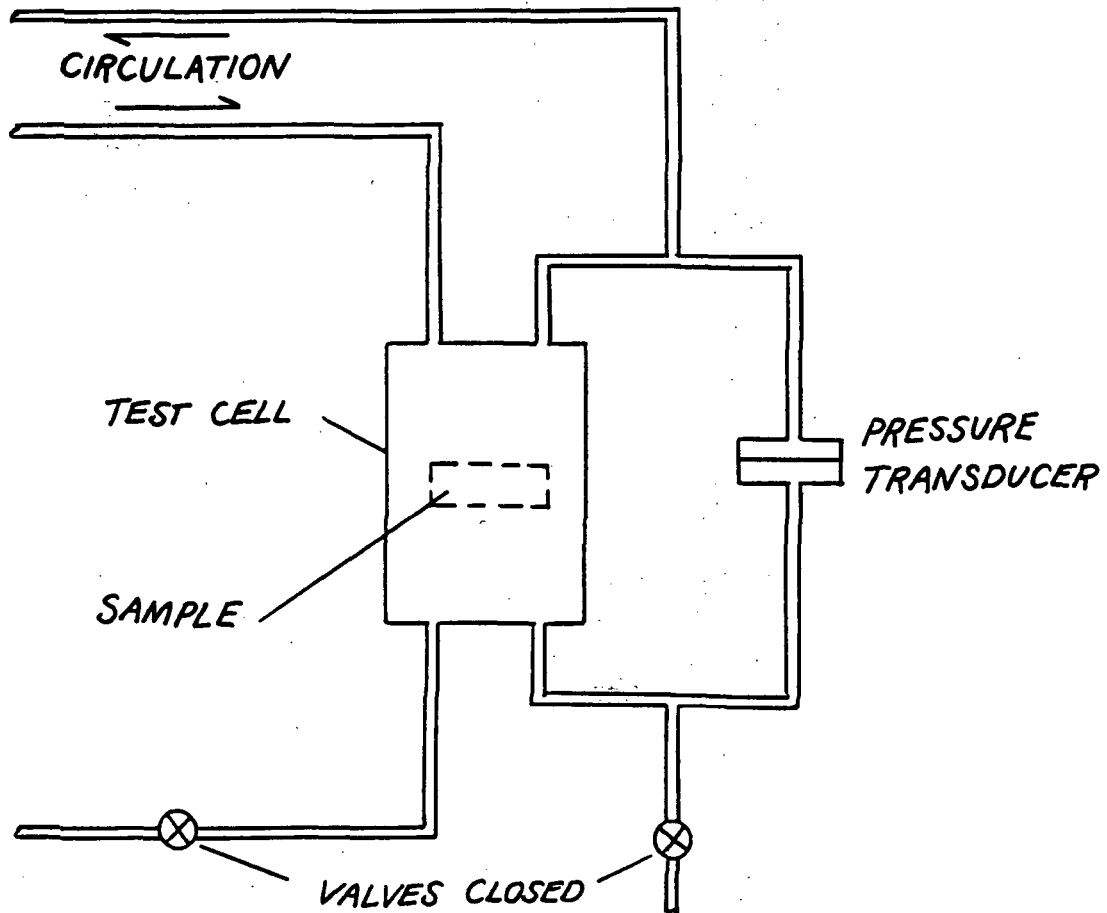
FIGURE 3.5: Configuration for zero flow through sample during circulation of pore fluid (shown here is circulation to top porous stone). Tubing lines to pressure transducer are dead-ended. No flow is permitted through the sample because the valve to the base porous stone is closed.

the manifold is configured to read $\triangle H$.

However, since the density gradients are not constant, and manifold short circuit and $\triangle H$ readings cannot be obtained simultaneously, some unknown error is present. Experience has indicated that this error is on the order of 20%; e.g., for a manifold short circuit reading of -0.4 cm, and a $\triangle H$ response of +0.2 cm, the estimated real hydraulic response is +0.6 cm plus or minus about 0.1 cm.

Calibration of the transducer itself is achieved with a column of water (35 cm at full scale). This method is very accurate, and readings are reproducible to within 5%.

Following the concentration gradient tests described above, the sample was saturated with the simulated in-situ pore fluid concentration (20 or 25 wt % TDS). This step requires flowing approximately 10 pore volumes of this pore fluid through the sample. During this flow period hydraulic and electric responses were recorded to provide information on hydraulic conductivity and streaming potential.

After the sample was saturated with the simulated in-situ pore fluid, external currents were imposed across the sample while both hydraulic and electric responses were recorded. A hydraulic response for the zero flow condition during an imposed current would be an indication of electro-osmosis. The electric potential response is a measure of the

electrical resistivity for the sample.

With regard to electrical resistivity, valid electrical data were confirmed by plotting the imposed current versus the resulting potential for several tests and checking for linearity, as prescribed by Ohm's law (an identical concept to that for hydraulic data). Figure 3.6 is an example of typical resistivity data. The slope of the line that connects the linear trend is the electrical resistance of the sample. The electrical resistivity of the rock (saturated with some particular pore fluid) is derived by considering the dimensions of the sample as follows:

$$R_o = R \ X \ A/L \qquad\qquad (3.2)$$

for: R_o = electrical resistivity

   R = electrical resistance (42 ohms, from Figure 3.6)

   A = sample cross-sectional area ($32 \ X \ 10^{-4} \ m^2$)

   L = sample length (.022 m)

Thus, for the data presented in Figure 3.6:

R_o = (42 ohms $X \ 32 \ X \ 10^{-4} \ m^2$) / .022 m = 6.1 ohm-m
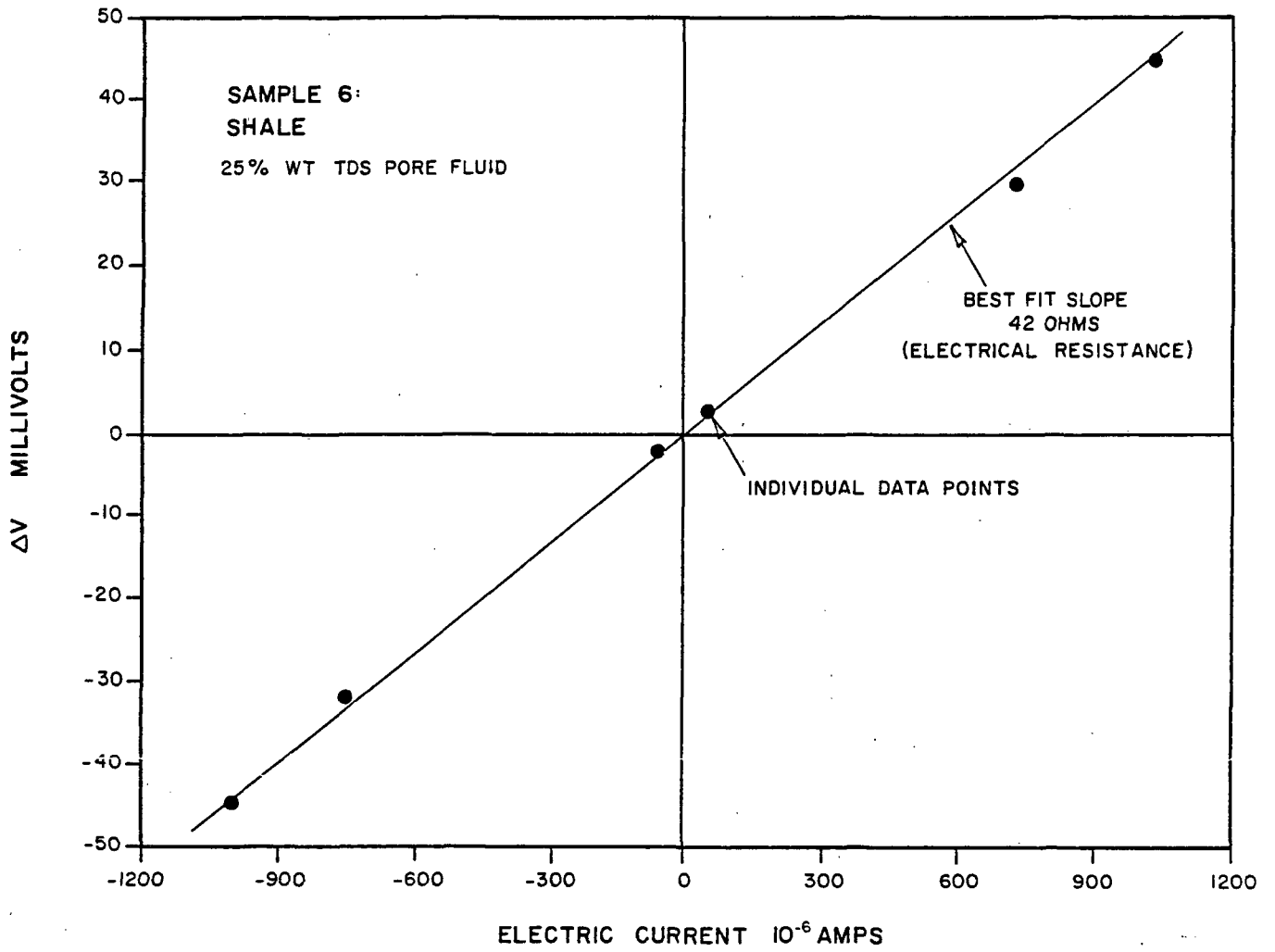
FIGURE 3.6: Typical electrical resistivity data.

The thermal tests were conducted last (while the sample was still saturated with the 20 or 25 wt % TDS pore fluid). The heater and thermistor wires were connected and power applied to the heater leads, which in turn produced a heat flux sourced from the heater embedded in the top instrument package. All valves were initially open in a manifold short circuit configuration until the heat flux reaches steady state. This is required to neutralize any effect due to thermal expansion of the water during transient heating.

After steady state was achieved, a zero flow condition is imposed and the hydraulic response recorded. For this zero flow condition, a hydraulic response due to the temperature gradient would be an indication of thermo-osmosis.

The steady state temperature difference between the ends of the sample is used to calculate thermal conductivity, which is derived according to Fourier's law. The temperature difference was approximately known by a formula that relates thermistor resistance difference to temperature difference, given by the manufacturer (Fenwal Electronics) as:

$$dT = dR/(\alpha R) \tag{3.3}$$

where:

dT = temperature difference between ends of the sample

R = average of top and bottom thermistor resistances

α = thermistor temperature coefficient (change in temperature with respect to resistance)

dR = net resistance difference between top and bottom thermistors:

$$dR = dR_t - \text{zero offset}$$

and: zero offset = constant resistance difference when no temperature difference exists (calibrated before thermistors are built into test cell and monitored thereafter)

dR_t = total measured resistance difference between ends of the sample (during steady state heat flow)

The heat flux through the sample is estimated by correcting the applied power for heat loss. For this purpose, a heat transfer ratio (HTR) has been calculated by calibrating for heat flux through an epoxy sample of known thermal conductivity. Calculation of the HTR is given in Appendix C.

Thus, the thermal conductivity can be calculated:

$$K_t = qL/AdT \qquad\qquad (3.4)$$

where: K_t = thermal conductivity

q = actual heat flux through sample:

q = applied power X HTR

L = sample length

A = sample cross-sectional area

In these experiments, generally only one thermal conductivity data set per sample was acquired, so that the confidence in these results is not as good as that for the hydraulic conductivity and electrical resistivity results. However, the reproducibility of thermal conductivity results is approximately confirmed by the two data sets taken for samples 4 and 6 (see Table 4.6).

Nevertheless, error in the thermal conductivity results might be substantial. Sources of error include:

1. Validity and accuracy of equation (3.3). (The manufacturer suggests that dT is good to 10%.)
2. Thermistors are not in contact with the sample, but actually measure the temperature of the pore fluid approximately 1/16" from the sample surface. This error could be large but should cancel when considering the influence of the HTR on the final calculation (see Appendix C).
3. The thermal conductivity of the epoxy sample used in the calculation of the HTR is not precisely known, but is estimated to within 10% (manufacturer suggestion).

The uncertainty in thermal conductivity varies with the temperature difference (dT), and is greatest for the smallest dT (see Table 4.6 and Appendix C).

The uncertainties in the hydraulic conductivity and electrical resistivity results derive from transducer and voltmeter calibration, the precision with which the sample dimensions are known, and averaging of the response over time. This last point addresses the fact that both the hydraulic and electrical data are recorded on a strip chart, and the recorded response is not necessarily a straight line, but may have some slope (electric data) or cyclic nature (hydraulic data). In the case of the hydraulic data, the cycle amplitude is typically less than 5% of the recorded response. The slope in the electric response can be ignored if the <u>change</u> in potential at the initial current on and final current off time steps are equal (which was always the case).

The effect of calibration drift and error in sample dimensions were also found to be minor, since calibrations were checked between samples and dimension measurements are known to within 5%.

Therefore, it can be stated that the uncertainties in the hydraulic conductivity and electrical resistivity

results are negligible compared to the significance of exact

values; i.e., it is not meaningful to know exact values. For

example, these measurements represent very small samples

from a large domain, and the data they provide are parametric

rather than existential in nature.

Error in the measurement of coupled flow phenomena is

difficult to assess. With regard to the hydraulic

measurements, the problem with density gradients in the

manifold has already been cited. Also, electrical activity

cannot neatly be separated into its potentially numerous

causes. Though great care was taken in the preparation of

the electrodes and to insulate the sample from extraneous

electrical influence, unexplained electrical activity was

observed. The calculation of uncertainties for coupled flow

phenomena is beyond the scope of this thesis.

Field Conditions vs. Laboratory Conditions

A goal of this study was to reproduce field conditions

in the laboratory. Experimentation on actual cores under in-

situ stress saturated with simulated pore fluid achieved a

large measure of this goal. However, high subsurface

temperatures (+300C) were not reproduced in the laboratory.

Direct conduction properties can be fairly well corrected for temperature, but extrapolating coupled flow data is a highly speculative exercise.

Table 3.1 presents the field conditions and the corresponding laboratory conditions for six key parameters.

TABLE 3.1

Field Conditions and Relationship to Laboratory Conditions

Parameter	Field Conditions	Laboratory Conditions
Lithology	Altered sedimentary	Actual cores
Salinity[1] gradient	Max. 10 ppm/cm (at 3000-3500')	Typical 50,000 ppm/cm (min. 5000 ppm/cm)
Pore fluid chemistry	20-25 wt % TDS: primarily NaCl, $CaCl_2$, and KCl	From 1.0 to 25 wt % TDS: NaCl, $CaCl_2$, and KCl
Thermal gradient	Max. .002C	Typical 0.5C/cm
Temperature	250-350C	20C
Flow rate	?	Typical 10^{-4} cm^3/sec

1 Gradient concentrations are in parts per million (ppm). Pore fluid concentrations are given in weight percent total dissolved solids (TDS). [ppm = wt % TDS X 10^4].

The maximum field salinity gradient in Table 3.1 is estimated from Figure 3.6., and field temperature information is from Sass et al. (1988).

Laboratory pore fluid composition was simulated from a geochemical analysis of produced formation water from 6000', which is given in Table 3.2. (In-situ pore fluid concentrations are discussed in Chapter I.)

TABLE 3.2

Pore Fluid Composition[1]

Potassium (K)	6.7%
Calcium (Ca)	10.6%
Sodium (Na)	20.7%
Chloride (Cl)	59.8%
Total	97.8%*

* Other species present in the analysis but not included in simulated pore fluid make up 2.2% of the total and include (in decreasing concentration): iron, manganese, zinc, silica, strontium, boron, barium, lithium, lead, and others.

1 Geochemical analysis provided by Don Michels (personal communication, 1988).

Actual field concentration gradients are too small to simulate at laboratory scale, where experiments are conducted on samples 7/8 to 1" in length, rather than hundreds of feet of geologic section. Likewise, laboratory thermal gradients are necessarily much larger than actual field thermal gradients. Still, this experimental work will provide qualitative indications of coupled processes and the lithologic controls on those processes.

Finally, simulation of effective stress is straight forward. Effective stress is defined as the difference between overburden stress and pore pressure, and represents the stress supported by the rock matrix. In the case of the SSSDP, these quantities are fairly well known. Overburden stress is estimated by knowledge of the sediment density, known from regional gravity surveys (Elders et al., 1972). Pore pressure is known from drilling and well test data, as interpreted by the writer.

Sample Description

Sample preparation:

Undisturbed 4" and 5" diameter cores received from the University of California (Riverside) were re-cored in our

lab to a uniform 2.45" diameter to fit inside the pre-
designed sample holders. Extreme care was taken to keep the
portion to be tested intact and undisturbed. These reduced
size cores were centered within the 2.65" inside diameter
sample holders to allow a 0.1" annulus to be filled with
epoxy. This epoxy procedure assured that no hydraulic short
circuit occurred between the sample and sample holder.

Once epoxied, the sample was trimmed to approximately
1" in length with a diamond cut off saw. Surface planing
refined the length and achieved smooth, even surfaces. It
was desirable for the sample length to be slightly greater
than that of the sample holder. This allowed the sample to
receive full compression from the pistons. Figure 3.7 shows
this relationship and the nominal dimensions of the prepared
samples.

Physical description of samples:

Rock encountered below 2500' in the SSSDP borehole is
thermally altered, highly consolidated, and often fractured.
Though there is a great deal of variability due to both
depositional facies and state of alteration (Mehegan et al.,
1986), the rock is generally represented by the six samples
chosen for testing in this thesis.

Sample depths range from 3113' to 8591'; and include
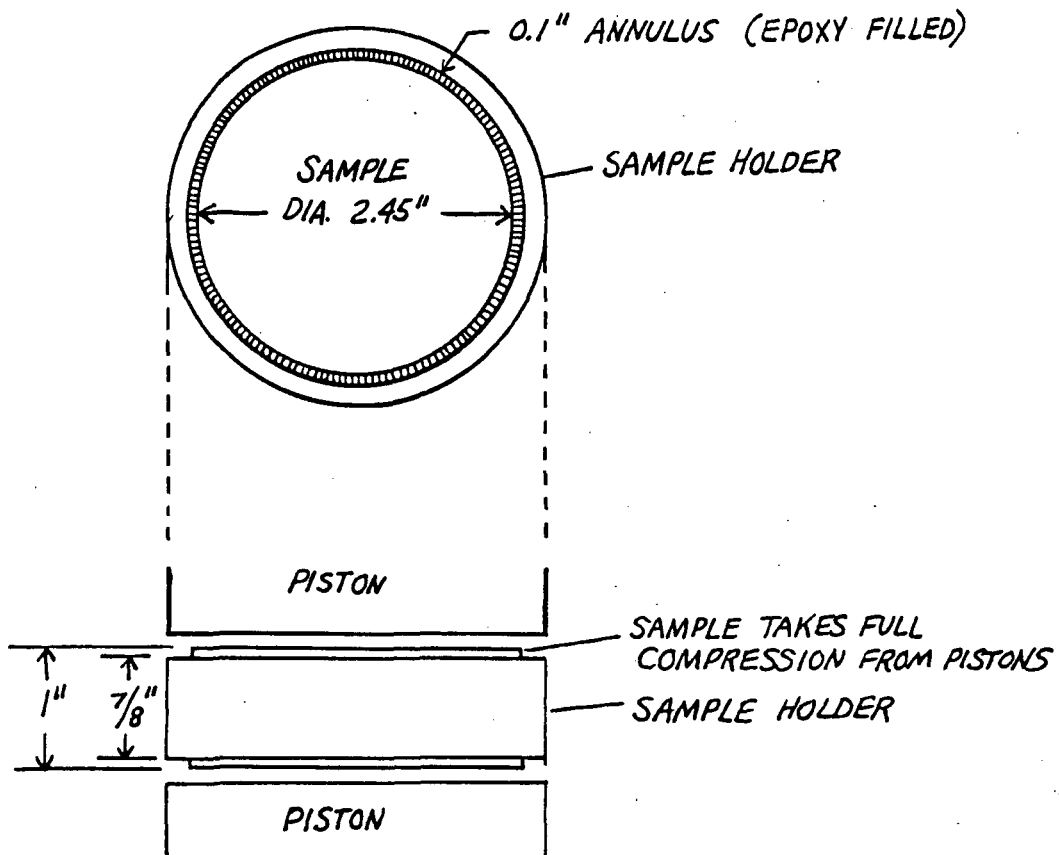
FIGURE 3.7: Sample dimensions. Note that the pistons contact the sample, rather than the sample holder. Thus the sample receives the full axial load from the pistons.

two shales, two siltstones; and two sandstones (grain size classification). Also, since most core recovered from the borehole was naturally fractured, these samples reflected this: four of the six samples tested had fractures. Furthermore, it was assumed in these experimentments that tests conducted under in-situ confining stress simulated actual subsurface fracture conditions.

A physical description of each sample is provided in Table 3.3. Following that is Table 3.4, which lists the estimated porosities of the samples from two methods: (a) laboratory estimates from water content calculations, and (b) geophysical log-derived estimates.

TABLE 3.3

Physical Description of Samples

Sample	Depth	Description
1	3808'	Light gray shalely siltstone. Chlorite imparts a slight greenish cast. No apparent fractures.
2	3808'	Same as sample 1 except subtle vertical to sub-vertical fractures are apparent.
3	3113'	Gray-green silty sandstone. Scattered pyrite and calcite. Obvious vertical to sub-vertical fractures.
4	8156'	Dark gray-green shale. Scattered pyrite and epidote. Anhydrite porphyroblasts. Obvious vertical to sub-vertical fractures.

TABLE 3.3 Continued:

Sample	Depth	Description
5	8591'	Light green sandstone. Abundant epidote. Obvious vertical to sub-vertical fractures.
6	6037'	Light gray-green silty shale. Greenish cast due to chlorite evident. Finely scattered epidote and pyrite. No apparent fractures.

TABLE 3.4

Estimated Porosities

Sample	Laboratory Porosity	Geophysical Log-derived Porosity
1	.06	.09
2	.06	.09
3	.20	.23
4	.03	N.M.*
5	.07	N.M.
6	.03	.02

* Not Measured (data not available from geophysical logs).

Laboratory porosities were estimated from the following

equations:

$$e = W \times G \qquad\qquad (3.5)$$

and, $\qquad\qquad n = e/1+e \qquad\qquad (3.6)$

For n = water filled porosity

   e = void ratio

   W = water content when saturated

   G = Grain density

Water content is known from the ratio the weight of

water to the weight of solids (corrected for original salt

content):

$$W = weight\ of\ water\ /\ weight\ of\ solids$$

The average grain density for all of the samples is

estimated at approximately 2.70 g/cm^3. This value assumes

that the rock is made up primarily of quartz or clay

minerals with minor amounts of hydrothermal minerals. Grain

densities for the predominant minerals in these samples is

given in Table 3.5.

TABLE 3.5

Grain Densities for the Predominant Minerals

Mineral	Density (g/cc)
Quartz	2.65
Clays	2.60 to 2.96
Anhydrite	2.96
Epidote	3.3 to 3.5
Sphalerite	3.9 to 4.2
Pyrite	5.0 to 5.2
Calcite	2.71

Geophysical log-derived porosities were estimated from the following equation:

$$n = (P_m - P_b)/(P_m - P_f) \qquad (3.7)$$

For: n = water filled porosity

P_m = grain density (assumed to be 2.7 g/cm^3 average)

P_b = bulk density (measured in the borehole with gamma-gamma density device*)

P_f = fluid density (1.0 g/cm^3)

* The gamma-gamma geophysical logs are measured by Schlumberger and made available by U.S.G.S. All log interpretation is done by the writer.

CHAPTER IV

DISCUSSION OF RESULTS

COUPLED FLOW DATA

Coupled flow data will be divided into four groups for purposes of presentation and discussion: (1) hydraulic response due to solute concentration gradients, (2) hydraulic response due to electric gradients, (3) hydraulic response due to thermal gradients, and (4) electric response due to solute concentration and hydraulic gradients.

Hydraulic response due to solute concentration gradients

These data will be presented in summary form that includes the sample number, pore fluid concentration, solute concentrations in the base and top porous stones, head difference developed across the sample for the zero-flow condition (with a notation as to whether the top or base is the higher pressure), and the mechanism of coupled flow that is indicated by the direction of the head difference. Table 4.1 lists these data.

TABLE 4.1

Hydraulic Response To Solute Concentration Gradients

Sample No.	Pore fluid conc.[1]	Porous stone conc.		Head Difference (cm H_2O)	Mechanism[2] Indicated
		top	base		
2[*]	D[3]	1.5	D	0.7 T[4]	C-O
2	D	1.5	20.0	0.8 T	D-O
3	D	6.0	D	0.3 B	D-O
3	D	6.0	20.0	0.3 T	D-O
3	20.0	18.0	20.0	0.6 B	C-O
4	2.0	2.0	1.0	0	None
4	2.0	2.0	25.0	0.6 B	C-O
4	25.0	23.0	25.0	0	None
4	25.0	11.3	25.0	0.1 T	D-O
5	1.0	11.3	1.0	0.1 B	D-O
5	11.3	25.0	11.3	1.4 B	D-O
5	25.0	22.5	25.0	0	None
6	D	1.0	D	0	None
6	1.0	11.3	1.0	0.2 T	C-O
6	1.0	25.0	1.0	0.8 T	C-O
6	25.0	11.3	25.0	0.3 T	D-O
6	25.0	1.0	25.0	1.2 T	D-O

* Data from sample 1 is omitted due to measurement problems; however, sample 2 represents the same lithology and depth.

See next page for Table 4.1 footnotes.

Footnotes from Table 4.1:

1 Concentrations given in wt % total dissolved solids (TDS)

2 C-O refers to Chemico-osmosis as dominate process
  D-O refers to Diffusion-osmosis as dominate process

3 D = Distilled water

4 T = flow tendency is toward top of sample
  B = flow tendency is toward base of sample

The data in Table 4.1 show in general that diffusion-osmosis (the tendency for water movement in the direction of solute diffusion) is more likely to occur in the coarser grained samples (see sample description, Table 3.3), or when the sample is saturated with a highly concentrated brine. The noteworthy exception to this is sample 3 (a sandstone), in the case where chemico-osmosis is indicated for the condition where the saturating pore fluid is a 20% brine solution.

The data in Table 1 also show that chemico-osmosis is indicated for the shales (samples 4 and 6) in the cases where the saturating pore fluid is relatively dilute. Sample 6 illustrates the effect that the concentration of the saturating fluid has on the hydraulic response and indicated mechanism of coupled flow. In the cases for sample 6 where the pore fluid is dilute (1%), solute concentration gradients result in chemico-osmosis. However, in the cases

where the pore fluid is concentrated (25%), the same solute concentration gradients result in diffusion-osmosis. These results are consistent with what is known about concentration effects on membrane efficiency, as stated in Table 2.3. It is tempting to speculate at what pore fluid concentration for sample 6 might the processes of chemico-osmosis and diffusion-osmosis be equal but opposite. The data plotted in Figure 4.1 suggest that a pore fluid concentration of approximately 10% wt TDS is the condition for which these processes cancel each other (in sample 6).

Data from sample 5 is anomalous because it is the only sample for which chemico-osmosis is not indicated under any conditions. Sample 5 is noted for the least amount of fine grained material (and presumably the least amount of clay). This suggests that diffusion-osmosis dominates under conditions where clays (and therefore membrane properties) are absent. Sample 5 is also highly fractured, which could facilitate the diffusion process. However, sample 4 is highly fractured as well, but exhibits chemico-osmosis for a dilute saturating fluid.

Clay mineralogy:

The role of clay minerals as membranes in the chemico-osmotic process was established in Chapter II. Here we will
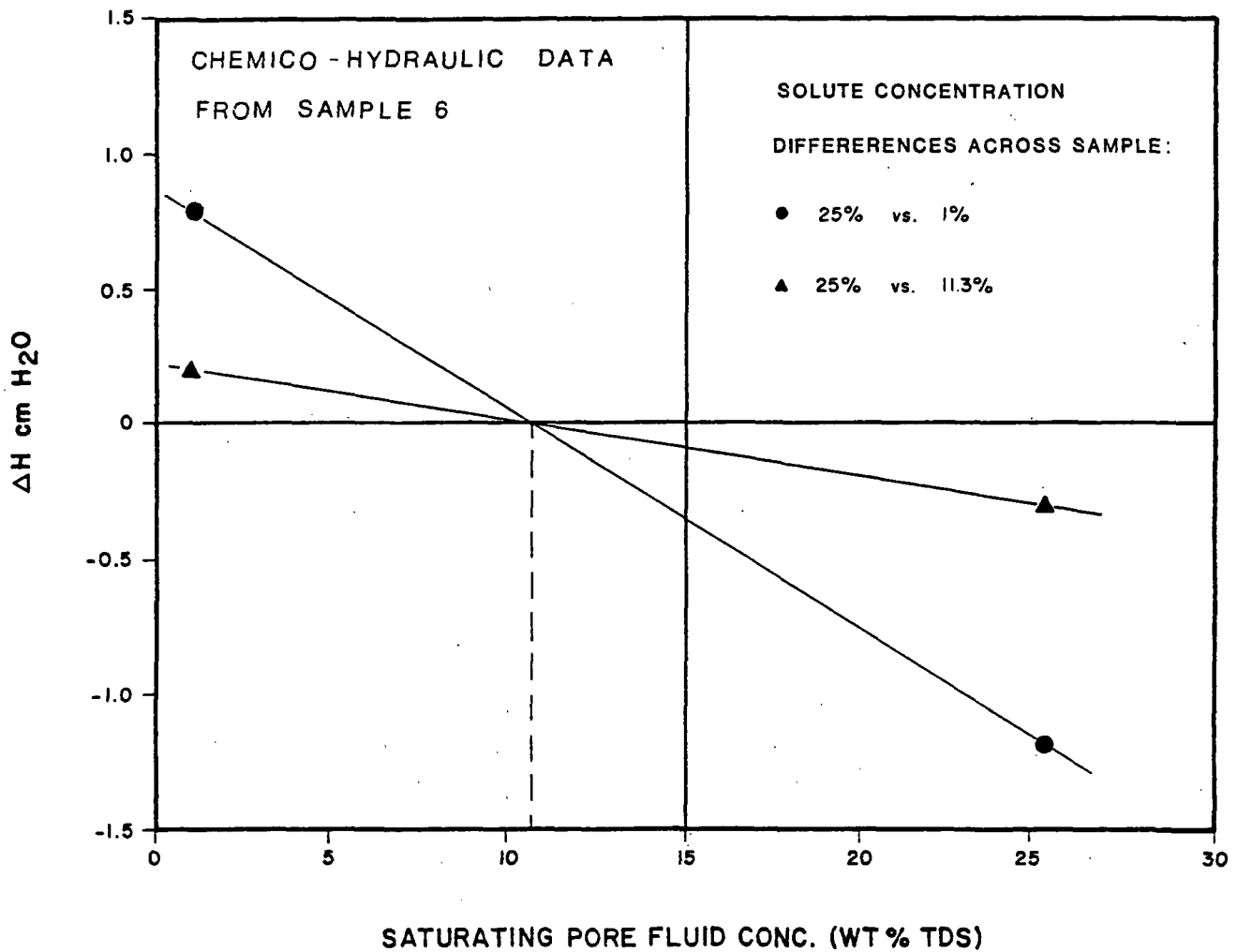
FIGURE 4.1: Chemico-hydraulic data from sample 6. Positive ΔH indicates flow consistent with chemico-osmosis and negative ΔH indicates flow consistent with diffusion-osmosis. Though the two lines represent different chemical gradients, they both intersect the $\Delta H = 0$ line at the same saturating pore fluid concentration. This may suggest that a pore fluid of approximately 10% wt TDS is the condition for which the processes of chemico-osmosis and diffusion-osmosis are equal but opposite.

expand on that concept to include the relative membrane efficiency of certain clays, and what types of clays we would expect in the SSSDP cores. The variation in membrane behavior among clays is due to, all else being equal, their variation in cation exchange capacity (CEC). The higher the CEC, the more effective the membrane in excluding ions from its pore space. Table 4.2 gives the CEC for selected clay minerals at 25C and pH 7.

TABLE 4.2

CEC For Selected Clay Minerals[1]

Clay mineral	CEC (milliequivalents per 100 grams)
Montmorillinite	80 - 150
Illite	10 - 40
Chlorite	10 - 40
Kaolinite	3 - 15

1 From Grim, 1953.

A study on clay mineral transitions in the SSSDP borehole by Donaghe and Peacor (1986) indicates that montmorillinite and illite are present to 4038', below which montmorillinite disappears. Illite decreases linearly to

8800', below which it disappears. Chlorite is abundant throughout the studied section. Data reported by Weaver (1979) on geothermal clay alteration in general (not site specific to the Salton Sea area) is in overall agreement with the temperature/depth relationship suggested by Donaghe and Peacor. Weaver also reports that kaolinite should be expected to be largely converted to illite and chlorite by 150C (2000 ft in the SSSDP borehole), and discusses the classical clay mineral transition sequence in which smectite converts to illite (190C), illite converts to chlorite (250-275C), and chlorite converts to feldspars (above 325C).

The depth/temperature range of our samples is 3113 ft (230C) to 8591 ft (325C), so that we can confine our interest primarily to illite and chlorite. Furthermore, the transition from illite to chlorite is attended by certain physical changes that may be noticeable on geophysical logs. Namely, illite is dehydrated to form chlorite, and the chlorite structure is more compact with fewer layers of bound water. This translates into a lower shale porosity for chlorite, and a corresponding higher resistivity. Muramoto and Elders (1984) have found also that sandstone resistivity increases in the illite to chlorite transition zone, due to the onset of hydrothermal mineralization of chlorite and epidote in the pore spaces (thereby deceasing porosity and

increasing resistivity).

A dramatic increasing resistivity trend is in fact noted in the SSSDP geophysical logs between 3800 and 4400 ft, which approximately corresponds with the expected temperature range (250-275C, Weaver) for the illite to chlorite transition (Figure 4.2). Therefore, it may be reasonable to expect that chlorite is the dominant clay mineral below 4400 ft (samples 4, 5, and 6), though illite is probably still present. In any case, for our purposes illite and chlorite have a similar range of CEC, so that their influence on membrane properties can also be considered to be similar.

As to the relative abundance of clays in specific samples, it is a practical assumption that grain size and the corresponding interpreted depositional environment provide an indicator as to the original amounts of clay material. For example, the shale samples (4 and 6) are interpreted to have been deposited as lacustrine muds with abundant detrital clays (smectites, kaolinite), whereas the sandstones (samples 3 and 5) are alluvial or deltaic deposits made up of mostly quartz grains. The siltstone samples (1 and 2) have been noted to contain abundant fine-grained material, presumably including clay.
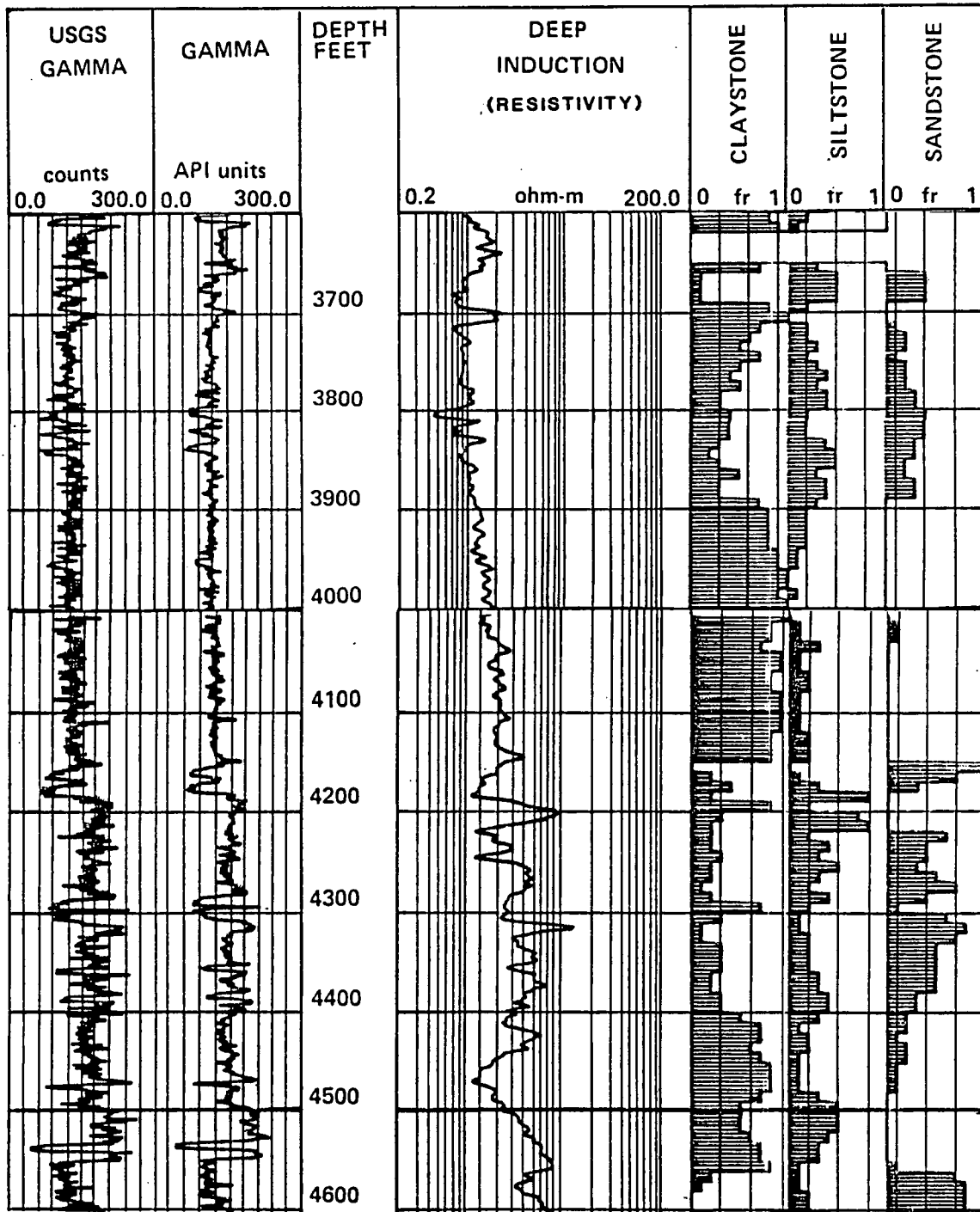
FIGURE 4.2: Geophysical log section from the SSSDP borehole (reproduced from U.S.G.S Open File report 86-544) showing the increasing resistivity trend between 3800 and 4400 ft. This trend may represent the illite to chlorite alteration transition zone.

Though these rocks have been thermally altered, the effect of that alteration on clay minerals is primarily the conversion of one type of clay to another, with no significant change in the overall clay percentage. The exception to this may be for the sandstones, where chlorite can be deposited in the pore space as a hydrothermal mineral, though no clays were originally present. Still, it is assumed that sediments originally more abundant in clays remain so, and the introduction of clay minerals to quartz sandstones is minor with respect to the membrane behavior of the rock.

Effect of temperature:

Temperature dependent factors that could influence chemico-osmotic and diffusion-osmotic processes include the membrane efficiency of the clays, diffusion coefficients, and the chemical potential of the water phase.

The clay minerals in these samples have already been subjected to high temperatures in the subsurface and have been altered accordingly. Therefore, only the temperature dependence of membrane efficiency for a specific clay mineral phase, not the effect of alteration, must be considered here. Haydon and Graf (1986) have reported increased filtration efficiencies for a compacted

montmorillinite with increasing temperature (up to 180C). However, they explain their results in terms of viscosity and hydraulic drag, not membrane efficiency. Their results are not conclusive for our purposes, and no other data concerning membrane temperature dependence were found.

The effect of temperature on the chemical potential of the water phase for a brine solution is complicated by the presence of the multi-component solute, and cannot be resolved here. However, it can be noted in these experiments that the occurrence of chemico-osmosis appears to be more controlled by the relative presence or absence of membrane properties (i.e. clay), and the concentration of the pore fluid, rather than by the magnitude of the chemical potential difference.

The effect of temperature on diffusion, at least, is well understood. Diffusion coefficients for disassociated ions increase with increasing temperature (Barrow, 1979). Hence the driving force for diffusion-osmosis logically also increases with increasing temperature.

Hydraulic Response Due to Electric Gradients

Each of the six samples were tested for electro-osmosis

as described in Chapter III. The test conditions, in terms

of the saturating pore fluid and range of imposed currents,

are listed with the hydraulic results in Table 4.3.

TABLE 4.3

Electro-hydraulic Data

Sample	Pore Fluid[1]	Range of Imposed Currents (uamps)	Corresponding Potentials (millivolts)	$\triangle$H [2]
1	20.0	1 - 100	NM[3] - 2.2	0
2	6.0	10 - 100	1.1 - 11.5	0
2	20.0	100 - 1000	2.5 - 25.0	0
3	D[4]	10 - 50	4.0 - 20.0	0
3	20.0	10 - 2500	NM - 31.0	0
4	2.0	10	11.5	0
4	25.0	10 - 100	2.0 - 20.0	0
5	1.0	50	25.0	0
5	11.3	50 - 500	2.8 - 29.0	0
5	25.0	100 - 1000	4.2 - 46.8	0
6	25.0	50 - 1000	2.1 - 45.1	3.5 cm @ 750 uamps 5.0 cm @ 1000 uamps

1 In wt % TDS

2 Head difference in cm H_2O (resolution 0.2 cm H_2O)

3 NM = Not Measurable

4 D = Distilled Water

As can be seen from Table 4.3, for a wide range of conditions tested, only sample 6 exhibits the tendency for electro-osmotic flow. Considering that previous work on electro-osmosis (see Chapter II) found that this process is associated with materials of high porosity, it may be surprising that electro-osmosis is observed at all in these highly consolidated samples. The porosity of sample 6, for example, is .02 (Table 3.4).

Furthermore, there are unexplained characteristics to the electro-osmosis observed in sample 6. Namely, that it occurs only for currents of 750 uamps and above, and only for positive current in the direction of the base of the sample (cathode at base). The two hydraulic responses that were observed were approximately proportional to the imposed currents (Figure 4.3), but smaller currents produced no hydraulic response, rather than correspondingly smaller hydraulic responses. Apparently, a threshold exists below which electro-osmosis does not occur.

Hydraulic Response Due to Thermal Gradients

Each of the six samples were tested for thermo-osmosis as described in Chapter III. No hydraulic response was
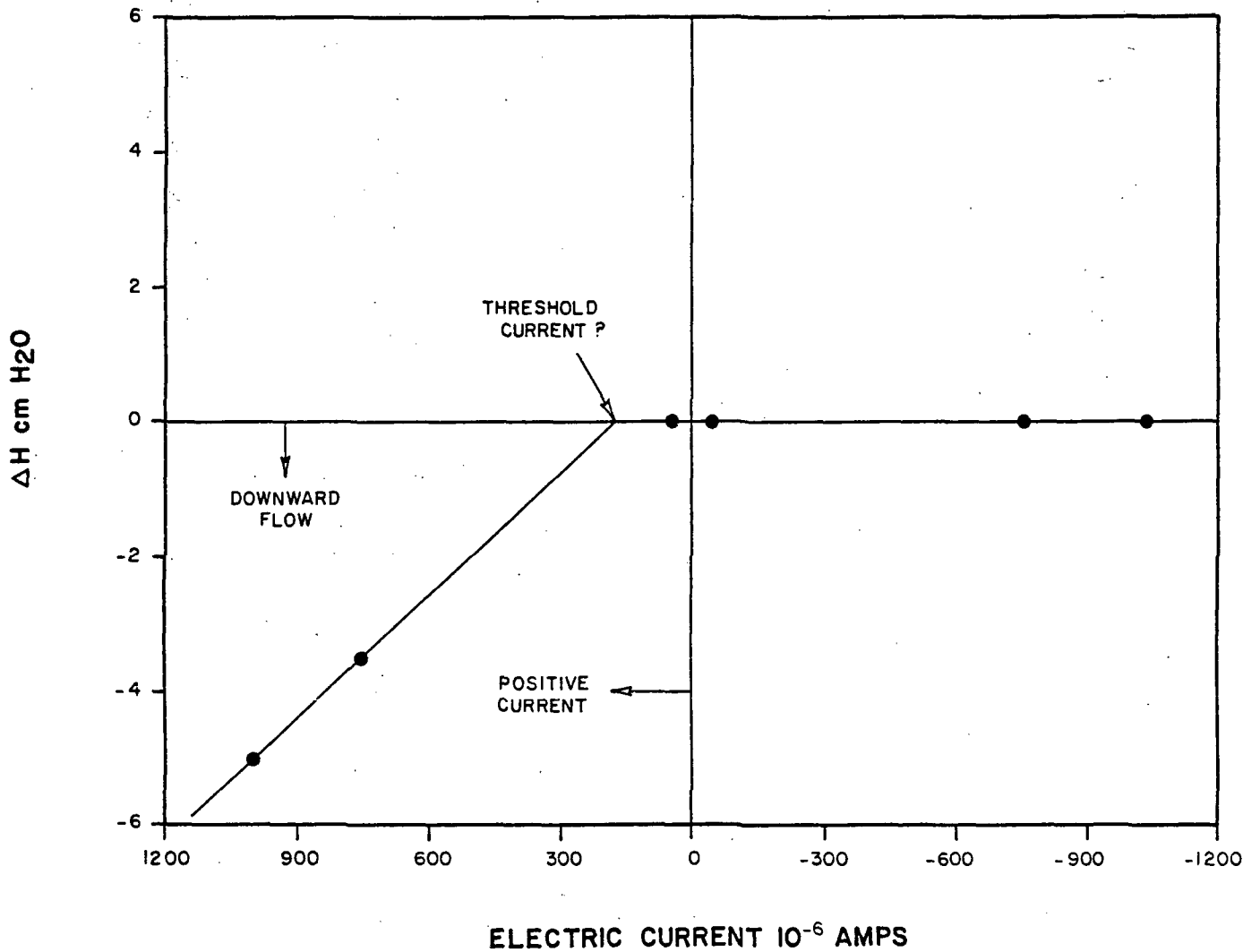
FIGURE 4.3: Hydraulic response to electric currents for

sample 6. Existence of a threshold current is conjecture,

and the reason for no response for the opposite currents is

not known.

detected for any of the samples (resolution 0.2 cm H_2O). The temperature differences imposed ranged from 0.3C for sample 4, to 3.1C for sample 6.

Since the mechanism for thermo-osmosis is not known, one can only speculate on the controlling factors that are present in these samples, or for these test conditions, that have prevented thermo-osmosis. There are two factors in these tests that are quite different from any previously reported conditions: (a) the high concentration of the saturating pore fluid; e.g., 20-25 wt % TDS here versus a maximum of .6 wt % NaCl in other work, and (b) the experiments in this thesis are performed on highly consolidated rock, whereas other work has been performed on loosely compacted clay samples (except Dirksen, 1969, who experimented on kaolinite compacted under a pressure of 6200 psi).

The prospect of extrapolating these low temperature results to in-situ temperatures cannot be evaluated here. But the fact that these tests were carried out on actual cores perhaps leaves us two fruitful avenues of exploration. If, for example, the driving force for thermo-osmosis were assumed to be a difference in chemical potential of the water phase, then thermodynamic calculations that show a

larger chemical potential difference at 25C than for 300C

for the gradients tested, could allow us to rule out thermo-

osmosis at the higher temperature. Also, field thermal

gradients are much smaller than the experimental gradients,

which suggests, but does not prove, that thermo-osmosis is

not likely to occur for these rocks at any temperature.

Electric Potential Response to Solute Concentration and Hydraulic Gradients

Electric potentials across the samples were

continuously recorded during all phases of experimentation.

This section will focus specifically on: (a) the net change

in electric potential from a condition of solute uniformity

to a condition where there is a difference in solute

concentration between the top and base porous stones, and

(b) electric potentials generated by hydraulic gradients.

Table 4.4 is a summary of the data described in (a),

above, and lists the same solute gradients shown in

Table 4.1. Table 4.4 includes the sample number, pore fluid

concentration, solute concentrations in the porous stones,

the net electric potential change with a notation as to a

hypothesized mechanism for that change, and a comment on

whether that mechanism is consistent with the hydraulic

response from Table 4.1 (i.e., chemico-osmosis and membrane

potential are consistent processes with respect to the

effect of membrane properties, whereas diffusion-osmosis and

liquid junction potential are consistent with respect to the

absence of membrane properties).

TABLE 4.4

Electric Potential Response to Solute Concentration Gradients

Sample No.	Pore fluid (wt % TDS)	Porous Stone conc. top	base	Net ΔE [1] (millivolts)	Consistent with ΔH Response
2	D [2]	1.5	D	None	--
2	D	1.5	20.0	+15 L [3]	Yes
3	D	6.0	D	+15 M	No
3	D	6.0	20.0	-60 L	Yes
3	20.0	18.0	20.0	None	--
4	2.0	2.0	1.0	+50 M	--
4	2.0	2.0	25.0	-50 M	Yes
4	25.0	23.0	25.0	None	--
4	25.0	11.3	25.0	None	--
5	1.0	11.3	1.0	+80 M	No

TABLE 4.4 Cont'd

Sample No.	Pore fluid (wt % TDS)	Porous Stone conc. top	base	Net E [1] (millivolts)	Consistent with H Response
5	11.3	25.0	11.3	+58 M	No
5	25.0	22.5	25.0	None	--
6	D	1.0	D	None	--
6	1.0	11.3	1.0	+110 M	Yes
6	1.0	25.0	1.0	+50 M	Yes
6	25.0	11.3	25.0	+14 L	Yes
6	25.0	1.0	25.0	+16 L	Yes

1 Base of sample is reference for sign; i.e., + means base is positive. "None" refers to none or negligible potential change observed. The potentials listed are the net change after circulation of the noted solute concentrations is complete.

2 D = Distilled water

3 L = same direction as Liquid junction potential
  M = same direction as Membrane potential

From the data in Table 4.4 it is evident that for samples 2 through 5, the processes of chemico-osmosis and diffusion-osmosis cannot reliably be linked with the mechanisms for membrane potential and liquid junction potential, respectively. Put another way, the membrane

properties which produce chemico-osmosis do not necessarily
result in membrane potentials in these samples. Likewise,
the lack of membrane properties which allow diffusion-
osmosis to occur do not necessarily result in liquid
junction potentials.

The potentials measured in sample 6, however, do appear
consistent. Sample 6 is the only sample in Table 4.4 which
is not fractured (sample 1, not in Table 4.4, is unfractured
also, but the direction of the electric potentials were not
recorded). The observation that the concentration-
induced electric potentials for the unfractured sample 6
alone were consistent with the presence or absence of
membrane properties may not be a coincidence. It is
tentatively suggested here that the presence of fractures
influences the concentration-induced potentials in such as
way as to overshadow the effect of the membrane or liquid
junction potentials.

Electric potentials were continuously monitored during
hydraulic flow through the sample in order to detect the
occurrence of hydraulically-induced electric potentials
(streaming potentials). The criteria for the identification
of streaming potentials as defined in Chapter II are: (1)
positive potential in the direction of flow (due to the

T-3678

surplus of cations in the membrane pore space), (2) the
potential must appear with the onset of hydraulic flow and
disappear with its termination, and (3) the measurement
should be repeatable.

Although every hydraulic flow-test resulted in some
change of potential, none satisfied the three criteria noted
above. In approximately 50% of the tests the sense of
direction of the potential was opposite that expected from
the commonly cited mechanism for streaming potential
(hydraulic convection of charge). Figure 4.4 is an example
of this: hydraulic flow is from the base to the top, but the
base has acquired the positive charge. Also in Figure 4.4,
transient responses of unknown cause are noted, as well as
a significant static drift preceding the flow-test. The
static potential drift may be related to the introduction of
the hypersaline brine to the manifold from the pore fluid
reservoirs, a process which could have influenced the
potentials in both the streaming potential tests and the
concentration-induced potential tests. Unfortunately, the
direction and degree of static drift due to the introduction
of the brine was not consistent, and could not be corrected
for.

TRANSIENT RESPONSE-
CAUSE UNKNOWN

HYDRAULIC FLOW ENDS

HOUR | TIME

TRANSIENT RESPONSE-
CAUSE UNKNOWN

BASE OF SAMPLE
BECOMING MORE
POSITIVE

HYDRAULIC FLOW
BEGINS
(BASE ──► TOP)

SCALE

10mV

STATIC DRIFT DUE
TO INTRODUCING
HYPERSALINE FLUID
TO MANIFOLD
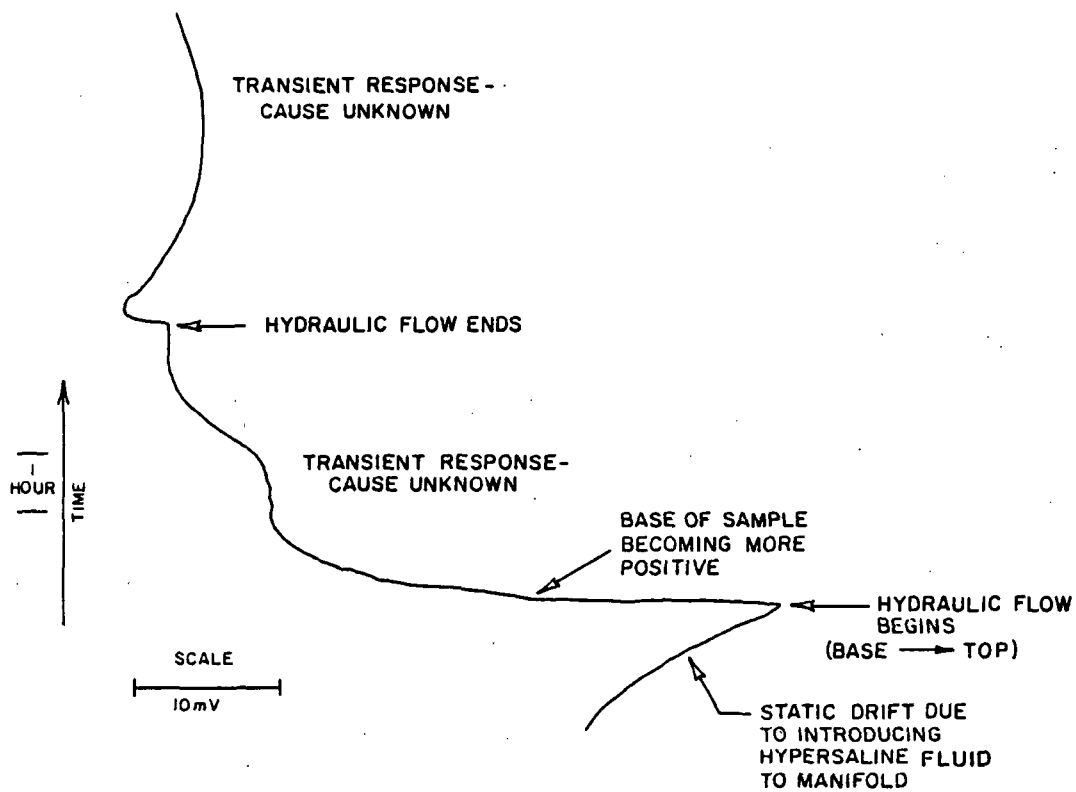
FIGURE 4.4: Example of strip chart data for electric response due to hydraulic flow.

DIRECT TRANSPORT DATA

Hydraulic Conductivity:

The direct transport properties measured in this thesis are hydraulic conductivity, thermal conductivity, and electrical resistivity. The data for hydraulic conductivity is analyzed as per Figure 3.4, and a summary of the results is presented in Table 4.5.

TABLE 4.5

Hydraulic Conductivity

Sample	K_h(Measured) (cm/s)	K_h(Corr.)* (cm/s)	In-situ Temp. (C)	Measured at in-situ effective stress (psi)
1	5.0×10^{-9}	3.3×10^{-8}	275	2400
2	4.3×10^{-7}	2.8×10^{-6}	275	2400
3	4.5×10^{-5}	3.0×10^{-4}	250	1900
4	2.7×10^{-2}	2.5×10^{-1}	325	5000
5	3.7×10^{-4}	3.4×10^{-3}	330	5300
6	3.3×10^{-7}	2.9×10^{-6}	300	3800

* Corrected to in-situ temperatures.

The magnitude of the temperature correction in Table
4.5 is a 6-9 fold increase in hydraulic conductivity due to
the temperature-dependent decrease in kinematic viscosity,
according to the following equation:

$$K_h(\text{Corr.}) = (\sqrt{}_{25}/\sqrt{}_T) \times K_h(\text{Measured}) \qquad (4.1)$$

For: $\sqrt{}_{25}$ = kinematic viscosity at 25C

$\sqrt{}_T$ = kinematic viscosity at the in-situ temperature
(estimated from temperature logs)

Data for this correction are from the Geothermal
Technical Data Book, published by Lawrence Berkeley
Laboratory (Phillips, 1981). These data are for NaCl
solutions only, but kinematic viscosities for a mixed
solution are not expected to deviate significantly
(Phillips, 1981).

The data in Table 4.5 demonstrate that hydraulic
conductivity in these samples is fracture controlled (see
sample descriptions, Table 3.3). For example, samples 1 and
2 are taken from the same depth and are the same lithology,
but the fractured sample (sample 2) is two orders of
magnitude greater in hydraulic conductivity than the
unfractured sample. Likewise, samples 4 and 6 are both

shales with similar porosities (.03), but are separated by five orders of magnitude due to fracturing (in sample 4).

It should be noted that the measured hydraulic conductivities listed in Table 4.5 are averages for different permanent concentrations. It was found that the concentration of the permanent did not significantly affect the hydraulic conductivity of these samples.

Thermal Conductivity:

Temperature and heat flux data are collected as described in Chapter III, and thermal conductivities are calculated by equation (3.2). Results are presented in Table 4.6, along with the associated uncertainty as described in Appendix C.

TABLE 4.6

Thermal Conductivity

Sample	Heat Flux[*] (W)	Temp. Diff. (C)	K_t (W/mC)	Uncertainty (W/mC)
1	.17	.55	2.4	1.3
2	.30	.93	2.5	0.7
3	.30	.70	3.3	1.0

TABLE 4.6 Cont'd

Sample	Heat Flux[*] (W)	Temp. Diff. (C)	K_t (W/mC)	Uncertainty (W/mC)
4	.07	.30	1.9	2.4
4	.30	1.15	2.0	0.6
5	.30	.67	3.3	1.0
6	.30	.85	2.6	0.9
6	1.19	3.10	2.8	0.2

* Corrected for heat loss as per Appendix C.

No corrections to in-situ temperatures are warranted. The thermal conductivity of the rock matrix is not expected to be significantly affected by temperature below 500C (Keller, personal communication, 1988). Also, there is little net change in the thermal conductivity of the brine pore fluid between 25C and 300C (Phillips, 1981).

Two important observations can be made from the results in Table 4.6: (1) that the thermal conductivities exhibit no increasing or decreasing trend with depth, and (2) if there is a lithology control on thermal conductivity, it appears that sandstones have a slightly higher thermal conductivity than shales and siltstones.

Electrical Resistivity:

The electrical resistivity data are collected as
described in Chapter III, and analyzed as per Figure 3.6. A
summary of these results is contained in Table 4.7.

TABLE 4.7

Electrical Resistivity

Sample	Pore Fluid (wt % TDS)	Resistivity (Ohm-m)
1	20.0	2.9
2	20.0	3.3
3	D	49.5
3	20.0	1.7
4	2.0	87.7
4	25.0	18.1
5	1.0	68.2
5	11.3	7.9
5	25.0	6.4
6	25.0	6.1

The data in Table 4.7 show that sample resistivity is
primarily controlled by the concentration of the pore fluid.

This is a well established relationship for the electrical properties of porous rock (Keller, 1982). In most porous rock, nearly all of the imposed electric current is transported by ions in solution, with little current transported by the matrix. Matrix conductance can, however, be significant, particularly in shales which can transmit current via the charged surfaces of clay minerals (Waxman and Smits, 1968).

With regard to matrix conductance, it can be noted in the results above that: (a) Although pore fluid concentration grossly controls resistivity, the relationship between concentration and resistivity is not proportional (see samples 4 and 5), and (b) there is a significant difference in the resistivities of samples 4 and 6 (18.1 and 6.3 Ohm-m, respectively), though both are shales with similar porosity, and both are measured with identical pore fluids. Observations (a) and (b) indicate the influence of matrix conduction on resistivity. This issue is further explored in the section on Electrical Resistivity in Chapter V.

Correcting to in-situ temperature:

Temperature corrections will be made on the basis of pore fluid resistivity. Ucok (1980), has tested the

relationship between sample resistivity and pore fluid
resistivity for sandstones saturated with a 20% by weight
NaCl solution. For a range of temperatures between 25C and
350C, he found the relationship almost linear (Figure 4.5).

Table 4.8 gives the data relevant to correcting the
resistivity of the 20% and 25% by weight TDS brines to in-
situ temperatures.

TABLE 4.8

Temperature Correction for Brines

Pore Fluid (wt% TDS)	Calculated R_w @ 25C (ohm-m)	Measured R_w @ 25C (ohm-m)	Calculated R_w @ 300C (ohm-m)
20.0	.047	.052	.0082
25.0	.038	Not Measured	.0066

The term R_w signifies the resistivity of the brine.
The resistivities of multi-solute solutions can be
calculated using an empirical "equivalent conductance"
technique that multiplies non-sodium/non-chloride ions by
factors which convert their conductance to equivalent NaCl
conductance (Ucok, 1980). The resistivity of the equivalent
NaCl solution can then be found in any borehole logging
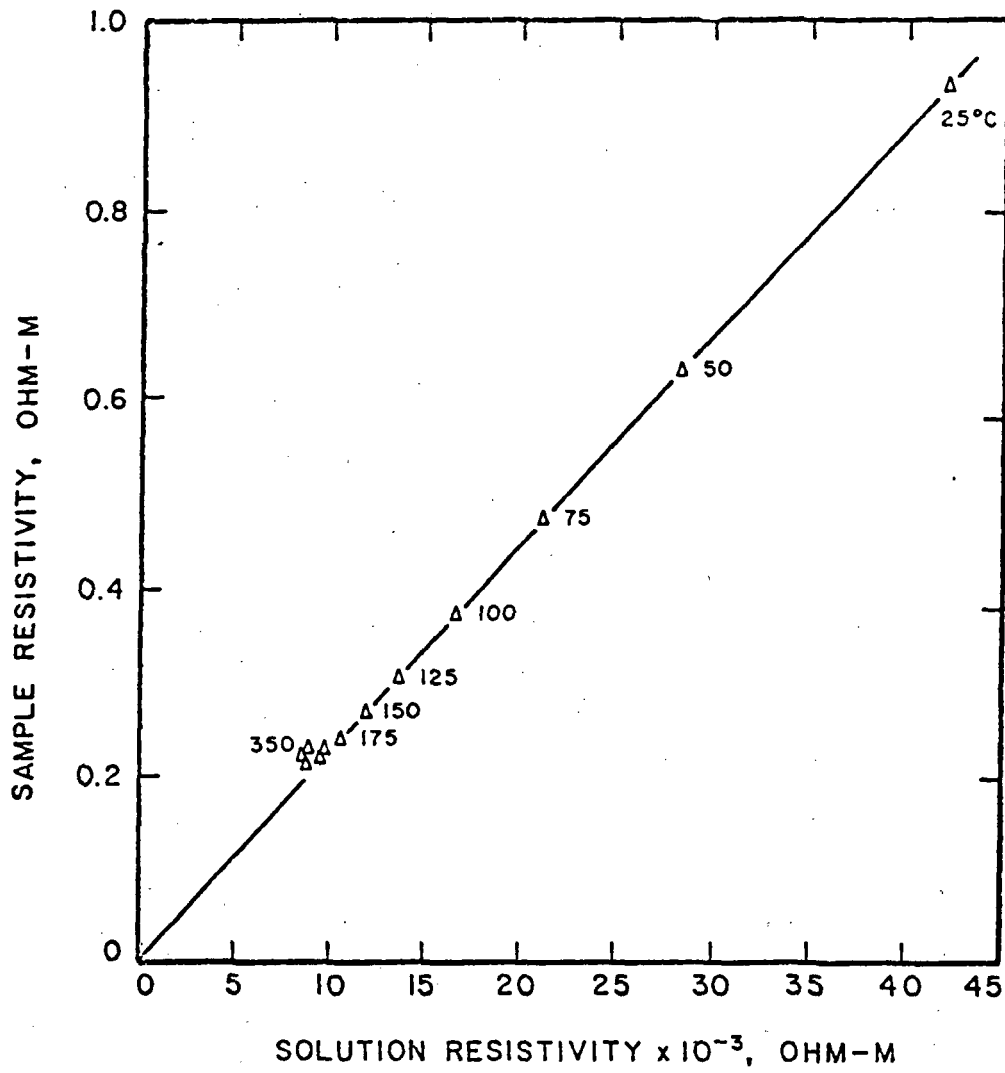chart book (i.e., Schlumberger, 1972).

FIGURE 4.5: Rock resistivity versus pore fluid resistivity
for a 20% NaCl solution saturated sandstone at various
temperatures (Ucok, 1980).

The temperature corrections are performed according to Ucok's data (1980). The brines are corrected to a uniform 300C, rather than a separate correction for each sample depth. Ucok has shown that temperature corrections are almost uniform between 250C and 350C. This interesting relationship is shown in Figure 4.6.

Based on the above temperature correction for brines, the rock resistivity can be corrected by the same ratio (resistivity is decreased by a factor of 5.7 when correcting from 25C to 300C). The temperature-corrected resistivity values, and geophysical log-derived resistivities are listed in Table 4.9.

TABLE 4.9

Temperature-corrected Sample Resistivity

Sample	Sample Resistivity Corrected to 300C (ohm-m)	Geophysical Log-derived resistivity[*] (ohm-m)
1	0.5	1.0
2	0.6	1.0
3	0.3	0.2
4	3.1	4.2 ?
5	1.1	0.8
6	1.1	6.5

* The geophysical log-derived resistivities are from representative induction log responses at or nearby the core depth.
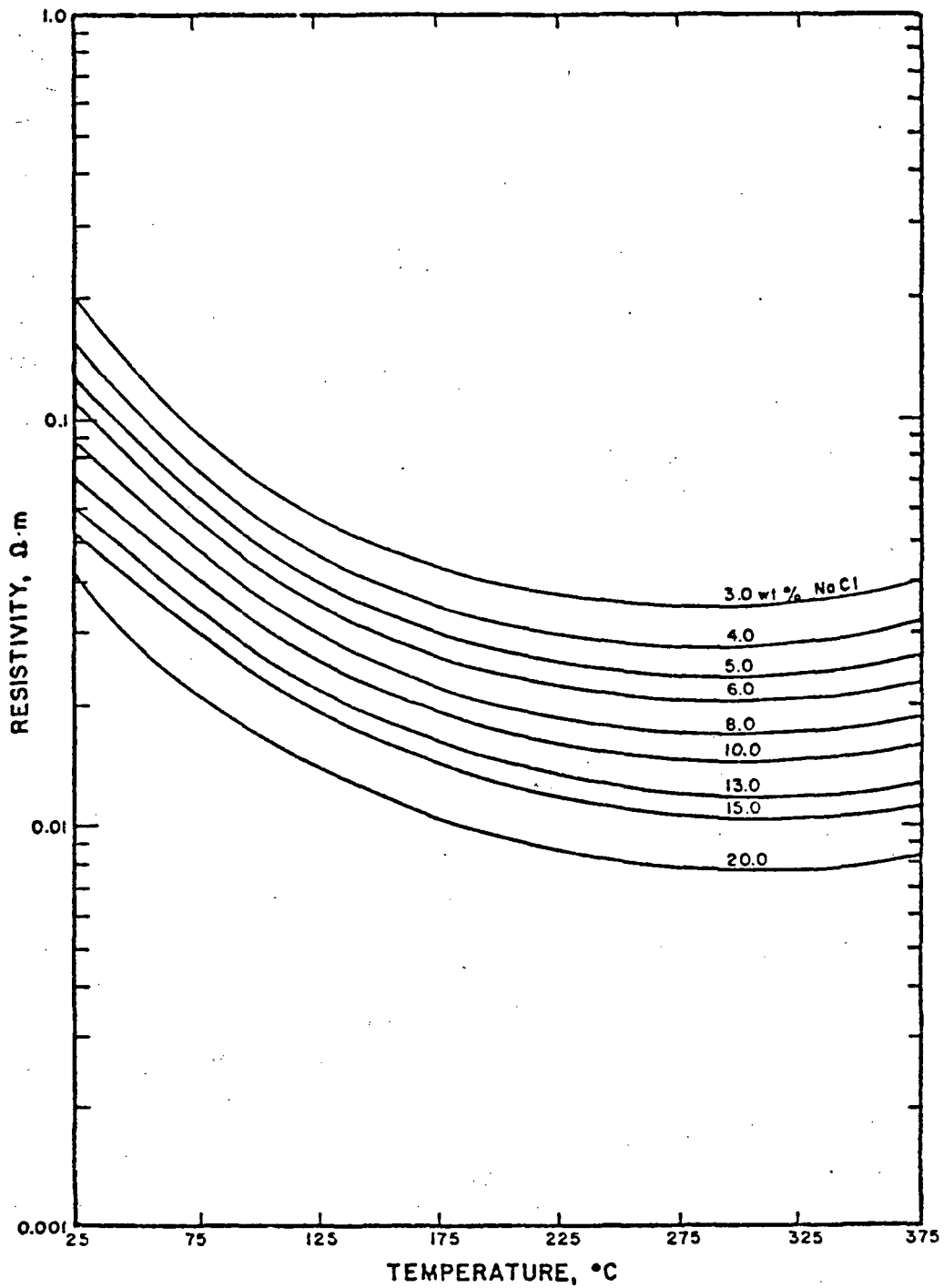
FIGURE 4.6: Resistivity of NaCl solution versus temperature and concentration (Ucok, 1980).

It is interesting to point out that the laboratory measured, temperature-corrected resistivities for the sandstones are fairly close to their respective log-derived values. However, the shales and siltstones deviate significantly from their log-derived counterparts. Although the log-derived values are subject to vertical averaging, the above observation may indicate that the temperature correction based solely on pore fluid resistivity is accurate for sandstones (as shown previously by Ucok), but inaccurate for siltstones and shales.

The observation can be taken one step further. Note that the laboratory corrected resistivities are, in each case for the shales or siltstones (samples 1,2,4,and 6), lower than the log-derived values. This is consistent with the idea that matrix conduction decreases rock resistivity; i.e., the resistivities for these samples have been "overcorrected" (reduced by too much) on the basis of pore fluid alone.

CHAPTER V

APPLICATIONS OF THE RESULTS TO THE

SALTON SEA GEOTHERMAL SYSTEM

Major issues of interest for the Salton Sea Geothermal System that may be addressed by results from this thesis are as follows:

(1) The effect of coupled pore fluid transport on heat transfer in the reservoir.

(2) The role of the hypersaline brine/dilute fluid interface in pore fluid movement.

(3) Controls on hydraulic and thermal conductivities.

(4) The relationship among electrical resistivity, surface conduction by clays, and pore fluid concentration.

Heat Transfer

Understanding the mechanism for heat transfer in the Salton Sea reservoir is critical to its long term energy management. In the subsurface, two types of heat transfer

are operating; conduction and convection, though it is not always clear to what extent each contributes to heat flow in particular subsurface regions. In plume-like advection driven by thermal fluid density gradients, or wherever pore fluid movement is significant, convective heat transfer is important. Heat is transported as latent energy contained in the fluid, and its rate of transfer is therefore influenced by the interstitial velocity of the fluid. Where advection, or hydraulic flow, is negligible, advective heat flow is also negligible, and thermal conductivity overwhelmingly controls the rate of heat transfer.

The question of fluid transport in the reservoir therefore precedes that of heat transfer. With this in mind, the following discussions will focus on the question of fluid convection in the Salton Sea Geothermal System.

It was noted in Chapter I that there is evidence for the existence of uniform fluid density below the brine interface, which, if true, would preclude thermal advection as a mechanism of heat transfer in that region. The observation of uniform fluid density has been reinforced by drilling and well test data from the SSSDP borehole. Daily drilling reports indicate that the drilling mud weights used to balance formation pressures remained within the narrow

range of 8.0 - 9.0 lb./gal during drilling of the well.
Also, a shut-in bottom hole pressure of 2492 psi recorded at
5950' represents a fluid gradient of .42 psi/ft, which is
equivalent to the hydrostatic head caused by a fluid with a
density of approximately 1.0 g/cc. This test is commensurate
with other well tests in the area (Unocal, personal
communication, 1988). Measurements of original formation
pressures elsewhere within the Salton Sea hypersaline
reservoir also show that natural state regional hydraulic
flow is negligible or non-existent (Unocal, personal
communication, 1988).

The apparent reservoir-wide uniform fluid density
exists in spite of, or perhaps because of, the extreme
chemical and thermal gradients. It is not known why the
fluid density should stabilize at the approximate density of
cool fresh water (1.0 g/cc). Still, the evidence noted above
suggests the lack of thermal advection and natural state
hydraulic flow in the reservoir.

This does not rule out convection from another
cause. Specifically, convection that may be caused by
coupled processes. It is clear that chemico-osmosis would
not be important in the hypersaline portion of the reservoir
because experiments in this thesis indicate that chemico-
osmosis is not likely to predominate in these rocks when

saturated with a highly concentrated pore fluid. However,
diffusion-osmosis could be a mechanism that drives water
upward in the reservoir, in the direction of solute
diffusion, without benefit of fluid density gradients or
hydraulic head differences.

Evidence for the occurrence of upward fluid convection
lies with the temperature profiles in the SSSDP borehole
(Sass et al., 1988). Figure 5.1 shows the temperature build-
up with time, which has still not reached steady state six
months after drilling has terminated. Nevertheless, the
SSSDP profile exhibits two distinct characteristics: (1) a
linear portion from near-surface to approximately 3000 ft,
and (2) a concave down portion from 3000 ft to at least 6000
ft. The significance of these characteristics can be seen
when compared to mathematically modeled temperature profiles
for various convection conditions. Figure 5.2 illustrates
these conditions (governing equations from Bredehoeft and
Papadopulos, 1965). Note that the linear curve (a)
represents conduction dominated heat transfer, which
probably occurs in the top 3000 ft of rock at the SSSDP
site. Note also that either of the concave down curves (c)
or (d) can represent the lower portion of the SSSDP
borehole. Curve (d) is the case for increasing thermal
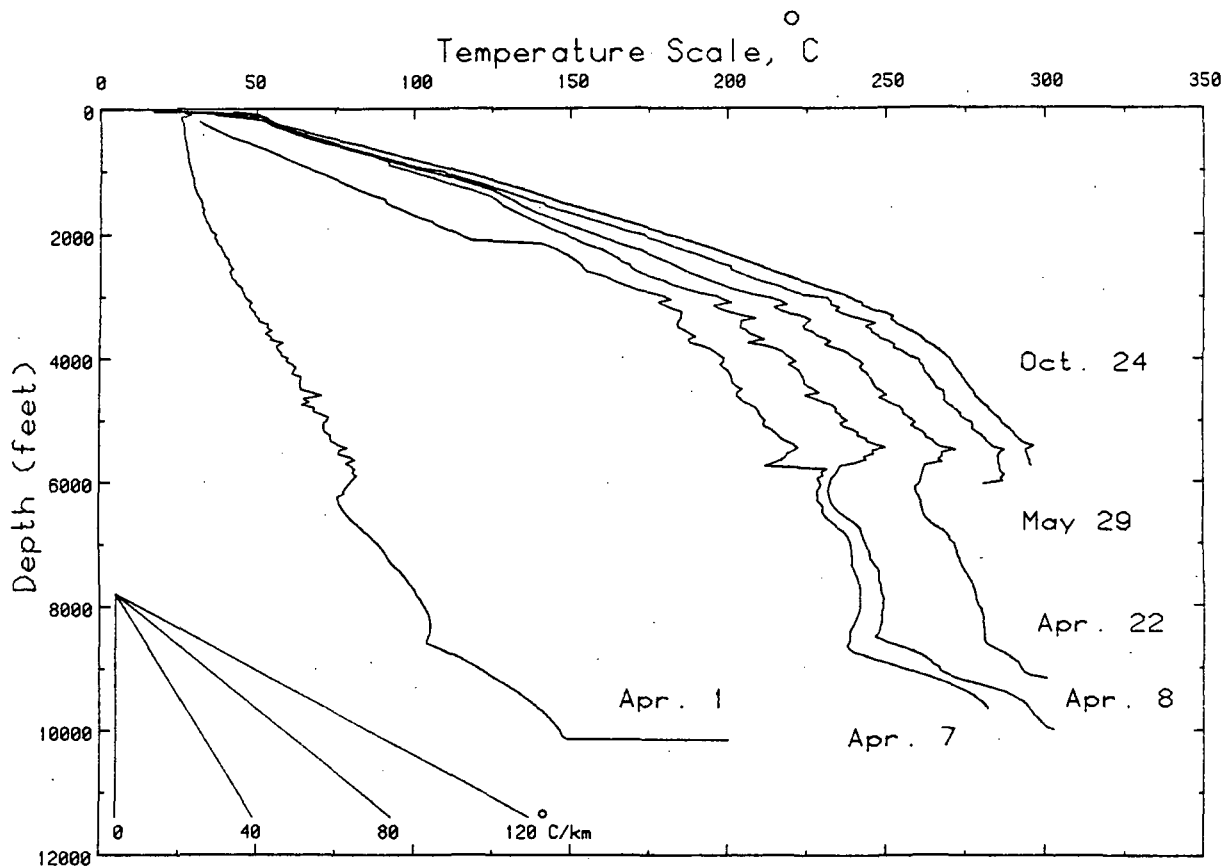
FIGURE 5.1: Thermal profiles for the SSSDP borehole. (Sass et al., 1988). A temperature log could not be obtained below 6000 ft, but a separate instrument measured a temperature of 355C at 10560', the highest temperature encountered in the SSSDP borehole.

Figure 5.2: Mathematically modelled temperature profiles. (a) constant thermal conductivity with no convection, (b) convection dominant, (c) mixed conduction/convection with upward convection and constant thermal conductivity), (d) increasing thermal conductivity with depth, and (e) mixed conduction/convection with downward convection and constant thermal conductivity.

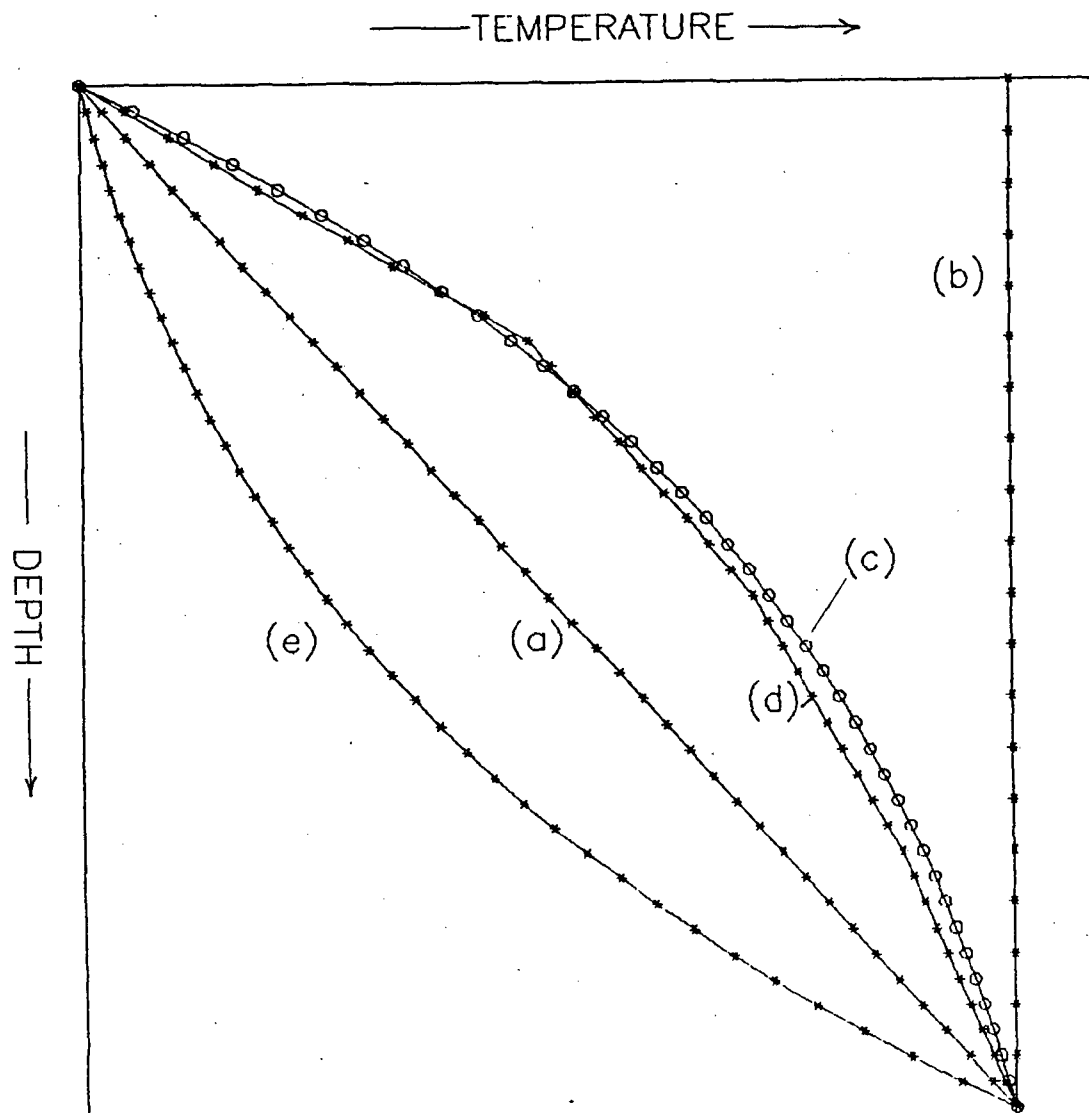conductivity with depth, but could be ruled out because thermal conductivity measurements in this thesis indicate that this property does not increase with depth. Curve (c) represents the case where upward convection influences the shape of the temperature profile.

Experimental evidence in this thesis indicates that diffusion-osmosis can and does occur in these rocks when saturated with a highly concentrated brine. Therefore, it seems possible that diffusion-osmosis could also occur in this reservoir, driving pore fluid upward and transferring heat from depth toward the brine interface.

The rate of upward convection may be estimated according to a relationship developed by Bredehoeft and Papadopulos (1965). Data on the curve marked Oct. 24 in Figure 5.1 between 3000 ft and 6000 ft suggest that for this interval convection velocity is approximately 6.0×10^{-10} ft/s.

Brine Interface

The break in slope of the temperature profiles shown in Figure 5.1 roughly coincides with the location of the brine interface. It follows that the brine interface may act as a barrier to the upward convection of hot fluids, either by virtue of a density inversion (fluids above the interface

are less dense due to their lower solute concentration), or by the elimination of diffusion-osmosis at the interface (chemico-osmosis may predominate in the less saline environment). The idea of the interface as a barrier departs from the prevailing theory that an "impermeable" thermally conductive caprock provides the barrier to advection (Kasameyer et al., 1984).

Thus, at least four different hypotheses attempt to explain the concave downward shape of the temperature profile in terms of heat transfer in the reservoir: (1) increasing thermal conductivity with depth, (2) plume-like advection occurs in the permeable portion of the reservoir, but is restricted by the impermeable caprock (Kasameyer et al., 1984), (3) plume-like advection occurs in the hypersaline portion of the reservoir, but is restricted by the density contrast at the brine interface (Williams, 1988), and (4) diffusion-osmosis drives pore fluid up toward the interface, but not beyond, as suggested in this thesis.

Above the interface, the fluids are relatively dilute and probably favor chemico-osmosis where clay minerals are present (there are ubiquitous shales throughout the entire SSSDP interval). Therefore, coupled processes would tend to drive pore fluid toward the interface from above due to chemico-osmosis, and from below due to diffusion-osmosis.

One final thought on the issue of the brine interface addresses the idea that the similarity in depth between the disappearance of montmorillinite, reported by Donaghe and Peacor (1986) at 4038', and the depth of the interface, at about 3000 ft, may not be a coincidence. For example, montmorillinite has a much higher cation exchange capacity than illite or chlorite (Table 4.2), perhaps tipping the balance in favor chemico-osmosis where montmorillinite is still present. This avenue of speculation presumes that the interface is controlled by the demarcation between chemico-osmosis and diffusion-osmosis, rather than vice-versa.

Hydraulic and Thermal Conductivity

Hydraulic conductivity in samples measured in this thesis is controlled by the presence or absence of fractures. Furthermore, fractures are frequently described in the cored interval (Mehegan et al, 1986). The significance of fracture controlled hydraulic conductivity is that completion zones for the production of geothermal fluids need not be targeted for sandstone intervals, as they are, for example, in the nearby Cerro Prieto field (Halfman et al, 1984). Rather, completion zones should be targeted for heavily fractured areas, as delineated by geophysical

logs or well tests.

Experimental results from samples in this thesis that range from 3113 ft to 8591 ft indicate that thermal conductivity is not controlled by depth. It should be noted that no prior data on thermal conductivity for this depth range in the Salton Sea Geothermal System could be found in the public record. However, Sass (1987) reported that thermal conductivity measurements on shallow drill cuttings (to 3000 ft) indicate an increasing trend with depth, due to decreasing porosity. If so, thermal conductivity does not increase sufficiently in that depth range, which includes most of the porosity reduction seen in the SSSDP (log analysis by writer), to influence the temperature profile (Figure 5.1).

The data that Sass reports and data from this thesis cannot be directly compared because the data sets are not from the same depth range, but a fundamental discrepancy between them exists. Data from this thesis indicate that the samples with the lower porosities (shale samples 4 and 6) also have the lower thermal conductivities (see Table 4.6). Whereas, the sample with the highest porosity (sample 3, a sandstone) shares the highest thermal conductivity (with sample 5, also a sandstone). These results suggest that

thermal conductivity for these rocks is more influenced by

lithology than an inverse relationship to porosity, with

sandstones possessing the higher thermal conductivity

compared to shales.

Electrical Resistivity

Information concerning clay content and pore fluid

concentration is contained in the measurement of the

electrical resistivity of rocks. Archie in 1941 proposed

relationships between formation resistivity, pore fluid

resistivity, and porosity that remain in wide use today. He

defined the formation factor for sandstones as:

$$F = R_o/R_w \qquad\qquad (5.1)$$

For: F = formation factor

R_o = resistivity of the rock when 100% saturated with a
fluid with resistivity of R_w.

Archie found experimentally that the formation factor

of sandstones can also be estimated by:

$$F = 1/n^m \qquad\qquad (5.2)$$

For: n = porosity

       m = an empirically determined exponent found to be

       about 2.0 for consolidated sandstones

Work done subsequent to Archie on shalely sands and shale conductance has shown that these relationships must be modified for fine-grained rocks to account for the surface conductance of clay minerals (summarized by Worthington, 1985). Furthermore, that significant deviation between formation factor (F) measured by the resistivity ratio method (Eq. 5.1) and F estimated by the porosity method (Eq. 5.2) usually indicates the contribution of surface conductance, and the presence of clay minerals.

Table 5.1 (following page) lists the formation factors for the six samples in this thesis as calculated both by the resistivity ratio and porosity methods.

TABLE 5.1

Formation Factors

Sample	R_O*	R_W*	F (Eq. 5.1)	n	F (Eq. 5.2)
1	0.5	.0082	61	.06	278
2	0.6	.0082	73	.06	278
3	0.3	.0082	36	.20	25
4	3.1	.0066	470	.03	1111
5	1.1	.0066	167	.07	204
6	1.1	.0066	167	.03	1111

* Corrected for temperature (Tables 4.8 and 4.9)

Samples 3 and 5 are roughly consistent with both of
Archie's relationships, indicating that these are fairly
clean sandstones, with little or no extraneous conductivity.
For the other samples, F by the resistivity ratio method
(Eq. 5.1) is much lower than that estimated by the porosity
method (Eq. 5.2), suggesting that the conductivity of the
bulk rock is greater than is predicted by the conductivity
of its pore fluid.

Three explanations for this result are explored here:
(1) Archie's relationships are not valid for non-sandstones,
(2) hydrothermal minerals contribute to rock conductivity,
and (3) the presence of fractures contributes to the
conductive path, resulting in excess conductivity not
indicated by porosity.

With regard to the latter, sample 6 possesses
significant excess conductivity, but is unfractured. The
possibility of conduction by hydrothermal minerals (i.e.,
pyrite, sphalerite) may not be realistic for disseminated
mineralization, as presumably exists in these rocks . Also,
it is puzzling why the sandstones would not also possess
excess conductivity due to hydrothermal minerals.

The validity of Archie's relationship for fine-grained
rocks (containing clay) has been the subject of discussion
for many years, but deviation from expected values is
usually assumed to be caused by the influence of clay
mineral conductance.

However, Waxman and Smits (1968), Ucok (1980), and many
others have found that surface conduction by clay minerals
is inversely related to pore fluid concentration. This is
explained by the reduction in the thickness of the clay
double layer, a phenomenon which would be expected where
there are a greater density of cations available to offset

the negative charge on the surfaces of clay particles. In fact, this is the very mechanism by which chemico-osmosis is eliminated under conditions of high pore fluid concentrations, as observed in this thesis. It would seem that under these conditions of high pore fluid concentration clay surface conductance would also be greatly reduced or eliminated.

Nevertheless, these experiments show, and Table 5.1 illustrates, that the bulk conductivity of the more fine-grained samples is significantly greater than expected by consideration of the pore fluid conductivity alone. It is therefore suggested here that the clay minerals present in these fine-grained rocks can still conduct an electric current although the ion-restricting property of those clays is suppressed by the presence of the hypersaline pore fluid.

CONCLUSIONS

Data from experimental work in this thesis show that both chemico-osmosis and diffusion-osmosis can cause pore fluid movement in cores from the SSSDP borehole. The process of chemico-osmosis tends to dominate for the cases where the core samples are saturated with a dilute fluid (1% wt TDS), whereas the process of diffusion-osmosis tends to dominate for the cases where the core samples are saturated with a hypersaline brine (20-25% wt TDS). Fine-grained samples exhibit a greater tendency toward chemico-osmosis due to their greater abundance of clay minerals, but the process can be transformed to diffusion-osmosis by replacing a dilute pore fluid with a concentrated pore fluid.

An important conclusion from the above results is that the membrane phenomenon of ion-exclusion is present in these thermally altered core samples, but can be suppressed by concentrated pore fluid. The mechanism of this suppression is proposed to be the reduction in the thickness of the clay double layer due to a greater concentration of cations available to offset the negative charge on the surfaces of clay minerals.

For the in-situ condition of hypersaline pore fluid known to exist in the Salton Sea Geothermal System below the brine/dilute interface, the process of diffusion-osmosis may be driving pore fluid upward toward the interface. This diffusion-driven process would allow the upward convection of pore fluid without the benefit of fluid density gradients or hydraulic head differences, proof for either of which has been difficult to establish with field data.

Electro-osmosis and thermo-osmosis are probably not important in these rocks. Thermo-osmosis was not detected at any time during experimentation with these samples. Electro-osmosis was recorded only for sample 6, and only in one direction. Streaming potentials were also not detected for these samples. Because of the reciprocal nature of electro-osmosis and streaming potential, the overall lack of detection of both is internally consistent. The writer concludes that the primary condition which is conducive to electro-osmosis and streaming potential is high porosity (above 20%), which is not present in these samples.

With regard to direct transport properties, hydraulic conductivity is overwhelmingly controlled by the presence or absence of fractures. Thermal conductivity appears to be controlled more by lithology than porosity or depth

(sandstones having the higher thermal conductivity compared to shales), but substantial uncertainties in the measurement of these values make this conclusion tentative.

Electrical resistivity is grossly controlled by pore fluid concentration, but the presence of excess conductivity in the fine-grained samples suggests that surface conductance by clay minerals may be significant. This conclusion does not conform to the concept that the hypersaline pore fluid suppresses all membrane properties. Therefore, the the writer concludes that the relative effect of pore fluid concentration on clay membrane properties is variable.

REFERENCES

Archie, G.E., 1941, The electrical resistivity log as an aid in determining some reservoir characteristics: Transactions, Society Petroleum Engineers annual meeting, pp. 54-61.

Barrow, G.M., 1979, Physical Chemistry, McGraw-Hill (fourth edition), New York, N.Y.

Berry, F.A.F., 1959, Hydrodynamics and geochemistry of the Jurassic and Cretaceous systems in the San Jaun Basin, northwestern New Mexico and southwestern Colorado: Ph.D. Thesis, Stanford University, California.

Berry, F.A.F, and B.B. Hanshaw, 1960, Geologic field evidence suggesting membrane properties of shales: Transactions XXI Geological Congress, Copenhagen, Denmark.

Biehler, S., 1964, Geophysical study of the Salton Trough of Southern California: PH.D. Thesis, California Institute of Technology, Pasadena.

Bredehoeft, J.D. and I.S. Papadopulos, 1965, Rates of vertical groundwater movement estimated from the earth's thermal profile; Water Resources Research, Vol. 1, No. 2, pp. 325-328.

Bredehoeft, J.D., C.R. Blyth, W.A. White, and G.B. Maxey, 1963, A possible mechanism for concentration of brines in subsurface formations: American Association of Petroleum Geologists Bull. 47, pp. 257-269.

Chen, H.C., and J.H. Fang, 1986, Sensitivity analysis of the parameters in Archie's water saturation equation: The Log Analyst, Vol. 27, No. 5, pp. 39-44.

Craig, H., 1966, Isotopic composition and origin of the Red Sea and Salton Sea geothermal brines: Science, Vol. 154, pp. 1544-1548.

Carr, C.W., and K. Sollner, 1962, New experiments on thermo-osmosis: Jour. Electrochem. Society, Vol. 109, pp. 616-622.

Carr, C.W. et al., 1962, Electro-osmosis in ion exchange membranes: Jour. Electrochem. Society, Vol. 109, pp. 251-255.

Cho, M., J.G. Liou, and D.K. Bird, 1988, Prograde phase relations in the State 2-14 well metasandstones, Salton Sea Geothermal Field, California: Journal Geophysical Research, Vol. 93, No. B11, pp. 13,081-13,104.

Crowell, J.C., 1974, The San Andreas fault system through time: Journal of the Geological Society of London, Vol. 136, No. 3, pp. 293-302.

Dirksen, C., 1969, Thermo-osmosis through compacted saturated clay membranes: Soil Science Society of America Proceedings, Vol. 33, No. 6, pp. 821-826.

Donaghe, L., and D.R. Peacor, 1986, Mineral transitions in Salton Sea argillaceous sediments: Abstract submitted to W.A. Elders, Chief Scientist, SSSDP.

Elders, W.A., R.W. Rex, T. Meidav, P.T Robinson, S. Biehler, 1972, Crustal spreading in Southern California: Science, Vol. 178, pp. 15-24.

Elders, W.A., 1979, The geological background of the geothermal fields of the Salton Trough: Campus museum contribution No. 5, Univ. of California, Riverside.

Elrick, D.E., D.E. Smiles, N. Baumgartner, and P.H. Groenevelt, 1976, Coupling phenomena in saturated homo-ionic montmorillinite I. Experimental: Soil Science Society of America Journal, Vol. 40, pp. 490-491.

Fritz, S.J., and I.W. Marine, 1983, Experimental support for a predictive model of clay membranes: Geochimica et Cosmochimica Acta, Vol. 47, pp. 1515-1522.

Fritz, S.J., 1986, Ideality of clay membranes in osmotic processes: Clays and Clay Minerals, Vol. 34, No. 2, pp. 214-223.

Fuis, G.S., W.D. Mooney, J.H. Healy, G.A. McMechan, and W.J. Lutter, 1982, Crustal structure of the Imperial Valley region: U.S.G.S Professional Paper No. 1254.

Graf, D.F., 1982, Chemical osmosis, reverse chemical osmosis, and the origin of subsurface brines: Geochimica et Cosmochimica Acta, Vol. 46, pp. 1431-1448.

Gray, D.H., 1966, Coupled flow phenomena in clay-water systems: Ph.D. Thesis, University of California, Berkeley.

Grim, R.E., 1953, Clay Mineralogy, McGraw-Hill, New York.

Groenevelt, P.H., and D.E. Elrick, 1976, Coupling phenomena in saturated homo-ionic montmorillinite II. Theoretical: Soil Science Society of America Journal, Vol. 40, pp. 820-823.

Halfman, S.E., M.J. Lippmann, R. Zelwer, and J.H. Howard, 1984, Geologic interpretation of geothermal fluid movement in Cerro Prieto Field: AAPG, Vol. 68, No. 1.

Hanshaw, B.B., 1962, Membrane properties of compacted clays: Ph.D. Thesis, Harvard University, Cambridge, Massachusetts.

Haydon, P.R., and D.L. Graf, 1986, Studies of smectite membrane behavior: Temperature dependence, 20-180C: Geochimica et Cosmochimica Acta; Vol. 50, pp. 115-121.

Helgeson, H.C., 1968, Equations of irreversible reactions in geochemical processes involving minerals and aqueous solutions: I. Thermodynamic relations: Geochemica et Cosmochemica Acta, Vol. 32, pp. 853-877.

Ingle, J.C., 1973, Pliocene-Miocene Sedimentary Environments and Biofacies: Society of Economic Paleontologists and Mineralogists Annual meeting, guidebook for field trip No.1.

Iwata, S., T. Tabuchi, and B.P. Warkentin, 1988, Soil-Water Interactions: Marcel Dekker, Inc., publisher, New York, N.Y.

Karig, D.E., and W. Jensky, 1972, The proto-Gulf of California: Earth and Planetary Science Letters, Vol. 17, pp. 169-174.

Kasameyer, P.W., L.W. Younker, and J.M. Hansen, 1984, Development and application of a hydrothermal model for the Salton Sea Geothermal Field: Geol. Soc. Amer. Bull. 95, pp. 1242-1252.

Katchalsky, A., and P.F. Curran, 1965, Non-equilibrium Thermodynamics in Biophysics, Harvard University Press,

Cambridge, Massachusetts.

Keller, G.V., 1982, Editor, Electrical Properties of Rocks,
CRC Handbook of Physical Properties of Rocks, Volume I: CRC
Press, Boca Raton, Florida.

Kemper, W.D., and J.C. van Schaik, 1966, Diffusion of salts
in clay-water systems: Soil Science Society of America
Proceedings, Vol. 30, pp.534-540.

Kemper, W.D., and J.B. Rollins, 1966, Osmotic efficiency
coefficients across compacted clays: Soil Science Society of
Proceedings, Vol. 30, pp. 529-534.

Kemper, W.D., and J.P. Quirk, 1972, Ion mobilities and
electric charge of external clay surfaces inferred
from potential differences and osmotic flow: Soil Science
Society of America Proceedings, Vol. 36, pp. 426-433.

Kharaka, Y.K., and F.A.F. Berry, 1973, Simultaneous flow of
water and solute through geologic membranes I. Experimental:
Geochimica et Cosmochimica Acta, Vol. 37, pp. 2577-2603.

Kobatake, Y., and H. Fujita, 1964, Osmotic flows in charged
membranes II. Thermo-osmosis: Journal of Chemical Physics,
Vol. 41, No. 10, pp. 2963-66.

Lachenbruch, A.H., J.H. Sass, and S.P. Galanis, 1985, Heat flow in southern-most California and the origin of the Salton Trough: Journal of Geophysical Research, Vol. 90, No. B8, pp. 6709-6736.

Marine, I.W., 1974, Geohydrology of a buried Triassic basin at Savannah River plant, South Carolina: American Association of Petroleum Geologists Bull. 58, pp. 1825-1837.

Marine, I.W., and Fritz, S.J., 1981, Osmotic model to explain anomalous hydraulic heads: Water Resources Research, Vol. 17, No. 1, pp. 73-82.

Mckibben, M.A., J.P. Andes, and A.E. Williams, 1988, Active ore formation at a brine interface in metamorphosed deltaic lacustrine sediments: The Salton Sea Geothermal System, California: Economic Geology, Vol. 83, pp. 511-523.

Mehegan, J.M., C.T. Herzig, and R.M. Sullivan, 1986, Visual core descriptions, SSSDP: Vols. I and II, Univ. of California, Riverside.

Michels, D.E., 1988, Salinity stabilization for non-advecting brine in a temperature gradient with applications to the Salton Sea geothermal system: Transactions Geothermal Resource Council, Vol. 12, pp. 127-130.

Mitchell, J.K., 1976, Fundamentals of Soil Behavior, John Wiley and Sons, New York, New York.

Mounce, W.D., and W.M. Rust, 1944, Natural potentials in well logging: Petroleum Transactions A.I.M.E., Vol. 155, pp. 47-55.

Muramoto, F.S., and W.A. Elders, 1984, Correlation of wireline log characteristics with hydrothermal alteration and other reservoir properties of the Salton Sea and Westmoreland geothermal fields, Imperial Valley, California: Los Alamos National Lab Report (LA-10128-MS), 101 pages, Los Alamos, New Mexico.

Olsen, H.W., 1969, Simultaneous fluxes of liquid and charge in saturated kaolinite: Soil Science Society of America Proceedings, Vol. 33, No. 3, pp. 338-344.

Olsen, H.W., 1972, Liquid movement through kaolinite under hydraulic, electric, and osmotic gradients: American Association of Petroleum Geologists Bull. 56, pp. 2022-2028.

Olsen, H.W., E.N. Yearsley, and K.R. Nelson, 1989, Chemical causes of pore fluid movement: International Association of Hydrological Sciences, Proceedings of the Third Scientific Assembly, Publ. No. 185, pp. 65-72.

Onsager, L., 1931, Reciprocal relations in irreversible processes I: Physical Review, Vol. 37, pp. 405-426.

Onsager, L., 1931, Reciprocal relations in irreversible processes II: Physical Review, Vol. 38, pp. 2265-2279.

Phillips, S.L., 1981, A Technical Databook for Geothermal Energy: Lawrence Berkeley Laboratory publication LBL-12810, Berkeley, California, 46 pages.

Rex, R.W., 1985, Temperature-chlorinity balance in the hypersaline brines of the Imperial Valley, California: Transactions ········hermal Resource Council, Vol. 9, pp. 351-356.

Robie, R.A., B.S. Hemingway, and J.R. Fisher, 1978, Thermodynamic properties of minerals and related substances: U.S.G.S. Bulletin 1452, p. 452.

Sass, J.H., 1987, Temperatures and Heat flow in the State 2-14 well, Salton Sea Scientific Drilling Program: Amer. Geop. Union Spring Meeting Poster Session.

Sass, J.H., S.S. Priest, L.E. Duda, C.C. Carson, J.D. Hendricks, and L.C. Robinson, 1988, Thermal regime of the State 2-14 well, Salton Sea Scientific Drilling Program; JGR, Vol. 93, No. B11, pp. 13005-13024.

Schlumberger, 1972, Log Interpretation Principles, Published by Schlumberger, New York, N.Y.

Shainberg, I., and W.D. Kemper, 1972, Transport numbers and mobilities of ions in bentonite membranes: Soil Science Society of America Proceedings, Vol. 36, pp. 577-582.

Spiegler, K.S., 1958, Transport processes in ionic membranes: Transactions Faraday Society, Vol. 54, pp. 1408-1428.

Srivastava, R.C., and P.K. Avasthi, 1975, Non-equilibrium thermodynamics of thermo-osmosis of water through kaolinite: Journal of Hydrology, Vol. 24, pp. 111-120.

Staverman, A.J., 1952, Non-equilibrium thermodynamics of membrane processes: Transactions Faraday Society, Vol. 48, pp. 176-185.

Tarif, P.A., R.H. Wilkens, C.H. Cheng, and F.L. Paillet, 1988, Laboratory studies of the acoustic properties of samples from SSSDP and their relation to microstructure and field measurements: Journal Geophysical Research, Vol. 93, No. B11, pp. 13,057-13,067.

Tasaka, M., 1986, Thermal membrane potential and thermo-osmosis across charged membranes: Pure and Applied Chemistry, Vol. 58, No. 12, pp. 1637-1646.

Taylor, S.A., and J.W. Cary, 1961, Analysis of the simultaneous flow of water and heat with the thermodynamics of irreversible processes: Transactions International Congress Soil Science, Vol. 1, pp. 80-90

Tsang, C.F., 1987, Proceedings of the International Symposium on Coupled Processes Associated with Nuclear Waste Repositories, Academic Press, New York, N.Y.

Ucok, H, 1980, Temperature dependence of the electrical properties of aqueous salt solutions and solution-saturated porous rocks: Ph.D. Thesis, Univ. of So. Cal., Los Angeles, California, 153 pages.

Waxman, M.H., and L.J.M. Smits, 1968, Electrical conductivities in oil-bearing shaly sands; SPE Jour., Vol. 8, pp. 107-122.

White, D.E., E.T. Anderson, and D.K. Grubbs, 1963, Geothermal brine well: Mile deep drill hole may tap ore-bearing magmatic water and rocks undergoing metamorphism: Science, Vol. 139, pp. 919-922.

White, D.E., 1968, Environments of generation of some base metal ore deposits: Economic Geology, Vol. 63, pp. 301-335.

Williams, A.E., 1988, Delineation of a brine interface in the Salton Sea Geothermal System, California: Transactions, Geothermal Resources Council, Vol. 12, pp. 151-157.

Weaver, C.E., 1979, Geothermal alteration of clay minerals and shales: Diagenesis, Office of Nuclear Waste Isolation Technical Report (ONWI-21), 176 pages, Battelle, Columbus, Ohio.

Worthington, P.F., 1985, The evolution of shaly sand concepts in reservoir evaluation; The Log Analyst, Vol. 26. No. 1, pp. 23-40.

Wyllie, M.R.J., 1949, A quantitative analysis of the electro-chemical component of the SP curve: Journal of Petroleum Technology, Vol. 1, pp. 17.

Wyllie, M.R.J., 1951, An investigation of the electro-kinetic component of the SP curve: Petroleum Transactions A.I.M.E., Vol. 192, pp. 1-18.

Young, A., and P.F. Low, 1965, Osmosis in argillaceous rocks: American Association of Petroleum Geologists Bull. 49, pp. 1004-1008.

APPENDIX A

DERIVATION OF OSMOTIC PRESSURE

The chemical potential for an ideal solution is given by Barrow (1979) as:

$$u_W = u_W^o(T) + RT\ln(c_W) \qquad (A.1)$$

and can also be approximated by (Barrow, 1979):

$$u_W = PV_W \qquad (A.2)$$

for: u_W = chemical potential of water phase

u_W^o = standard state at temperature T

V_W = partial molar volume of water

 P = Partial pressure of the water phase

 R = gas constant

 T = absolute temperature

c_W = molar concentration of water phase

Real solutions approach the behavior predicted by equation (A.1) only at infinite dilution. To account for the deviation from ideality, the common practice is to introduce an activity coefficient γ, by which c_W is multiplied to

give the "active concentration" or activity, a_w.

$$a_W = \gamma\, c_W \qquad (A.3)$$

Thus, the chemical potential for a real solution is approximated by:

$$u_W = u_W^O + RT\ln(a_W) = PV_W \qquad (A.4)$$

The <u>difference</u> in chemical potentials between arbitrary solution 'A' and arbitrary solution 'B' is given by:

$$\triangle u_W = V_A P_A - V_B P_B = RT\ln(a_A/a_B) \qquad (A.5)$$

Where, for the isothermal condition, the standard states of solution 'A' and solution 'B' are equal and therefore cancel.

Now, if we set $V_W = (V_A + V_B)/2$, and call V_W the mean partial molar volume of the water, then:

$$P_B - P_A = RT\ln(a_A/a_B)/V_W \qquad (A.6)$$

The difference, $P_B - P_A$, is defined as the osmotic pressure between solution 'A' and solution 'B', which are separated by an ideal membrane; thus:

$$P_B - P_A = \pi = RT\ln(a_A/a_B)/V_W$$

Which is identical to equation (2.6.)

APPENDIX B

CONSTRUCTION AND ASYMMETRY TESTING FOR SILVER-SILVER CHLORIDE REVERSIBLE ELECTRODES

An electrode is "reversible" if it allows the exchange of anions and electrons between itself and a solution with negligible energy loss. Pure silver wire mesh that is electro-plated with chloride ions makes an excellent medium for reversible electrodes.

The electrodes used in this thesis are 2" diameter circles cut from pure silver wire mesh (80 strands to the inch); electro-plated with chloride ions in a 1.0 molar NaCl solution. The electrode leads are pure silver wire (.012" diameter) mechanically bonded to the mesh (cold rolled). For reliable, accurate results it is important that the silver mesh and leads be 100% pure and perfectly clean (store in plastic before use and soak in acetone before plating). The electro-plating process is depicted in Figure B.1.

These electrodes can be used to detect an electric potential or generate a current. In either case, stability is desirable - with little or no electric asymmetry between electrode pairs. Several arrangements were used to test the

electrodes for asymmetry, and confirm that no spontaneous
plating or de-plating occurs as a result of the electrode
pairs being immersed in solutions of different
concentrations. The results of these tests are shown in
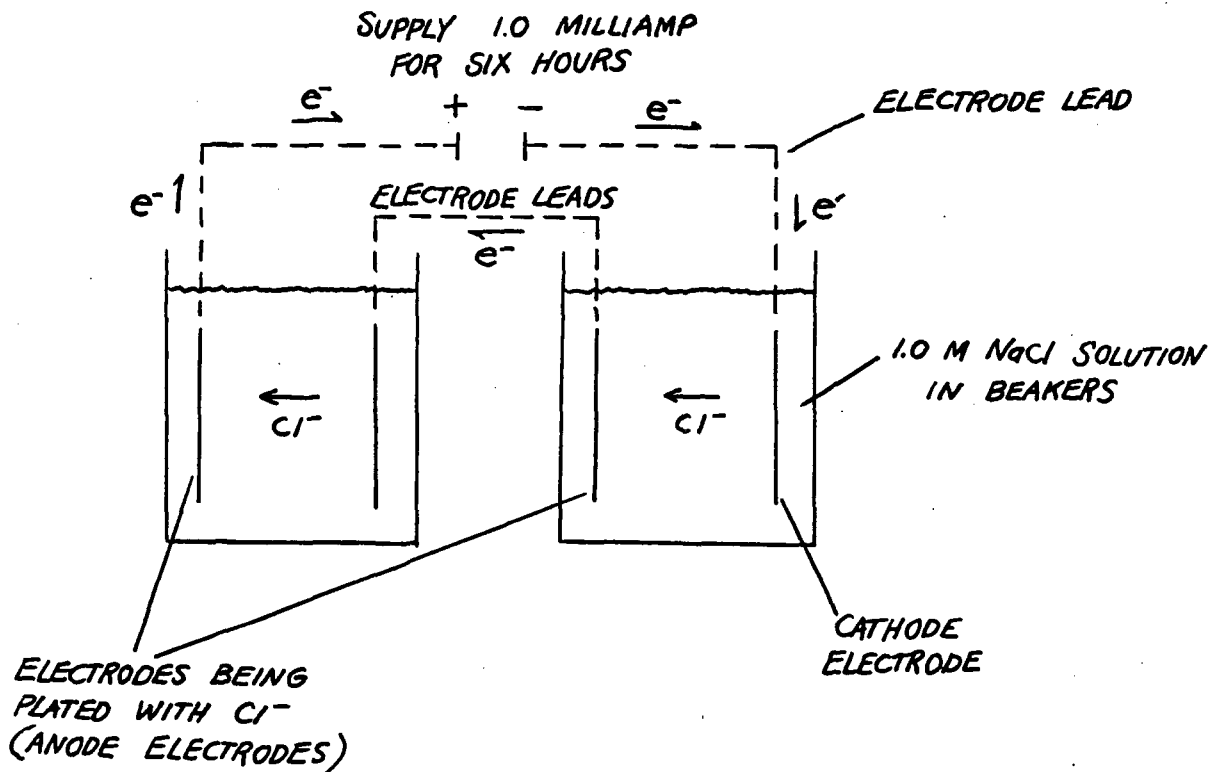Figures B.2 - B.4.

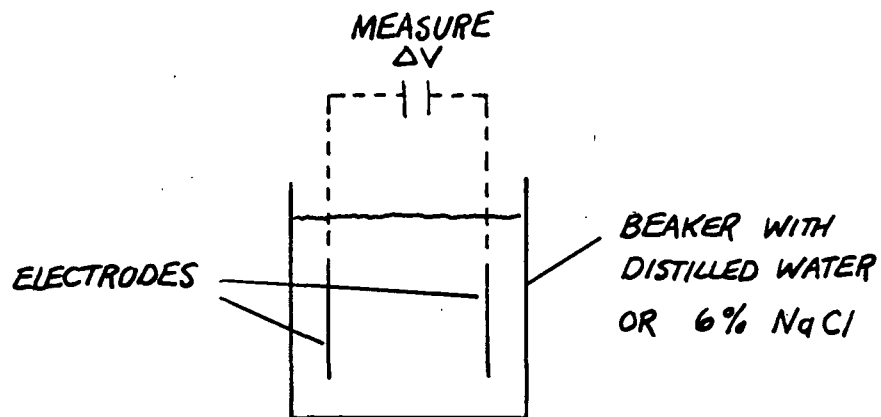Figure B.1: Electro-plating process for reversible
electrodes.

Figure B.2: Asymmetry test: two electrodes in the same solution. Results: V = 0.0 (24 hrs.) - No measurable asymmetry.
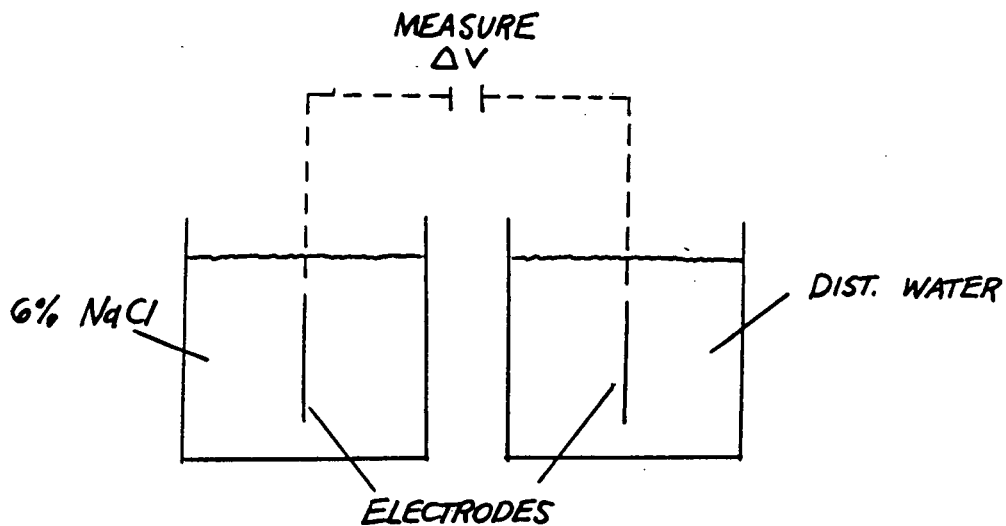

Figure B.3: Asymmetry test: two electrodes in different solutions. Results: V= 0.0 (24 hrs.) - No measurable asymmetry.
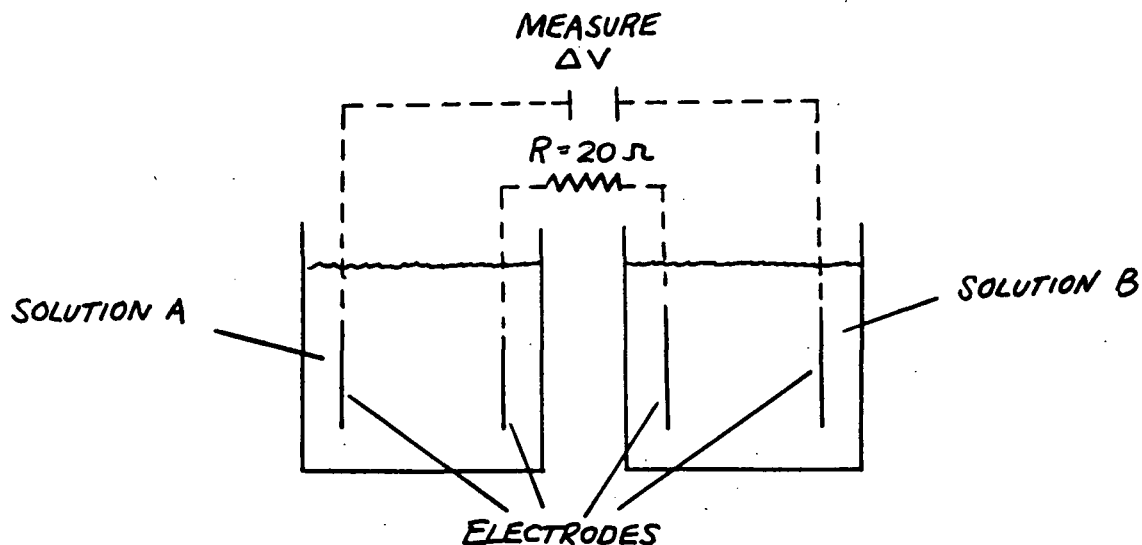
MEASURE
ΔV

$R = 20 \, \Omega$

SOLUTION A

SOLUTION B

ELECTRODES

Figure B.4: Asymmetry and spontaneous plating test: two electrodes in different solutions with parallel circuit to simulate current path in sample.

Results:

Soln. A	Soln. B	V (60 min.)
6 % NaCl	20 % TDS	0.3 mV
6 % NaCl	Dist. water	0.1 mV
20 % TDS	Dist. water	0.4 mV

Very little asymmetry; little or no spontaneous plating observed (spontaneous plating would be a transient process resulting in larger asymmetry potentials with time).

APPENDIX C

CALCULATION OF THE HEAT TRANSFER RATIO AND

UNCERTAINTIES IN THERMAL CONDUCTIVITY

Because of heat loss from the test cells, all of applied power of the heater is not manifested as heat flow through the sample. To evaluate this heat loss, a sample "blank" (made of epoxy) of known thermal conductivity is tested under the same conditions that real samples are: a constant voltage is applied and a temperature difference (dT) is measured at thermal equilibrium. Since the thermal conductivity of the blank is known, the actual heat flow can be calculated and compared to the applied power. The ratio between the actual heat flow and the applied power is the heat transfer ratio.

The calibration arrangement for the derivation of the heat transfer ratio (HTR) is shown on the following page in Figure C.1.
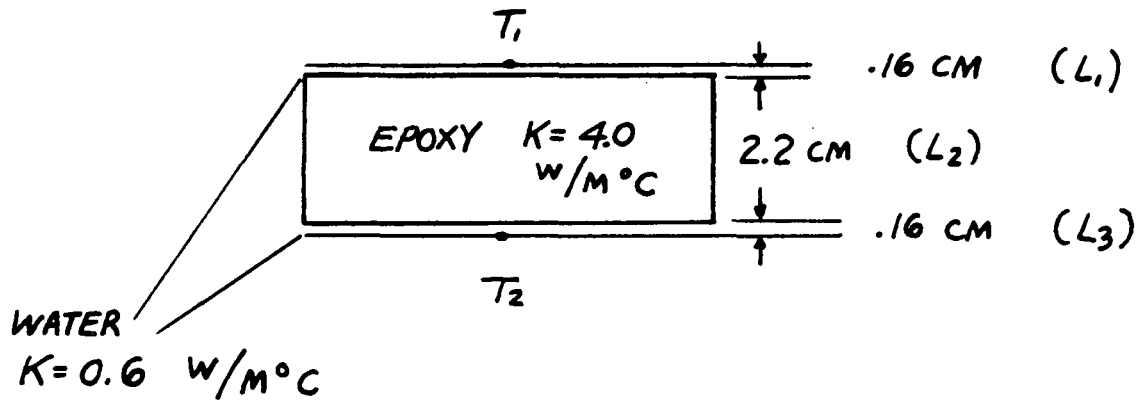
WATER
$K = 0.6$ W/M°C

FIGURE C.1: Calibration arrangement for the derivation of the heat transfer ratio (HTR).

For an applied voltage of V = 5.0 volts, the applied power is given by:

$$P_w = V^2/R = 25/21 = 1.19 \text{ Watts} \qquad \text{(C.1)}$$

where R = resistance of the heater wire (21 ohms)

For applied power the calculated dT was 1.1C (as per equation (3.3) in the text). The thermal circuit is shown in Figure C.2.
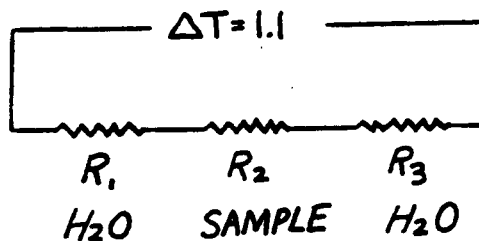
$$\Delta T = 1.1$$

R₁   R₂   R₃
H_2O SAMPLE H_2O

FIGURE C.2: Thermal circuit for HTR calibration.

The actual heat flux through the sample is given by:

$$q = dT/R_s \qquad\qquad (C.2)$$

where: $R_s = R_1 + R_2 + R_3$

and: $R_1 = R_3 = L_1/K_w = .00267 \ m^2/W \ C$

$R_2 = L_2/K_e = .00625 \ m^2/W \ C$

For: K_w = thermal conductivity of water (0.6 W/m C)

K_e = thermal conductivity of epoxy (4.0 W/m C)

Now, R_s = .00267 + .00625 + .00267 = .01159 m^2/W C

Thus, q = 1.1/.01159 = 95 W/m^2, and the actual heat

transfer is: Q = q X A = 95 X .003 = .29 Watts

(where A is the cross-sectional area equal to 30 X 10^{-4} m^2)

Therefore, the heat transfer ratio is:

$$HTR = Q/P_w = .294/1.19 = 0.25, \text{ or } 25\% \qquad (C.3)$$

This value (.25) is multiplied by the applied power in each

case to obtain the actual heat transfer. It is assumed for

the tests in this thesis that this HTR is constant for the

conditions tested, though this is only an estimate.

APPENDIX C CONTINUED:

UNCERTAINTY IN THERMAL CONDUCTIVITY MEASUREMENTS

Error analysis for a derived quantity that depends on single-measurement parameters is developed in Chen and Fang (1986). The following error analysis for thermal conductivity measurements in this thesis adheres to the methods and assumptions contained therein.

For the working equation:

$$K_t = (Q/\Delta T) \times (L/A) \qquad\qquad (C.4)$$

where:

K_t = thermal conductivity

Q = actual heat transfer

ΔT = temperature difference

L = length of sample

A = cross-sectional area of sample.

The variance in thermal conductivity is:

$$\sigma^2_{K_t} = \left(\frac{\partial K_t}{\partial Q}\right)^2 \sigma^2_Q + \left(\frac{\partial K_t}{\partial \Delta T}\right)^2 \sigma^2_{\Delta T} \qquad\qquad (C.5)$$

If we assume that the uncertainties in sample length and cross-sectional area are negligible.

For the sake of example, the partial derivatives in equation (C.5) are evaluated for specific heat transfer and ΔT values; namely, those values used in the calibration of the heat transfer ratio (HTR). The partial derivatives, and therefore the variances, will vary with the single-measurement values.

For: Q = .29 watts

         ΔT = 1.1°C

$$\frac{\partial K_t}{\partial Q} = \frac{L}{A \; \Delta T} = \frac{.022}{(.003)(1.1)} = 6.67 \qquad (C.6)$$

$$\frac{\partial K_t}{\partial \Delta T} = \frac{QL}{A} = \frac{(.29)(.022)}{.003} = 2.13 \qquad (C.7)$$

The variance in the single-measurement parameters is obtained from an estimated uncertainty associated with their measurement. This is subjective, but there is no statistical alternative. For this example, and for the calculation of measured values in this thesis, a 10% uncertainty is assigned to both Q and ΔT.

Thus,

$$\sigma_Q = .10, \qquad \sigma_Q^2 = .01$$

$$\sigma_{\Delta T} = .10, \qquad \sigma_{\Delta T}^2 = .01$$

For these assumed parameter variances, and the partial derivatives evaluated in equations (C.6) and (C.7), the variance in thermal conductivity can now be calculated from equation (C.5):

$$\sigma_{K_t}^2 = (6.67)^2 \times .01 + (2.13)^2 \times .01 = .49$$

Therefore, the 68% confidence level uncertainty in the thermal conductivity measurement of the epoxy sample used to calculate the HTR is given by:

$$\sigma_{K_t} = \sqrt{.49} = .7$$

Uncertainties calculated in a similar manner are listed in Table 4.6 with their respective measured thermal conductivities.